RECLAMATION

Managing Water in the West

Desalination and Water Purification Research and Development Program Report No. 127

Boron Rejection by Reverse Osmosis Membranes: National Reconnaissance and Mechanism Study

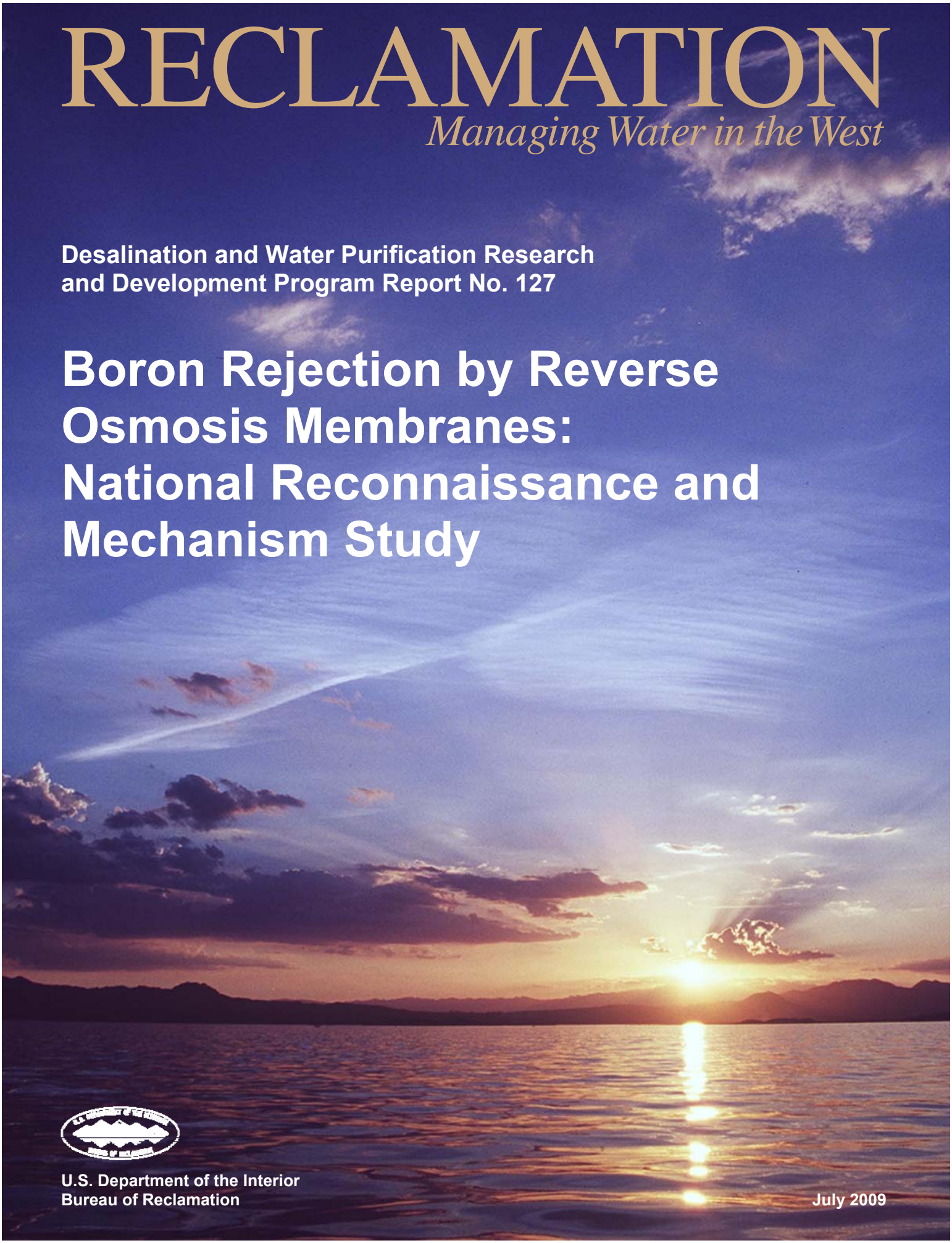

U.S. Department of the Interior
Bureau of Reclamation

July 2009

REPORT DOCUMENTATION PAGE

Form Approved
OMB No. 0704-0188

1. REPORT DATE *(DD-MM-YYYY)*	2. REPORT TYPE	3. DATES COVERED *(From - To)*
July 2009	Final	September 2004 - December 2005

4. TITLE AND SUBTITLE
Boron Rejection By Reverse Osmosis Membranes: National Reconnaissance And Mechanism Study

5a. CONTRACT NUMBER
Agreement No. 04-FC-81-1050

5b. GRANT NUMBER

5c. PROGRAM ELEMENT NUMBER

6. AUTHOR(S)
Jaehong Kim, Ph.D. and Hoon Hyung, School of Civil and Environmental Engineering, Georgia Institute of Technology
Mark Wilf, Ph.D., Hydranautics
Jong-Sang Park, Ph.D., Saehan Industry, Inc.
Jess Brown, Ph.D., Carollo Engineers, P.C.

5d. PROJECT NUMBER

5e. TASK NUMBER
Task F

5f. WORK UNIT NUMBER

7. PERFORMING ORGANIZATION NAME(S) AND ADDRESS(ES)
Georgia Institute of Technology, School of Civil and Environmental Engineering, 311 Ferst Dr., Atlanta, Georgia 30332-0512
Hydranautics, 401 Jones Rd., Oceanside, California 92054
Saehan Industry, Inc., 12th Floor, Hanshin Bldg., 254-8, Kongduk-Dong, Mapo-Ku, Seoul, Korea 121-710
Carollo Engineers, P.C., 401 N. Cattlemen Rd., Suite 306, Sarasota, FL 34232

8. PERFORMING ORGANIZATION REPORT NUMBER

9. SPONSORING / MONITORING AGENCY NAME(S) AND ADDRESS(ES)
U.S. Department of the Interior
Bureau of Reclamation
Denver Federal Center
PO Box 25007
Denver CO 80225-0007

10. SPONSOR/MONITOR'S ACRONYM(S)
Reclamation

11. SPONSOR/MONITOR'S REPORT NUMBER(S)
DWPR No. 127

12. DISTRIBUTION / AVAILABILITY STATEMENT
Available from the National Technical Information Service
Operations Division, 5285 Port Royal Road, Springfield VA 22161

13. SUPPLEMENTARY NOTES
Report can be downloaded from Reclamation Web site: www.usbr.gov/pmts/water/publications/reports.html

14. ABSTRACT ***(Maximum 200 words)***

The mechanism of boron rejection by and transport through RO membrane was studied with bench-scale experiments using six commercial RO membranes. Boron rejection was governed by speciation of boric acid and affected by temperature but did not relate to other measurable parameters including rejection of mono- and divalent ions and surface properties. A mathematical model was developed to predict the boron rejection by RO membranes under different operating conditions such as pressure, pH, and temperature. Boron concentrations in the feed and product waters from nine pilot- or full-scale plants were analyzed in parallel. Comparison to bench-scale data suggested that much lower level of boron rejection was observed in the field data, primarily due to high target recovery. A comprehensive cost estimate for RO processes designed for boron removal was performed. The economics of boron removal processes is expected to be governed by the target permeate water quality driven by the regulations. In addition, when the boron removal is of concern in the RO process, the development of RO membranes with improved boron rejection capabilities is critical to achieve target boron removal in full-scale membrane plants.

15. SUBJECT TERMS
reverse osmosis, desalination, boron, transport model, mechanism

16. SECURITY CLASSIFICATION OF:			17. LIMITATION OF ABSTRACT	18. NUMBER OF PAGES	19a. NAME OF RESPONSIBLE PERSON
a. REPORT	b. ABSTRACT	c. THIS PAGE			19b. TELEPHONE NUMBER *(include area code)*
UL	UL	UL	SAR	140	Frank Leitz 303-445-2255

Standard Form 298 (Rev. 8/98)
Prescribed by ANSI Std. 239-18

Desalination and Water Purification Research and Development Program Report No. 127

Boron Rejection by Reverse Osmosis Membranes: National Reconnaissance and Mechanism Study

Prepared for Reclamation Under Agreement No. 05-FC-81-1050

by

Jaehong Kim, Ph.D. and Hoon Hyung, School of Civil and Environmental Engineering, Georgia Institute of Technology

Mark Wilf, Ph.D., Hydranautics

Jong-Sang Park, Ph.D., Saehan Industry, Inc.

Jess Brown, Ph.D., Carollo Engineers, P.C.

U.S. Department of the Interior
Bureau of Reclamation
Technical Service Center
Water and Environmental Resources Division
Water Treatment Engineering Research Group
Denver, Colorado

July 2009

MISSION STATEMENTS

The mission of the Department of the Interior is to protect and provide access to our Nation's natural and cultural heritage and honor our trust responsibilities to Indian tribes and our commitments to island communities.

The mission of the Bureau of Reclamation is to manage, develop, and protect water and related resources in an environmentally and economically sound manner in the interest of the American public.

Disclaimer

The views, analysis, recommendations, and conclusions in this report are those of the authors and do not represent official or unofficial policies or opinions of the United States Government, and the United States takes no position with regard to any findings, conclusions, or recommendations made. As such, mention of trade names or commercial products does not constitute their endorsement by the United States Government.

Acknowledgements

Funding for this project was provided by the Desalination and Water Purification Research and Development Program of the Bureau of Reclamation, Denver, Colorado. In-kind contributions from participating organizations includ**ing** Hydranautics, Saehan Industries, Inc., and Carollo Engineers, P.C. are thankfully acknowledged. The authors also would like to thank Lynne Gulizia at Toray America and William Mickols at Dow (Filmtec) corporation for their donation of RO membranes.

The authors are grateful for Junsuk Kim, Sungpyo Hong**,** and Younghun Kim at Saehan Industries, Inc. for their efforts in some of the instrumental analyses performed**;** Dr. Guangxuan Zhu, a laboratory manager at School of Civil and Environmental Engineering, Georgia Institute of Technology, for maintenance and troubleshooting of the analytical instruments**;** and Frank Leitz at the Bureau of Reclamation for administrative support and guidance throughout the project.

Table of Contents

Contents (continued)

List of Figures

List of Figures (continued)

List of Figures

List of Tables

List of Tables

Glossary

a	pre-exponent value of boric acid (T^{-1})
b	pre-exponent value of borate (T^{-1})
C	superficial aqueous-phase solute concentration, which is assumed to be in equilibrium with concentration of solute in the membrane phase (ML^{-3})
c	concentration of salts (ML^{-3}; kg/m^3)
$\overline{C}$	average solute concentration of feed and permeate side (ML^{-3})
Cl	chlorinity, (dimensionless; ‰)
C_f	solute concentration in the feed side (ML^{-3})
C_m	concentration at membrane surface (ML^{-3})
C_p	solute concentration in the permeate side (ML^{-3})
$C_{T,B}$	total concentration of boron species (ML^{-3})
D	molecular diffusion coefficient (L^2T^{-1})
D_{AM}	diffusion coefficient of solute in the membrane (L^2T^{-1})
$D_{AM}K/\Delta x$	solute transport parameter (LT^{-1})
$[H^+]$	concentration of proton (ML^{-3})
$\{H^+\}$	activity of proton (ML^{-3})
$[H_2BO_3^-]$	concentration of borate (ML^{-3})
$\{H_2BO_3^-\}$	activity of borate (ML^{-3})
$[H_3BO_3]$	concentration of boric acid (ML^{-3})
$\{H_3BO_3\}$	activity of boric acid (ML^{-3})
i	interest rate
J_s	gravimetric solute flux ($ML^{-2}T^{-1}$)
J_v	volumetric water flux (LT^{-1})
K	partition coefficient between solvent (water) and membrane (dimensionless)
k	mass transfer coefficient (LT^{-1})
k_t	mass transfer coefficient of boron at t ^oC (LT^{-1})
k_{25}	mass transfer coefficient of boron at 25 ^oC (LT^{-1})
K_{a1}	the first acid constant of boric acid (ML^{-3})
K_{a1}'	apparent first acid constant of boric (ML^{-3})
L_p	hydraulic permeability (LT^{-1})
n	system life
P	hydraulic pressure ($ML^{-1}T^{-2}$)
p_h	specific hydraulic permeability (T^{-1})
P_s	overall permeability constant (LT^{-1})
p_s	local solute permeability coefficient (L^2T^{-1})
$P_{s,B}$	overall permeability constant of boron (LT^{-1})
$P_{s(H2BO3-)}$	permeability constant of borate (LT^{-1})
$P_{s(H2BO3-)0}$	pre-exponential value of borate (LT^{-1})
$P_{s(H2BO3-)25}$	permeability constant of borate estimated at 25 ^oC (LT^{-1})
$P_{s(H3BO3)}$	permeability constant of boric acid (LT^{-1})
$P_{s(H3BO3)0}$	pre-exponential value of boric acid (LT^{-1})

$P_{s(H3BO3)25}$	permeability constant of boric acid estimated at 25 ^{o}C (LT^{-1})
R	intrinsic rejection (dimensionless) = $(C_m - C_p)/C_m$
R_0	apparent rejection (dimensionless) = $(C_f - C_p)/C_f$
S	standard deviation of the replicate analyses
T	Temperature (K)
t	temperature (^{o}C)
Δx	distance from feed/membrane interface toward permeate/membrane interface across the membrane (L)
α_0	fraction of boric acid (dimensionless)
α_1	fraction of borate (dimensionless)
μ	viscosity ($ML^{-1}T^{-1}$; Pa·s)
π	osmotic pressure ($ML^{-1}T^{-2}$)
ρ	density (ML^{-3}; kg/m^3)
σ	reflection (coupling) coefficient which indicates degree of solute/water coupling (dimensionless)
σ_B	reflection coefficient of boron (dimensionless)
$\sigma_{(H2BO3-)}$	reflection coefficient of boric acid (dimensionless)
$\sigma_{(H3BO3)}$	reflection coefficient of boric acid (dimensionless)

Abbreviations and Acronyms

$/1,000 gal	dollars per thousand gallons
$/kw-hr	dollars per kilowatthour
$/$m^3$	dollars per cubic meter
%	percent
μm	micrometers
μg/L	micrograms per liter
AAES	Anionic Atlas Electrolytic suppressor
AFM	Atomic Force Microscopy
B	boron
BWRO	brackish water RO
CDHS	California Department of Health Services
Cl	chloride
DI	deionized
gal/day	gallons per day
gfd	gallons per square foot day
gpm	gallons per minute
HCl	hydrochloride
IC	Ion Chromatography
ICP-AES	Inductively Coupled Plasma Mass Spectrometer-Atomic Emission Spectroscopy
IX	ion exchange
kw-hr/m^3	kilowatthour per cubic meter
m/s	meters per second
m^3/day	cubic meters per day
MDL	method detection limit
Mg	magnesium
$MgSO_4$	magnesium sulfate
$MgCl_2$	magnesium chloride
mL/min	milliliters per minute
mm	millimeters
mV	millivolts
Na	sodium
Na_2CO_3	sodium carbonate
NaCl	sodium chloride
NaOH	sodium hydroxide
nm	nanometers
ppm	parts per million
psi	pounds per square inch
RO	reverse osmosis
SEM	Scanning Electron Microscopy
SO_4	sulfate
SS	stainless steel
SWRO	seawater RO
TMP	transmembrane pressure

Executive Summary

Seawater desalination has become an important process in many areas of the United States and worldwide due to increased water demand and decreased suitable water sources. As our knowledge of trace contaminant occurrence and related environmental and human health impacts expands and water quality standards become increasingly stringent, seawater desalination processes will continue to be challenged by new types of contaminants, such as boron. Boron is naturally occurring and is present in seawater at an average concentration of 4.6 milligrams per liter (mg/L). While boron is a vital element for organism growth, excessive exposure can cause detrimental effects to plants, animals, and possibly humans. Consequently, World Health Organization Guidelines for Drinking Water Quality propose a maximum recommended boron concentration of 0.5 mg/L. This value is considered provisional due to the lack of a comprehensive toxicological assessment and the limited availability of technologies to remove boron. Boron is also on the U.S. Environmental Protection Agency's (EPA) Drinking Water Contaminant Candidate List, but there is a limited amount of information on the occurrence of boron in drinking water supplies in the United States.

The first part of this project involved bench-scale cross-flow filtration experiments, which were performed to evaluate rejection of boron and ionic species in synthetic seawater by six commercial reverse osmosis (RO) membranes. Overall, boron rejection was strongly affected by acid-base dissociation of boric acid. Experimental results were analyzed and explained using a nonequilibrium thermodynamic model coupled with film theory. Equations to predict the parameters in the model at various operating conditions (pH, operating pressure, and temperature) were further developed. Parameters such as membrane surface characteristics and apparent rejection of ionic species did not correlate with boron rejection.

For the second part of the project, boron concentrations in raw and finished waters from nine RO treatment facilities were analyzed. The results showed that product water of the all the seawater desalination facilities tested in this study could not meet WHO guidelines for the boron concentration of 0.5mg/L, except two brackish water treatment facilities where boron concentration in the feed was low. However, most of the plants were in compliance with the European Communities Drinking Water Regulations and California Department of Health Services action level of 1 mg/L. It was also observed that boron rejection by full- or pilot-scale RO membranes were much lower than those estimated in the lab-scale experiment. This was most likely due to differences in overall system recoveries. An accurate extrapolation of full-scale boron rejection from bench-scale results

would require the use of a predictive model that factors the increase in boron concentration as RO concentrate flows into successive membrane elements.

The third task of the project was to identify appropriate RO configurations (i.e., configurations that would produce water containing regulatory level of boron) and develop associated cost estimates for full-scale installation and operation. The results indicated that multistage processes would be required to achieve the boron concentration of 0.5 mg/L, but it would also involve much higher costs relative to simple systems. This evaluation also shows that the development of RO membranes with higher boron rejection capabilities and the optimization of multistage treatment processes are critical to the establishment of cost-effective RO processes designed for boron removal.

This project was a collaborative effort among the Georgia Institute of Technology, two leading membrane manufacturers (Hydranautics and Saehan Industry, Inc.), an engineering consulting firm (Carollo Engineers), and drinking water utilities.

1. Introduction

1.1 Project Objectives

Seawater desalination has become an important process in many areas of the United States and worldwide due to increased water demand and decreased suitable water sources. As our knowledge of trace contaminant occurrence and related environmental and human health impacts expands and water quality standards become increasingly stringent, seawater desalination processes will continue to be challenged by new types of contaminants, such as boron (B).

Boron is naturally occurring and is present in seawater at an average concentration of 4.6 milligrams per liter (mg/L). While boron is a vital element for organism growth, excessive exposure can cause detrimental effects to plants, animals, and possibly humans. Consequently, current World Health Organization (WHO) Guidelines for Drinking Water Quality propose a maximum recommended boron concentration of 0.5 mg/L. This value is considered provisional due to the lack of a comprehensive toxicological assessment and the limited availability of technologies to remove boron. Boron is also on the U.S. Environmental Protection Agency's (EPA) Drinking Water Contaminant Candidate List, but there is little information on the occurrence of boron in drinking water supplies in the United States.

Unfortunately, it is generally difficult for a reverse osmosis RO process to achieve an average boron rejection over 90 percent (%), which is typically required to produce permeate that meets the provisional WHO boron guidelines. Improved rejection can be achieved by adding treatment stages or polishing steps, which could increase costs substantially, though there has been minimal work done on the impact of boron regulation on water production costs. The development of RO membranes that inherently achieve high boron rejection is critical for meeting the provisional boron standard. To that end, a study on boron transport mechanisms through RO membranes was performed and the relationship between boron rejection and characteristics of RO membranes was evaluated.

The first objective of this study was to understand the mechanism of boron rejection by and transport through RO membranes and to elucidate the effects of operating condition such as pH and temperature on boron transport. Bench-scale experiments were performed with synthetic seawater to evaluate boron rejection using commercially available RO membranes. A mathematical model was applied to quantitatively analyze membrane performance.

The second objective of this study was to characterize ambient boron concentrations in various water bodies and assess removal of boron at existing

RO facilities. Raw and treated samples from participating utilities were analyzed to provide a comprehensive seasonal and geographical map of boron occurrence and treatment in the United States.

The third objective of this study was to identify appropriate RO configurations (i.e., configurations that would produce water containing < 0.5 mg/L boron) and develop associated cost estimates for full-scale installation and operation. This work will ultimately help evaluate the impact of a potential boron regulation on the desalination industry.

1.2 Background

1.2.1 Occurrence and Environmental Concern

Boron is a nonmetallic element with an atomic number of five and atomic weight of 10.81. Boron exists as a mixture of two stable isotopes, ^{10}B (19.8%) and ^{11}B (80.2%). Most of the Earth's soils typically have less than 10 mg/L of boron, although concentrations as high as 100 mg/L have been reported in some shale and soils (EPA, 2001). Seawater contains 4.6 mg/L boron on average, with concentrations ranging from 0.5 to 9.6 mg/L (Woods, 1994). Freshwater boron concentrations range from <0.01 to 1.5 mg/L. In natural environments, boron exists as a boric acid (H_3BO_3) and its dissociated forms ($H_2BO_3^-$, HBO_3^{2-}, and BO_3^{3-}). Since boric acid is weak (pK_a = 9.14), H_3BO_3 is the predominant form in the environment (Woods, 1994).

Natural weathering processes are largely responsible for the presence of boron in seawater. It is also of anthropogenic origin in certain locations, such as in estuarine water, due to its use as a fungicide, insecticide, disinfectant, cleaner, fertilizer, antioxidant, borosilicate glass additive, and flame retardant (EPA, 2001). Humans are exposed to boron mainly through the consumption of fruits and vegetables, though ingestion through water and consumer products can also be significant. Although boron has been found in animal tissue, human exposure through meat consumption is estimated to be negligible (Agency for Toxic Substances and Disease Registry [ATSDR], 1992).

Boron is an essential element for the growth of plants and can be found in fertilizers and fungicidal agents as sodium borate and boric acid. However, if the concentration of boron is too high, massive leaf damage and/or premature ripening can occur, leading to reduced yields (EPA, 1975). The optimal boron concentration for agriculture ranges from 0.3 mg/L to 0.5 mg/L (Nadav, 1999). However, animal infectivity studies indicate that excess boron inhibits male reproductive capabilities and may have teratogenic properties (WHO, 1998). Consequently, the WHO Guidelines for Drinking Water Quality proposed a maximum recommended boron concentration of 0.5 mg/L (WHO, 1998). This

value is, however, considered provisional due to the lack of a comprehensive toxicological assessment and the limited availability of technologies to remove boron and currently being reevaluated by the WHO (Voutchkov, 2005). It should be noted that the WHO guideline level for boron is not a mandatory water quality parameter. Therefore, even though boron is listed on the EPA's Drinking Water Contaminant Candidate List, the EPA has not adopted the present WHO guideline level in the Safe Drinking Water Act. The only State with a regulation for boron is California, where a drinking water quality requirement of the boron is 1 mg/L. This level is, however, not a compliance limit but only a notification level. In addition, regulation for boron in the drinking water seems to vary greatly from country to country. For example, boron concentration limit in the European Union is 1 mg/L (Weinthal et al., 2005), while the limit in Canada is 5 mg/L (Mose and Nagpal, 2003).

1.2.2 Boron Removal by RO Membrane Process

RO processes have been widely used for seawater desalination. Despite high removal (>99%) of other ionic species from seawater, the removal of boron by RO has proven challenging. Due to the recent improvement of membrane performance, seawater RO (SWRO) membranes, which achieve up to 95% rejection of boron in the manufacturer's testing condition, have been commercialized. However, this nominal level of boron removal corresponds to 88~90% boron rejection under the higher recovery conditions of SWRO plants. It is difficult for a single-stage RO process to achieve an average rejection over 90% and to produce permeate that meets the provisional WHO boron guideline. Generally, the rejection of boron has been lower than 90% and has been reported to be as low as 40% with low-pressure brackish water RO membranes. An 80 cubic meter per day (m^3/day) (21,000 gallons per day [gal/day]) pilot-scale experiment performed at Sesoko Island in southern Japan (Magara et al., 1996) showed 43 to 78% boron rejection by the first-stage SWRO process, depending on the operating conditions. Subsequent work by Magara et al. (1998) indicated that in order to produce permeate with boron levels consistently below 1 mg/L, a minimum two-pass RO configuration would be necessary. From their 140 m^3/day (36,900 gal/day) pilot-scale experiment, Taniguchi et al. (2001) reported permeate boron concentration in the range of 0.4 to 1.0 mg/L using a single-pass RO configuration. The 50,000 m^3/day (13,200,000 gal/day) plant at Larnaca, Cyprus, constructed in 2001 with a partial two-pass configuration, produced permeate with 0.8 to 1.2 mg/L of boron from seawater that contained 4.5 to 6.5 mg/L of boron. In a study performed at a two-stage SWRO plant operated at 12 m^3/day (3,190 gal/day) and 55% recovery, Redondo et al. (2003) demonstrate boron removal of 90.0 to 90.6%, resulting in permeate boron concentrations of 0.79 to 0.86 mg/L. Table 1.1 summarizes RO boron removal data to date.

Table 1.1 Summary of Boron Removal by RO Membrane Processes

Author (Year)	Membrane Type	Feed Water	Experimental Conditions	Reported Rejection (concentration)
Mariñas (1991)	Cellulose acetate RO (Model not specified)	Tap water spiked with 5 mg/L boron	Pressure = 400 psi pH = 7.1~11.4 Temp = 28 ºC	<30~>99%
Magara et al. (1996)	Polyaromatic-amide (Model not specified)	Sea and brackish groundwater with 0.07~4.3 mg/L boron	Pressure = 40~65 kPa pH = 5~7.8 Temp = 20~35 ºC	43~78%
Magara et al. (1998)	NTR-70SWC-S8 ES10-D4	Various synthetic water spiked with 0.2~30 mg/L boron	Pressure = 5.7 MPa for NTR-70SWC-S8 and 0.5~1.0 MPa for ES10-D4 pH = 5.4~11Temp = 20~35 ºC	50~>99%
Prats et al. (2000)	Hydranautics 4040-LHA-CPA2 Toray SU-710 Toray SUL-G10	Brackish water	Feed flow rate per vessel < 60 L/min, pH = 5.5~10.5	39~100%
Taniguchi et al. (2001)	Toray UTC-80	Seawater	Temp = 25~30 ºC	0.4~1 mg/L
Rodrígez-Pastor et al. (2001)	Toray SUL-C10	Brackish water containing 4 mg/L boron	Feed flow rate per vessel < 50 L/min pH = 3~10	40~100%
Glueckstern et al. (2003)	SWRO membrane (not specified in the manuscript)	Seawater containing 5~6 mg/L boron	pH = 7~8 Temp = 25~30 ºC	76~90%
Redondo et al. (2003)	FILMTEC SW30HR-380 FILMTEC SW30HR-320 FILMTEC SW30-380 FILMTEC BW30-400 FILMTEC BW30LE-440	not clearly stated	Pressure = 10.7~55 bar pH = 6~12 Temp = 25 ºC	88~92% (pH=8) 88~92% (pH=8) 85~90% (pH=8) 55~75% (pH=8) 43~63% (pH=8)

Previous studies have shown that boron rejection by RO membranes improves as pH increases (i.e., as major species shift toward increasingly deprotonated forms), as operating temperature decreases, and as transmembrane pressure increases (Magara et al., 1996; Prats et al., 2000; Glueckstern and Priel, 2003; Busch et al., 2003). Considering the wide range of reported boron rejection by RO membranes (table 1.1), it is apparent that boron removal performance is significantly impacted by the physical and chemical characteristics of a given RO membrane. Figure 1.1 shows the symmetric structure of boric acid as well as a size comparison of major species of interest. Boric acid is uncharged and has trigonal structure. Therefore, boric acid is nonpolar, which causes it to interact very differently with membrane materials relative to charged salt ions and polar water molecules. RO membranes that permit high boron rejection along with high salt rejection and high water permeation might be manufactured through careful consideration of physical structure and chemical composition.

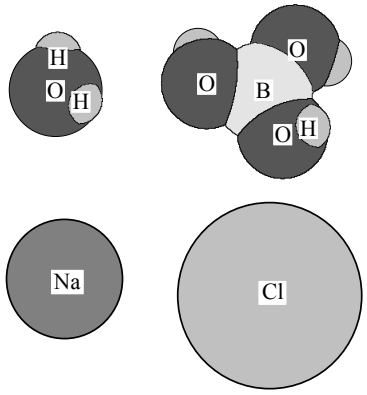

Figure 1.1 Computer rendering of a water molecule, boric acid, sodium ion, and chloride ion with actual size comparison.

Recently, the use of boron-specific ion exchange (IX) resins to polish RO treated water has been studied (Popat et al., 1988; Badruk et al., 1999a, 1999b; Nadav, 1999). Multi stage RO processes with pH adjustment have also been investigated (Magara et al., 1998; Pastor et al., 2001). These studies indicated that target boron concentrations could be achieved by using an IX or RO polishing step. However, adding treatment stages results in higher treatment costs, which could be a limiting factor for many utilities.

2. Conclusions and Recommendations

1. Surface analyses showed that all membranes tested had a negative surface charge and a ridge and valley structure. The negative charge of the membrane played an important role in boron removal, since charge repulsion is one of the important mechanisms of boron rejection. No relationship was found between solutes rejection and membrane surface roughness or hydrophilicity.

2. Bench-scale experiments performed with six commercialized RO membrane sheets showed that pH and temperature had substantial impact on boron rejection. At higher pH, boron rejection increased significantly, which was likely due to the enhanced charge repulsion from the dissociation of boric acid. Boron rejection was directly proportional to water temperature.

3. The Spiegler-Kedem model was combined with the film theory and applied to explain the boron rejection. Three parameters (mass transfer coefficient (k), overall permeability constant of boron ($P_{s,B}$), and reflection coefficient of boron (σ_B) in the model were successfully estimated from nonlinear optimization. The model with estimated parameters could accurately predict the boron transport through (rejection by) different SWRO membranes at various pressure, temperature, and pH conditions.

4. The overall permeability constant and reflection coefficient of boron were largely dependent on pH and temperature. Equations were developed to predict the effect of temperature and pH on the overall permeability constants and the effect of pH on the reflection coefficients.

5. Boron rejection was compared with the rejection of other ionic species, including sodium (Na^+), chloride (Cl^-), magnesium (Mg^{2+}), calcium (Ca^{2+}), and sulfate (SO_4^{2+}). While the observed transport behaviors of these ionic species were consistent with the current understanding of RO processes, they did not show any meaningful relationship with respect to the transport of boric acid or borate. This suggests that it would not be possible to estimate the level of boron rejection from other readily measurable parameters for SWRO membranes.

6. Analysis of the feed, permeate ,and concentrate from nine RO plants for seawater and brackish water treatment suggested that while most ionic species generally showed > 99% removal, rejection of boron was between 65 and 85% and largely dependent on membrane type, operating condition, and sampling location in the membrane vessel (brine side and feed side). Consistent with the bench-scale experiment, the rejection of boron showed a different rejection tendency relative to other solutes.

7. Based on the permeate boron concentrations, no seawater treatment plant could produce permeates to meet the current WHO guidelines of 0.5 mg/L, even though two brackish water treatment facilities could meet the guidelines since boron concentration in the feed was low. However, most of the plants were in compliance with the California Department of Health Services action level of 1 mg/L.

8. Boron rejection performance observed during bench-scale testing did not correlate well with the rejection performance observed in the full- or pilot-scale plants. This was mainly due to the higher recoveries used at the full- or pilot-scale plants. Accurate extrapolation of bench-scale boron rejection data to full- or pilot-scale boron rejection performance requires mathematical models that factor nonhomogenous conditions along the membrane element (Mi et al., 2005). Some of the modeling equations developed during this study can serve as a basis for such models.

9. Cost estimates suggest that a single-pass RO system (configuration 1), which could produce 1.2 parts per million (ppm) permeate boron concentration from the seawater with feed boron concentration of 5 ppm, would cost approximately \$0.518 per cubic meter (\$/m^3) or \$1.96 per thousand gallons (\$/1,000 gal) water production. Detailed cost estimation methods are provided later in this report.

10. A single-pass RO system with increased feed pH (configuration 2), a partial double-pass RO (configuration 3), and a single-pass RO system with IX polishing (configuration 4) could produce permeate containing <1 mg/L of boron, but configuration 2 cost \$0.520 /m^3 (\$1.96/1,000 gal) and was the most cost-effective option, with very slight increased water production cost from the configuration 1. To meet the provisional WHO boron guideline of 0.5 mg/L, double-pass RO with a concentrate recovery system was required. However, these configurations would be approximately 20 to 25% more expensive than other configurations.

11. The development of RO membranes with higher inherent boron rejection capabilities will be critical for establishing cost-effective treatment for boron removal.

3. Lab-Scale Evaluation of Boron Rejection

3.1 Overview

Bench-scale cross-flow filtration experiments were performed to evaluate boron transport through and rejection by commercial RO membranes. Six representative SWRO membranes obtained from four membrane manufacturers (Hydranautics, Saehan, Dow Filmtech, and Toray) were tested using feed water containing 10,500 mg/L sodium, 19,000 mg/L chloride, 1,350 mg/L magnesium, 450 mg/L calcium, and 2,700 mg/L sulfate (i.e., total dissolved solids [TDS] of 34,000 mg/L) which represented the average inorganic composition of seawater (Snoeyink and Jenkins, 1980). Five mg/L of boron as a boric acid was spiked to the water. Experiments were performed at different temperatures, raging from 15 to 35 degrees Celsius (^{o}C) and pHs ranging from 6.2 to 9.5. For each experimental condition, trans-membrane pressure (TMP) was gradually increased from 600 to 1,000 pounds per square inch (psi) to obtain the data required for modeling input. This model was applied to describe the transport mechanism of boron across RO membrane and to develop a tool to predict boron rejection under various operating conditions.

3.2 Materials and Methods

3.2.1 Membranes

Flat-sheet samples of six SWRO membranes were donated from four different membrane manufacturers. All samples were polyamide thin-film composite membranes. Salt rejection and permeate flux of selected membranes ranged from 99.6 to 99.8% and 15 to 22.5 gallons per square foot-day (gfd), respectively. Specifications of these membranes provided by the manufacturers are summarized in table 3.1. Note that SWC4+ from Hydranatics and TM820A from Toray are the membranes specifically developed for high boron rejection.

Table 3.1 Manufacturer's Specification of the SWRO Membranes

Maker	Saehan	Hydra-nautics	Dow (Filmtec)	Dow (Filmtec)	Toray	Toray
Model	SR	SWC4+	SW30 HR XLE	SW30 HR LE	TM820	TM820A
Material	Polyamide composite	Polyamide composite	Polyamide composite	Polyamide composite	Polyamide composite	Polyamide composite
Rejection[1]	99.6%	99.8%	99.7%	99.75%	99.75%	99.75%
Flux (gfd)[1 2]	15.79	17.1	22.5	18.75	16.5	15

[1] Test condition: 25 ^{o}C, 800 psi, 32,000 mg/L NaCl solution.
[2] Calculated based on the flux and area of the membrane module.

3.2.2 Membrane Surface Characterization

Surface charge of each membrane was determined by a Brookhaven BI-EKA Electro-Kinetic Analyzer (Brookhaven Instruments Corp., Worcestershire, United Kingdom) through streaming-potential measurements following a procedure described in the literature (Childress and Elimelech 2000). Ionic strength of the testing solution was maintained at 0.005 M using sodium chloride (NaCl). Solution pH was controlled at between 4 and 10 by adding hydrochloride (HCl) and sodium hydroxide (NaOH). To measure Atomic Force Microscopy (AFM), Scanning Electron Microscopy (SEM), and contact angle, samples were prepared by drying the membranes in a 35 °C oven for over 12 hours. Membrane surface roughness was analyzed using an Autoprobe M5 (PSIA, Sungnam, Korea) scanning probe microscope equipped with a silicon nitride cantilever (PSIA model UL06C, Sungnam, Korea). The scanning resolution of the membrane surface was 10 micrometers (μm) × 10 μm. Scanned data was processed by Proscan image processing program (PSIA, Sungnam, Korea) to obtain parameters related to the surface roughness such as root mean square roughness, average roughness, and surface area. Image of membrane surface was obtained by a Jeol Corp. Model JSM840 Scanning Electron Microscope (SEM) (Peabody, Massachusetts) at magnifications of 5,000 and 20,000. A cross-section image of each membrane was also analyzed at 200X and 2,000X magnifications. Samples for cross section measurement were prepared by drying the membranes in a 35 °C oven for over 12 hours. After carefully cutting the membranes in liquid nitrogen, cross-section images were analyzed. Contact angle of the membrane surface was measured by a VCA Optima Contact Angle Analyzer (AST Products, Inc., Billerica, Massachusetts) using a sessile drop method. Contact angles of at least 10 different locations on each membrane coupon were analyzed and averaged.

3.2.3 Experimental Setup

A bench-scale membrane filtration test unit was constructed for this project (figure 3.1). The test unit was equipped with four plate-and-frame test cells (designed and provided by Saehan Industries, Inc. as an in-kind contribution) which enabled simultaneous comparison of up to four different membranes or quadruplicating the measurements for a single membrane. Two sets, with each set having two cells in series, were placed in parallel as shown in figure 3.2. The feed channel in each membrane cell was rectangular, 73 millimeters (mm) long, and 38 mm wide to provide an effective filtration area of 2.774×10^{-3} square meter (m^2). The feed flow channel height was 5 mm. Each cell had upper and lower stainless steel (SS)-316 plates with a flat-sheet membrane sandwiched in between, which was sealed with silicon rubber rings. Permeate could be collected through the membrane support to the permeate line located in the upper plate. Feed water stored in a 40-liter (L) polypropylene tank was circulated and pressurized through the cells by a positive-displacement high-pressure pump (Hydra-Cell D10S,

Wanner Engineering, Minneapolis, Minnesota) (figure 3.1). This high-pressure pump can deliver 8.0 gallons per minute (gpm) of water at up to 1,200 psi discharge pressure.

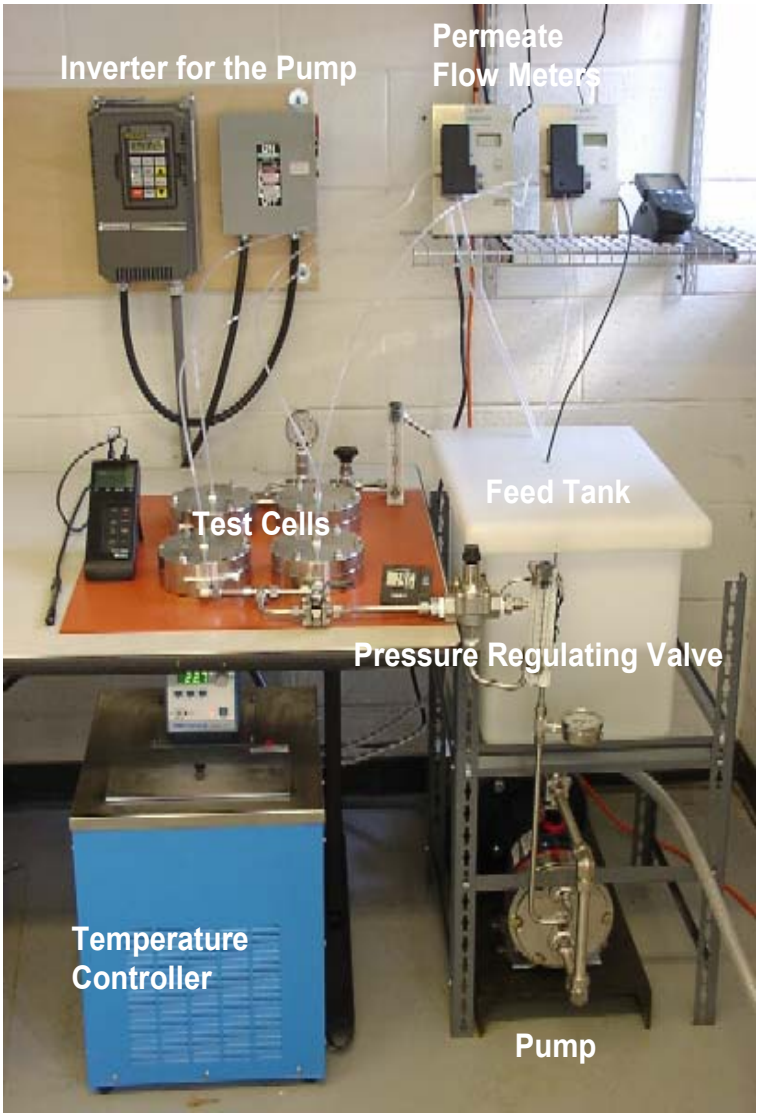

Figure 3.1 Photograph of the bench-scale filtration test unit.

Both retentate and permeate were returned to the cell to maintain a constant total solute concentration in the feed tank without a biocide. Feed pressure to the cell was controlled by a needle valve (Swagelok, Solon, OHIO) located downstream of the cells. To prevent the over-pressurization of the system, a safety valve (C22AB, Wanner Engineering, Minneapolis, Minnesota) was installed next to the pump outlet. This valve regulated the pressure by automatically bypassing a part of the feed flow, if the system pressure exceeded the preset level. Bypass and feed flow rate was measured by a hydraulic flow meter (Mcmaster, Atlanta, Georgia). Permeate flow rate from each cell was measured using an HFM 1000 Digital Flow Meter (Agilent, Palo Alto, California).

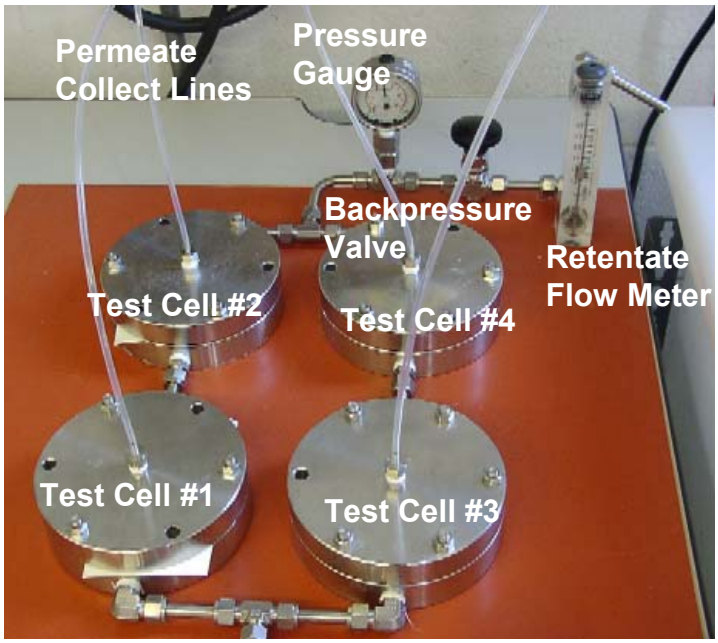

Figure 3.2 Photograph of test cells and their configurations.

Pressure was measured with analogue gauges (Swagelok, Solon, Ohio) located before and after the test cells. A temperature controller (Polystat, Cole parmer, Vernon Hills, Illinois) circulated the water through the heat-exchange coil immersed inside the feed tank. All experimental components were made of SS-316 and/or Teflon® to avoid corrosion. A schematic of the experimental setup is provided in figure 3.3.

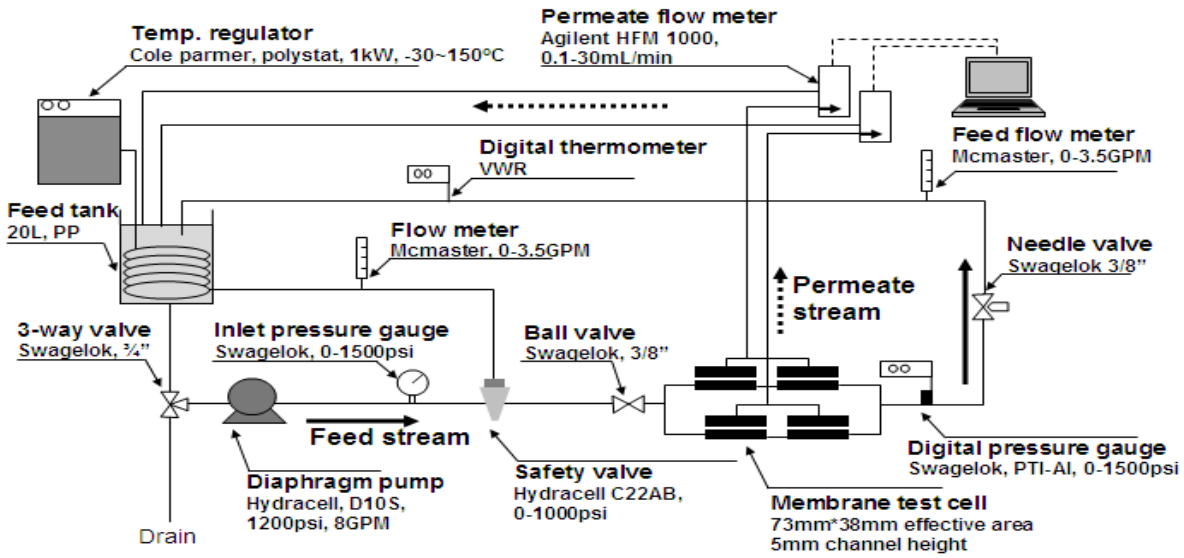

Figure 3.3 Schematic representation of bench-scale membrane filtration test unit.

3.2.4 Experimental Procedure

(1) Feed Solution Preparation

Synthetic seawater (total dissolved solids of 34,000 mg/L) containing 10,500 mg/L sodium, 19,000 mg/L chloride, 1,350 mg/L magnesium, 450 mg/L calcium, 2,700 mg/L sulfate, and 5 mg/L boron was prepared as follows. Stock Solution I was prepared by dissolving 587.62 grams (g) NaCl and 91.37 g magnesium sulfate ($MgSO_4$) and 175.52 g magnesium chloride ($MgCl_2$) in 3 L Milli-Q water (i.e., water purified by a Milli-Q Ultrapure Gradient Water System (Millipore, Billerica, Massachusetts) with resistance >20 μΩ/cm at 25 °C). To facilitate dissolution, 42.56 g calcium sulfate ($CaSO_4$) was separately dissolved in the 3 L Milli-Q water to prepare Stock Solution II. Stock Solution III was prepared by dissolving 0.63 g boric acid in the 100 mL Milli-Q water. These stock solutions were stored at 4 °C prior to the experiments.

(2) Membrane Preparation

Flat-sheet coupons of SWRO membranes with dimensions of 50 mm × 100 mm were cut from different locations on the membrane sheets. The membrane coupons were washed with overflowing deionized (DI) water for 10 minutes. After washing, the coupons were placed with skin side down in a closed container filled with Milli-Q water and stored for at least 24 hours at room temperature to remove contaminants or preservatives, which may exist on the membrane surface and inner matrix. Before being placed in the test cells, the coupons were rinsed with Milli-Q water.

(3) Filtration Experiment

Coupons of membrane were carefully placed on the lower plate of the membrane test cells with skin side down. After adding 10 L of Milli-Q water to the feed tank, the temperature regulator and high-pressure pump were switched on. A feed flow rate of 1.0 gpm, which corresponded to an average cross-flow velocity of 0.17 meters per second (m/s), was achieved by gradually increasing motor speed with an inverter motor drive. The system was gradually pressurized from 0 to 400 psi by closing a needle valve, while monitoring for any leakage or abnormality at every 100 psi increment. Solution I (3 L), solution II (3 L), and 4 L of Milli-Q water were then carefully added to the feed tank to reach total feed water volume of 20 L. The solution pH was then adjusted to 6.2 (or 7.5, 8.5, 9.5) by adding NaOH or HCl, while pH was monitored using a Thermo Orion 230+ pH meter (Waltham, Massachusetts). Note that the pH of the unadjusted solution was 6.2. The above process was developed to avoid any potential damage to the membrane samples due to a sudden development of osmotic pressure caused by any step addition of highly concentrated solutes. The target filtration pressure was gradually reached, and leak and abnormality monitoring was performed every 100 psi increment. Thirty minutes after startup, the conductivities of the feed water and the permeate from each cell were measured and used to calculate percent rejection. The flux was also measured by the digital flow meter. For

quality control purposes, experiments started only when the rejection and the flux of membranes were within the 0.5% and 10% of those specified by the manufacturer, respectively. If these criteria were not met, the membrane was replaced with another coupon. After 48 hours of operation to stabilize membrane performance, boric acid solution (solution III, 100 mL) was added to the feed tank. Operating conditions for the filtration experiments are summarized in table 3.2.

Table 3.2 Operation Conditions for the Bench-Scale Filtration Experiments

Feed volume	21.8 L
Flow rate	0. 5 gpm per cell/1.0 gpm overall
Cross-flow velocity	0.17 m/s
Operating pressure	600, 700, 800, 900, 1,000 psi
pH	6.2, 7.5, 8.5, 9.5
Temperature	15, 25[1], 35 °C

[1] Baseline condition

(4) Sampling and Data Acquisition

Sixty minutes after boron was spiked, water samples were collected. Before each sampling, the needle valve was regulated to adjust the target system pressure. A permeate tube was then placed into the sampling bottle and 20 mL of permeate was collected from each membrane. Feed water samples were collected directly from the feed tank using a micropipette. To prevent leaching of boron from the glassware, polyethylene sample bottles were used. After analyzing the feed and permeate concentrations of the samples, solute passage was calculated as follows:

$$\text{Solute Passage } (\%) = C_p / C_f \times 100 = (1 - R_0) \times 100 \qquad (1)$$

where, C_p = solute concentration in the permeate side [ML-3]; C_f = solute concentration in the feed side [ML-3]; R0 = (C_f - C_p)/C_f = apparent rejection [dimensionless]; C_f= feed concentration [ML-3] and C_p = permeate concentration [ML-3].

3.2.5 Analytical Methods

(1) Boron and Metals Analysis

Concentrations of boron, sodium, calcium, and magnesium were measured using an Inductively Coupled Plasma Mass Spectrometer-Atomic Emission Spectroscopy (ICP-AES) (Model ICAP 61E Trace Analyzer, Thermo Jarrell Ash, Franklin, Massachusetts) equipped with an autosampler. Samples were introduced into a cross-flow nebulizer, contained within a room-temperature spray chamber, at a pump speed of 100 revolutions per minute. A sipper was used to induce the sample to the reactor. Prior to analysis, trace metal grade nitric acid was added to feed and permeate samples stored in polyethylene containers to meet

1% v/v of nitric acid concentration. For instrument calibration, standard solutions of each species were prepared using High-Purity Standards (Charleston, South Carolina) and Milli-Q water in polyethylene or polytetrafluoroethylene bottles. Analyses were performed six times for each sample and the average value was recorded.

(*2) Anion Analysis*
Concentrations of chloride and sulfate were measured using a Dionex DX-600 Ion Chromatography (IC) system (Sunnyvale, California) which consisted of a GP50 gradient pump, IonPac AG9 HC guard column, IonPac AS9 HC analytical column (4 mm x 250 mm), Anionic Atlas Electrolytic suppressor (AAES), and ED50 conductivity detector. Samples were injected by an AS50 autosampler. The flow rate of the 9.0 mm sodium carbonate (Na_2CO_3) eluent was 1.3 milliliters per minute (mL/min). Back pressure was adjusted to approximately 2,500 psi. Standard solutions of chloride and sulfate for instrument calibration were prepared using High-Purity Standards (Charleston, South Carolina) and Milli-Q water.

3.2.6 Method Detection Limit

The method detection limit (MDL) is a measure of the precision of replicate analyses of a low-concentration sample. The MDL for boron was determined by making seven injections of deionized water containing boron at a concentration of 10 micrograms per liter (µg/L), five times the estimated instrument detection limit. Using the concentrations calculated from the calibration curve, the MDL can be calculated as:

$$MDL = 3.14 \times S \quad (2)$$

where, 3.14 = student's *t* value for a 99% confidence level and a standard deviation estimate with *n*-1 degrees of freedom (*t* = 3.14 for seven replicates) and *S* = standard deviation of the seven replicate analyses. From the seven replicate injections of 10 µg/L boron standard solution, a standard deviation of 1.52 was obtained. Consequently, the MDL for boron was determined to be 4.73 µg/L. Note that this level was approximately two orders of magnitude lower than the provisional standard of 0.5 mg/L. MDLs of other ionic species were also measured using the same procedure as that used for boron. Table 3.3 shows the fortified concentration of each ion, standard deviation, and method detection limit of the ionic species analyzed during this experiment.

Table 3.3 Method Detection Limit of Ionic Species

	B	Na	Ca	Mg	Cl	SO_4
Fortified Concentration (mg/L)	0.01	1	0.02	0.04	0.01	0.01
Standard Deviation of Seven Measurement	0.00152	0.93913	0.00055	0.00307	0.00134	0.00096
Method Detection Limit (mg/L)	0.00473	2.94887	0.00173	0.00963	0.00421	0.00301

3.3 Model Development

3.3.1 Mathematical Models for Solute Rejection by RO Membranes

According to the nonequilibrium thermodynamic model developed by Spiegler and Kedem (1966), transport of water and solute across RO membranes can be expressed as follows:

$$J_v = -p_h\left(\frac{dP}{dx} - \sigma\frac{d\pi}{dx}\right) \tag{3}$$

$$J_s = -p_s\frac{dC}{dx} + (1-\sigma)J_v\overline{C} \tag{4}$$

where J_v = volumetric water flux (LT^{-1}); J_s = gravimetric solute flux ($ML^{-2}T^{-1}$); p_h = specific hydraulic permeability (T^{-1}); p_s = local solute permeability coefficient (L^2T^{-1}); P = hydraulic pressure ($ML^{-1}T^{-2}$); π = osmotic pressure ($ML^{-1}T^{-2}$); σ = reflection coefficient which indicates degree of solute/water coupling [dimensionless]; C = superficial aqueous-phase solute concentration which is assumed to be in equilibrium with concentration of solute in the membrane phase (ML^{-3}); and $\overline{C}$ = average solute concentration of feed and permeate side (ML^{-3}).

Equation (3) implies water permeation through the membrane is proportional to the difference between the applied hydraulic pressure and the osmotic pressure. Note that the effect of osmotic pressure is influenced by the reflection coefficient, which represents the extent of convective transport of solute coupled with solvent (water) through the membrane. The reflection coefficient approaches unity for an ideal membrane and zero for a porous membrane (i.e., no osmotic pressure). Equation (4) represents the transport of solutes through the membrane. The first term in the right hand side of equation (4) denotes the solute transport by diffusion, which is proportional to the concentration gradient. The second term represents the solute transport by convection, which is determined by the coupling between solute and water, water flux, and average concentration of solutes on feed and permeates side. When there is little or no coupling between the solute and water (i.e., $\sigma \approx 1$), solute transport by convection becomes negligible.

The concentration of solute near the membrane surface is different from that in the bulk phase due to concentration polarization, which is caused by the accumulation of solutes rejected by a membrane. The expression representing the transport of solutes in the concentration polarization layer can be derived from film theory:

$$\frac{C_m - C_p}{C_f - C_p} = \exp\left(\frac{J_v}{k}\right) \tag{5}$$

where C_f = feed concentration (ML^{-3}); C_p = permeate concentration (ML^{-3}); C_m = concentration at membrane surface (ML^{-3}); and k = mass transfer coefficient (LT^{-1}). Combining equations (4) and (5), the transport (rejection) of the solute through the membrane can be expressed as follows:

$$\frac{R_0}{1 - R_0} = \frac{C_f - C_p}{C_p} = \frac{\sigma}{1 - \sigma} \cdot \frac{1 - \exp(-J_v \cdot (1 - \sigma) / P_s)}{\exp(-J_v / k)} \tag{6}$$

where, R_o = apparent rejection (dimensionless); $P_s = p_s/\Delta x$ = overall permeability constant (LT^{-1}); Δx = distance from feed/membrane interface toward permeate/membrane interface across the membrane (L). Equation (6) has successfully described the transport of solutes through RO membranes in the past studies (Murthy and Gupta, 1997; Taniguchi and Kimura, 2000). In order to predict the performance of membranes from this model, it is necessary to determine the unknown parameters such as mass transfer coefficient (k), solute permeability coefficient (P_s) and reflection coefficient (σ) in equation (6). These parameters can be experimentally obtained by several methods briefly described in the following sections.

3.3.2 Estimation of Transport Parameters

Transport parameters (k, P_s, and σ) can be estimated by linearization of equation (6) under the assumption of no coupling (e.g., very high rejection) ($\sigma = 1$) and/or infinite mass transfer (e.g., ideally dilute solution) ($k = \infty$) (Urama and Marinas, 1997). However, such simplification might not be appropriate for solutes like boron that show moderate rejection by membranes and concentrated feed solution showing non-negligible concentration polarization.

Alternatively, all three parameters can be simultaneously evaluated by a nonlinear optimization of equation (6) with experimentally determined apparent rejection (R_0) and water flux (J_v) (Lee et al., 2004; Murthy and Gupta, 1997; Murthy and Gupta, 1999). Unfortunately, this method, depending on the numerical algorithm, could suffer from uncertainties in the accuracy (Lee et al., 2004) and the uniqueness of the solution.

The parameters can be obtained by combining nonlinear parameter estimation with the independent evaluation of mass transfer coefficient (k). To reduce the number of unknowns and eliminate possible uncertainties from the numerical estimation, one of the parameters, mass transfer coefficient k, can be experimentally measured. σ and P_s are then obtained by nonlinear optimization of equation (6) with experimentally measured apparent rejection (R_0) and water flux (J_v). This approach was employed in this research to determine the parameters in the Spiegler-Kedem model. The nonlinear optimization was performed using a curve-fitting tool box in Matlab with a trust region method, which proved to be successful in obtaining unique solutions (i.e., no local convergence). However, since the accuracy of the solution could be highly dependent on the accuracy of mass transfer coefficient evaluation, several different methods were evaluated and the results were compared in the subsequent section.

3.3.3 Evaluation of Mass Transfer Coefficient

A widely-adopted and well-established method to estimate mass transfer coefficients is based on the assumption that the reflection coefficient (σ) is very close to 1 (Taniguchi and Kimura, 2000). This assumption is valid for the case of rejection of most of the salts by SWRO membranes. However, boron rejection by SWRO membranes is typically much less than 100% and this assumption is not likely valid. Therefore, in this study, an indirect method using the following empirical equation was employed to calculate the mass transfer coefficient of boron based on that of salt, which was determined experimentally.

$$\frac{k_{Salt}}{k_{H_3BO_4}} = \left(\frac{D_{Salt}}{D_{H_3BO_4}} \right)^{\beta} \tag{7}$$

where D = molecular diffusion coefficient (L^2T^{-1}); $\beta = 2/3$ for a clean membrane or $\beta = 1$ for fouled membrane [dimensionless] (Urama and Marinas, 1997). Note that the boron in the boundary layer is undergoing the similar mixing condition (i.e., determined by channel configuration and flow rate) as salt ions and, under such a condition, mass transfer coefficient is proportional to molecular diffusion coefficient (Taniguchi et al., 2001; Winograd et al., 1973).

The following four methods were used to obtain mass transfer coefficients of salt.

(1) Flux variation method from film theory

Equation (5), which described the film theory, could be rearranged as follows (Nakao and Kimura, 1981):

$$\ln\left(\frac{1-R_0}{R_0} \right) = \ln\left(\frac{1-R}{R} \right) + \frac{J_v}{k} \tag{8}$$

where intrinsic rejection (R) is defined as

$$R = \frac{C_m - C_p}{C_m} \tag{9}$$

Using equation (8), k can be calculated from the linear plot of J_v versus $\ln[(1-R_0)/R_0]$. In order for the plot to be linear, however, the intrinsic rejection (hence the degree of concentration polarization) should be independent of the permeate flux, J_v, which is not necessarily true, especially when the feed solute concentration is relatively high.

(2) Flux variation method from Spiegler-Kedem model combined with film theory

Combining equations (4) and (5) and assuming σ is equal to one, the following equation could be developed (Sutzkover et al., 2000) and $1/k$ can be obtained from the slope of the linear plot of $\ln[J_v \cdot (1-R_0)/R_0]$ versus J_v:

$$\ln\left(J_v \cdot \frac{1-R_0}{R_0}\right) = \ln P_s + \frac{J_v}{k} \tag{10}$$

(3) Osmotic pressure method

Taniguchi and Kimura (2000) developed an alternative method to estimate k by deriving the following equation from equation (3):

$$J_v = L_p[\Delta P - \{\pi(C_m) - \pi(C_p)\}] \tag{11}$$

where, $L_p = p_h/\Delta x$ = hydraulic permeability (LT^{-1}) and Δx = membrane thickness (L). Note that σ was assumed to be unity considering the high rejection of salt by the SWRO membranes. Using equation (11), the filtration coefficient (L_p) is first calculated from pure water flux (i.e., $C_m = C_p = 0$) at a specific pressure. From another filtration experiment at the same pressure with water containing a known concentration of salt (C_f), the concentration of permeate (C_p) and solution flux (J_v) are measured. Since J_v, L_p, and C_p are known, the concentration at membrane wall (C_m) can be calculated from equation (11). Finally, the value of k can be calculated using equation (5).

(4) Measurement from the flux decrease induced by salinity

Sutzkover et al. (2000) suggested following equation to calculate k based on equations (3) and (5).

$$k = \frac{J_v(Salt)}{\ln\left[\frac{\Delta P}{\pi_f - \pi_p} \cdot \left(1 - \frac{J_v(Salt)}{J_v(H_2O)}\right)\right]} \tag{12}$$

Therefore, the mass transfer coefficient can be obtained by measuring the flux of pure water, $J_v(H_2O)$, and that of a salt solution, J_v(salt). Osmotic pressures of the feed (π_f) and the permeate (π_p) can be calculated from the measurement of salt concentration in the feed and the permeate. This method is conceptually identical to the osmotic pressure method described above, as both methods are based on equations (3) and (5).

3.3.4 Empirical Equations for the Seawater Properties

For modeling purposes, the following empirical equations were used to estimate the relevant properties of synthetic seawater (Sagiv and Semiat 2004; Taniguchi and Kimura 2000; Taniguchi et al. 2001):

$$\pi(c,t) = (0.6955 + 0.0025t) \times 10^8 \frac{c}{\rho} \tag{13}$$

$$\rho = 498.4m + \sqrt{248{,}400m^2 + 752.4mc} \quad (\text{where } m = 1.0069 - 2.757 \times 10^{-4} t) \tag{14}$$

$$D = 6.725 \times 10 - 6 \exp(0.1546 \times 10^{-3} c - \frac{2{,}513}{273.15 + t}) \tag{15}$$

$$\mu = 1.234 \times 10^{-6} \exp(0.00212c + \frac{1965}{273.15 + t}) \tag{16}$$

where π = osmotic pressure ($ML^{-1}T^{-2}$; Pa); c = concentration of salts (ML^{-3}; kg/m^3); t = temperature (T; ^oC); ρ = density (ML^{-3}; kg/m^3); D = diffusion coefficient of salt (L^2T^{-1}; m^2/s); μ = viscosity ($ML^{-1}T^{-1}$; Pa·s).

3.4 Results and Discussions

3.4.1 Surface Characterization

As will be discussed in subsequent sections, boron rejection varied greatly depending on the type of SWRO membranes used. To relate boron rejection to parameters that vary among membranes, surface characteristics of membranes were analyzed using several different, commonly used, analytical tools. In this project, surface charge, surface roughness, effective surface area, and contact angles were analyzed and images of membrane surfaces were obtained by AFM and SEM.

(1) Surface Charge

Surface charge of the SWRO membranes at pHs 4.0, 6.0, 8.0, and 10.0 and ionic strength of 0.005 are shown in figure 3.4. Generally, the surface charge of polyamide-based thin-film composite membranes is negative and decreases as pH

increases due to the dissociation of carboxylic functional groups at the membrane surface (Petersen 1993). All membranes tested were negatively charged for the range of pHs evaluated, but the absolute values of surface potentials varied greatly from -5 to -75 millivolts (mV).

The TM820A membrane had the most negative surface charge at low pHs, and the SWC4+ had the most negative surface charge at high pHs. The XLE membrane was the least negatively charged across the whole pH range. pH dependency of surface charge also varied greatly by the membranes. Surface charges of the LE, XLE, and TM820A membranes decreased slightly as pH increased, while those of the TM820 and SWC4+ membranes decreased substantially as pH increased. The surface charge of the SR membrane changed minimally with pH.

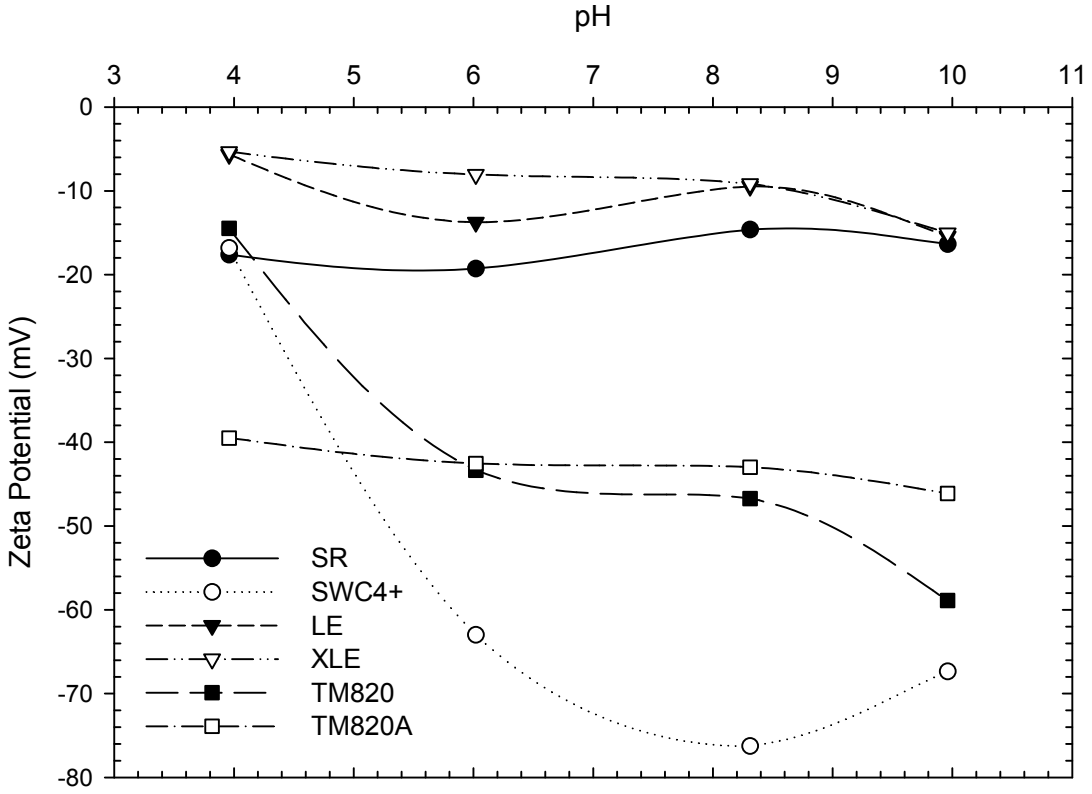

Figure 3.4 Surface charges of SWRO membranes at different pHs (I = 0.005, 25 °C).

(2) Atomic Forces Microscopy (AFM)

Images of the SWRO membrane surfaces analyzed by the AFM are presented in figure 3.5. All membranes showed a typical "ridge and valley" structure (Petersen, 1993) of polyamide membranes. Table 3.4 lists values for roughness and effective surface area for each membrane, as determined by AFM analysis.

The membranes showed diverse roughness values ranging from 36.77 to 80.45 nanometers (nm) and effective surface areas ranging from 124.2 to 143.3 μm. The TM820 membrane had the smoothest surface and the lowest surface area. The XLE membrane showed the roughest surface and highest membrane surface area.

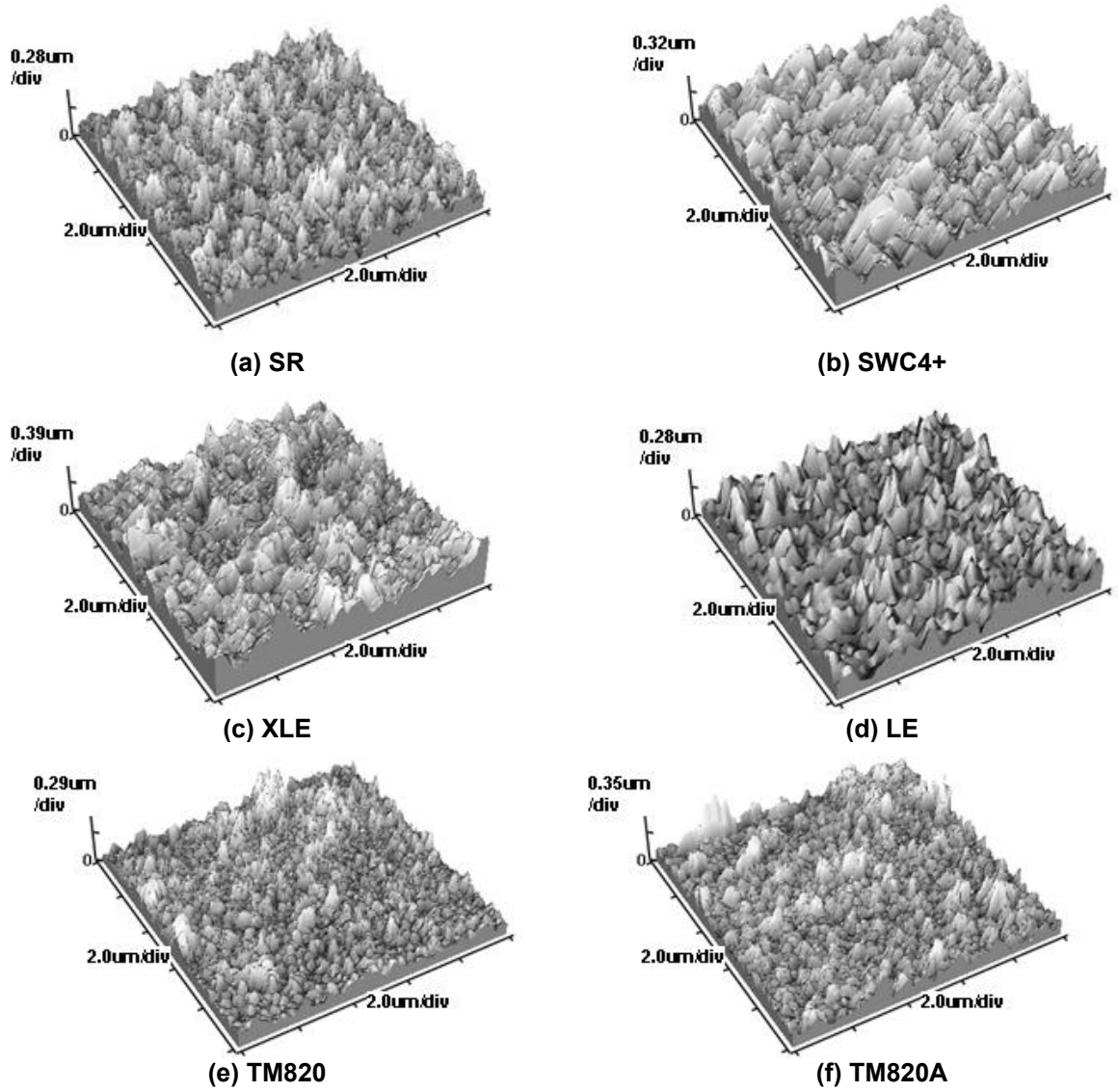

Figure 3.5 Microscopic surface image of the SWRO membranes analyzed by AFM.

Table 3.4 Roughness and Surface Area of the SWRO Membranes

	Roughness (nm)	Effective Surface Area[1] (μm^2)
SR	49.79	136.8
SWC4+	67.26	139.8
XLE	80.45	143.3
LE	60.65	137.8
TM820	36.77	124.2
TM820A	46.7	131.8

[1] Effective Surface Area: the area considering the roughness of the membrane surface.

(3) Scanning Electron Microscopy

Figure 3.6 shows images of membrane surfaces analyzed with 5,000X and 20,000X magnifications by the SEM. As confirmed by the AFM analysis, all membranes had the surface with ridge and valley structure typical of polyamide thin-film composite membranes. Also consistent with the quantitative analysis by the AFM, the SEM images indicated that the TM 820 and TM820A membranes had the smoothest surfaces and the XLE membrane had the roughest surface. Figure 3.7 shows the cross-section images of the membranes with 500X and 2,000X magnifications. The SWRO membranes consist of three layers: polyamide thin-film layer, polysulfone layer, and nonwoven fabric support layer (Petersen, 1993). Cross-section images show the layered structure of these membranes. Surface images with 500X magnification clearly showed the nonwoven fabric layer at the bottom, but it was difficult to distinguish the polyamide layer from the polysulfone layer even at high magnification.

(4) Contact Angle Measurement

Contact angles of membrane surfaces determined by the sessile drop method are presented in table 3.5. In the sessile drop method, a more hydrophilic surface shows a lower contact angle. All membranes, except the XLE and TM820A, showed similar hydrophilicity with contact angles ranging from 52.4^o and 60.6^o. The XLE membrane was the most hydrophilic with the lowest contact angle of 26.7^o followed by the TM820A membrane, which had a contact angle of 41.5^o.

Table 3.5 Contact Angle of the SWRO Membranes

Membrane	SR	SWC4+	XLE	LE	TM820	TM820A
Contact Angle	52.4^o	54.1^o	26.7^o	60.6^o	53.4^o	41.5^o

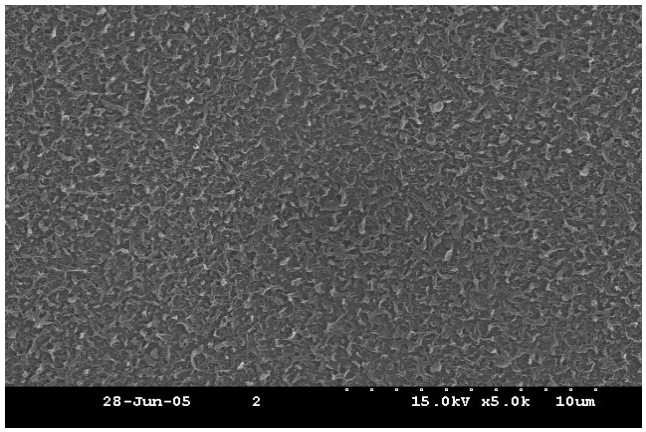

(a) SR 5,000X

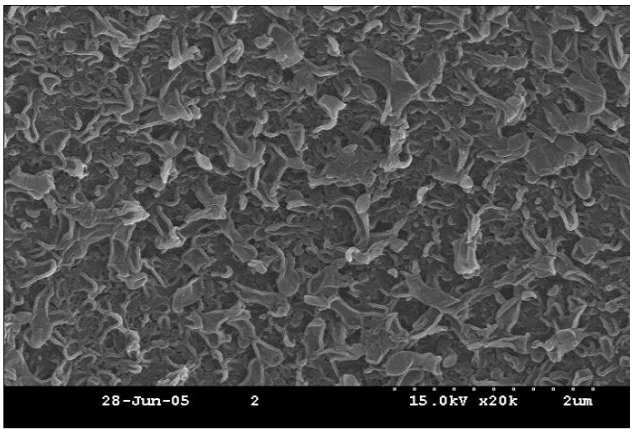

(b) SR 20,000X

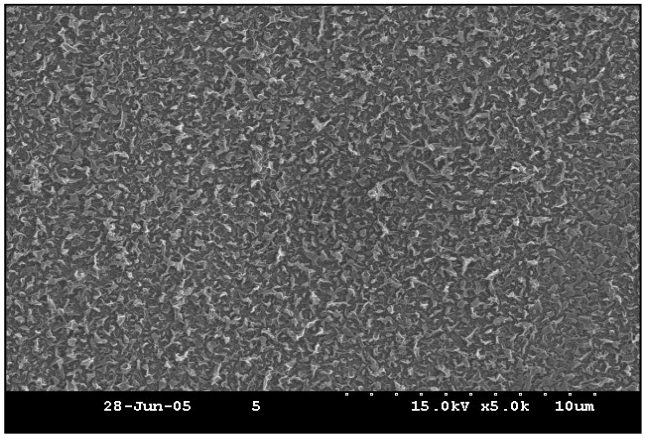

(c) SWC4+ 5,000X

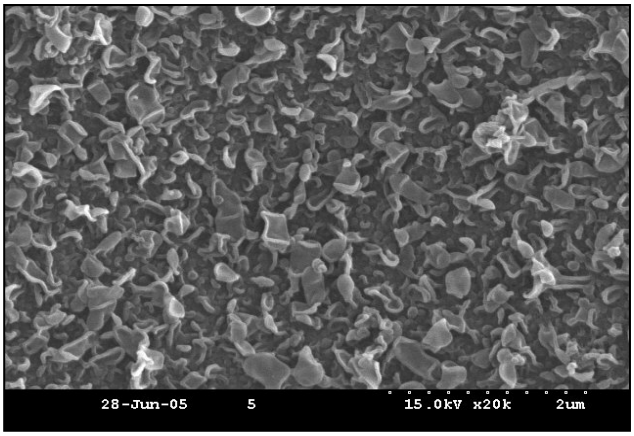

(d) SWC4+ 20,000X

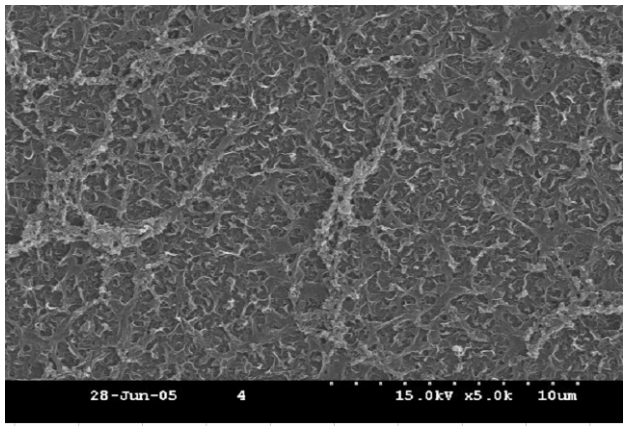

(e) XLE 5,000X

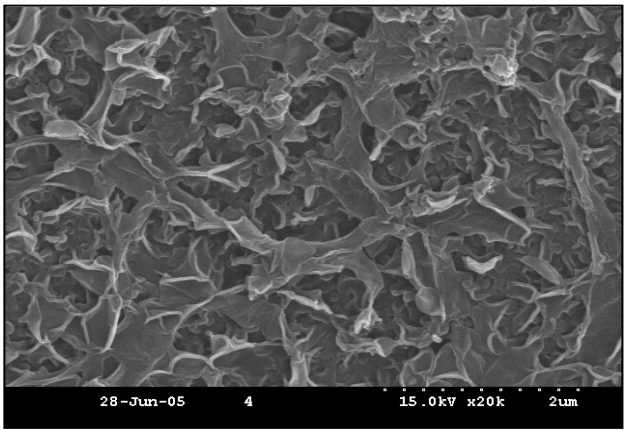

(f) XLE 20,000X

Figure 3.6 Microscopic surface image of the SWRO membranes analyzed by SEM.

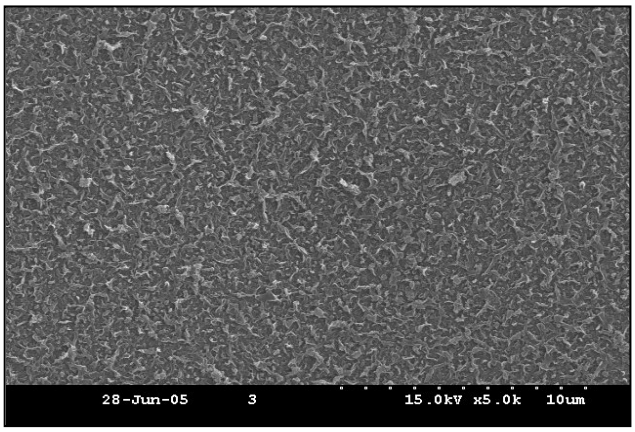

(g) LE 5,000X

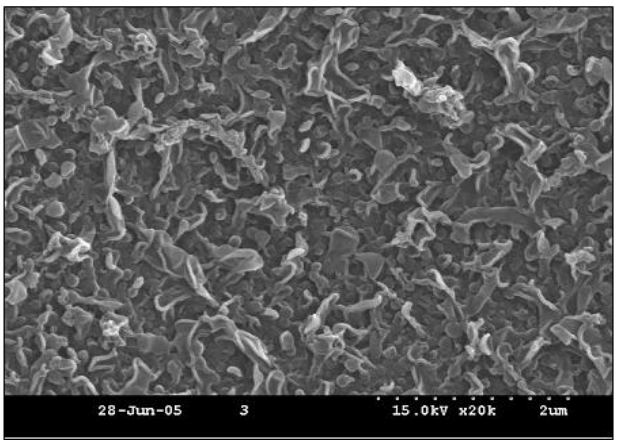

(h) LE 20,000X

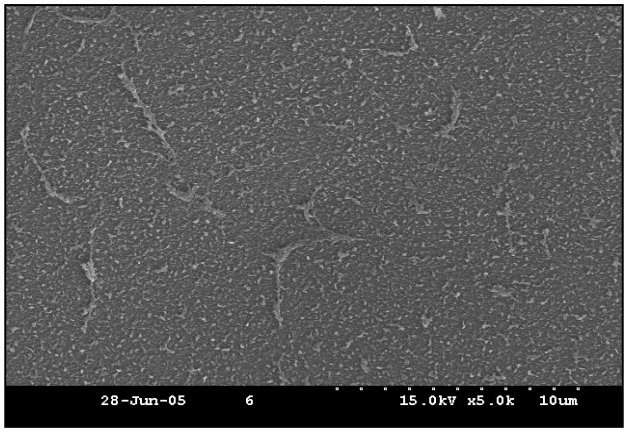

(i) TM820 5,000X

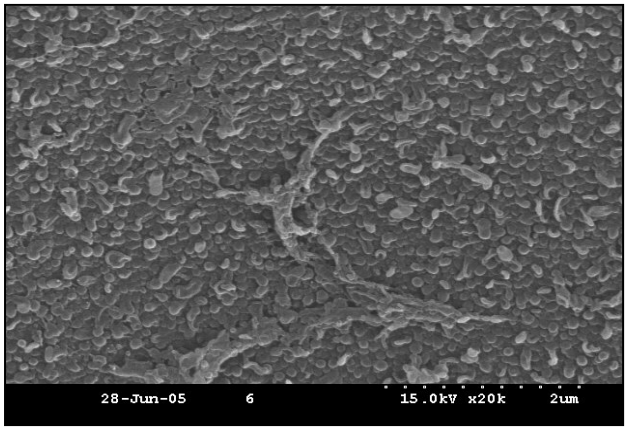

(j) TM820 20,000X

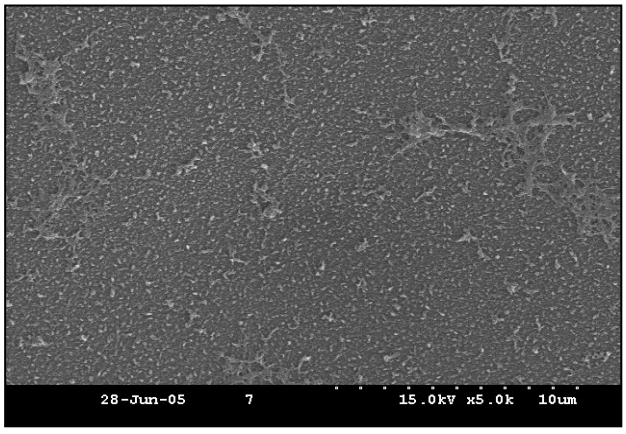

(k) TM820A 5,000X

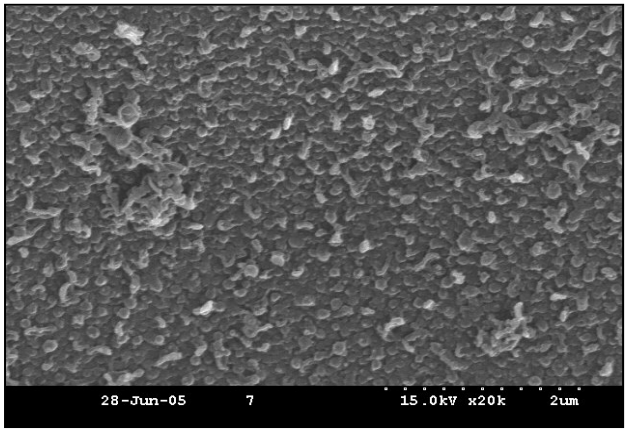

(l) TM820A 20,000X

Figure 3.6 Microscopic surface image of the SWRO membranes analyzed by SEM (continued).

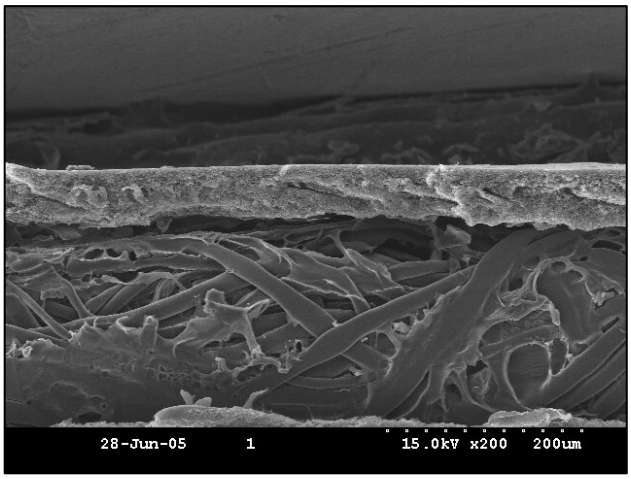

(a) SR 200X

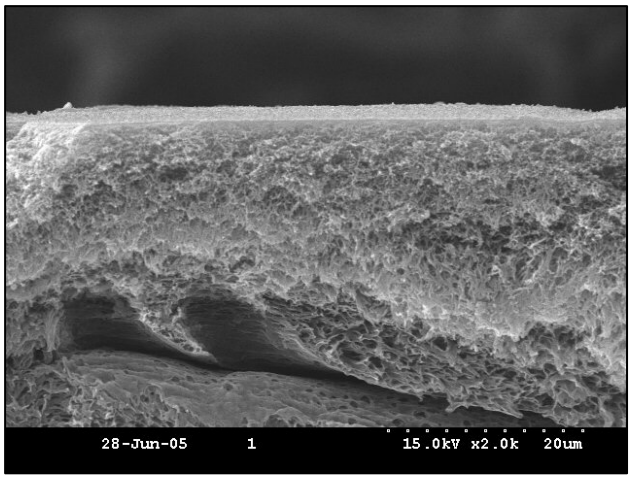

(b) SR 2,000X

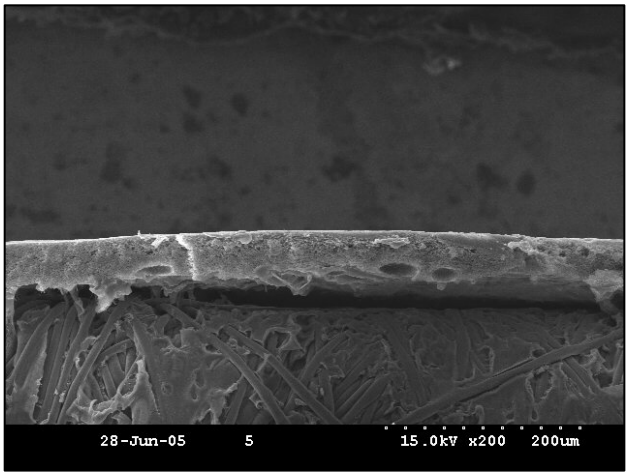

(c) SWC4+ 200X

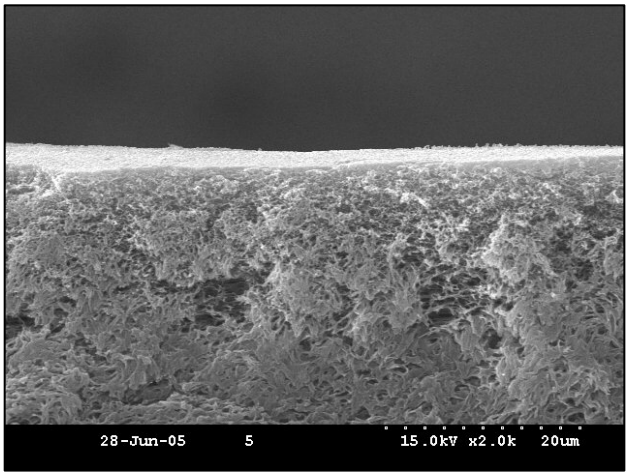

(d) SWC4+ 2,000X

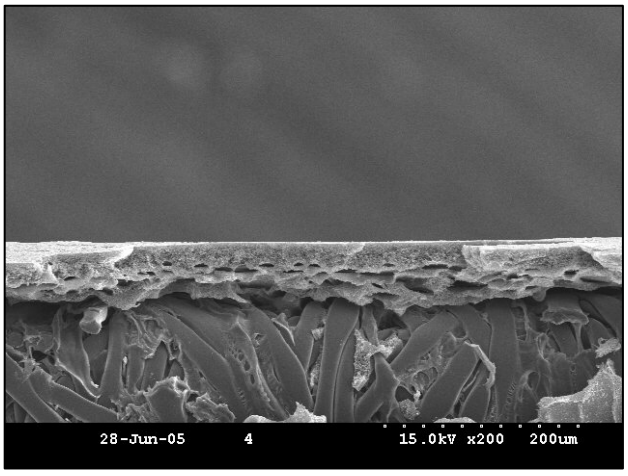

(e) XLE 200X

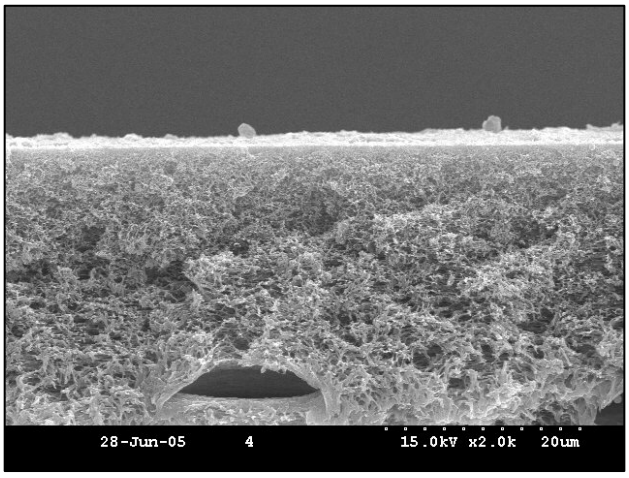

(f) XLE 2,000X

Figure 3.7 Microscopic cross-section images of the SWRO membranes analyzed by SEM.

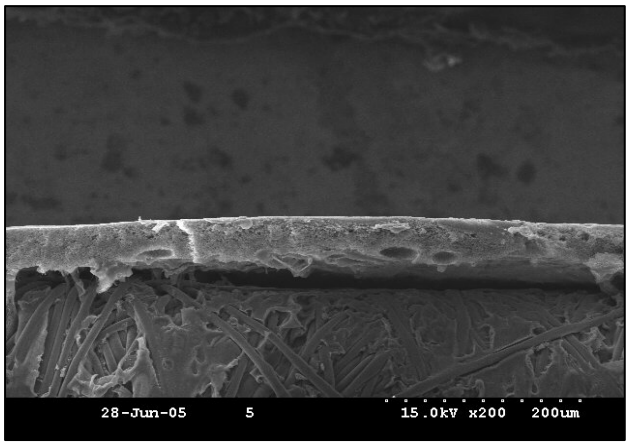

(g) LE 200X

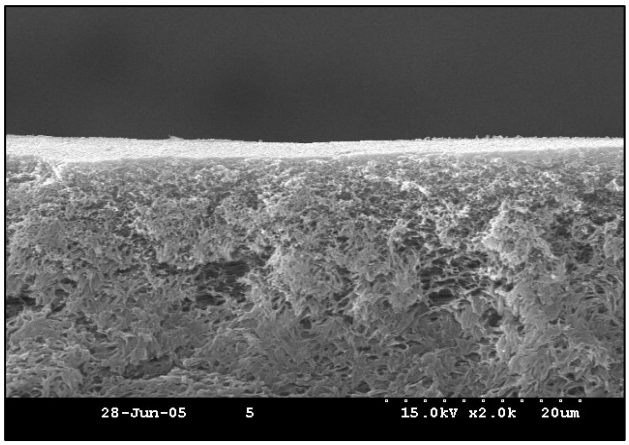

(h) 2,000X

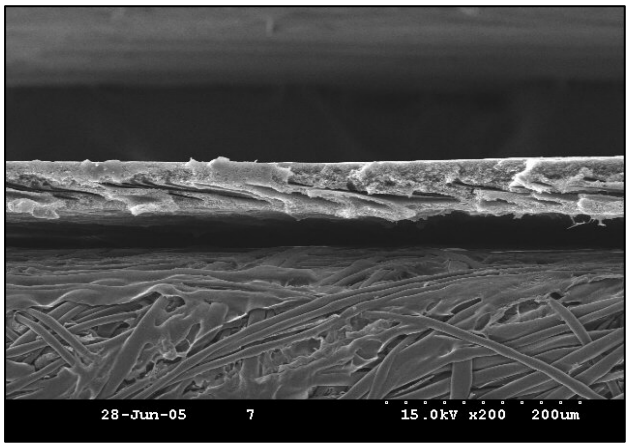

(i) TM820 200X

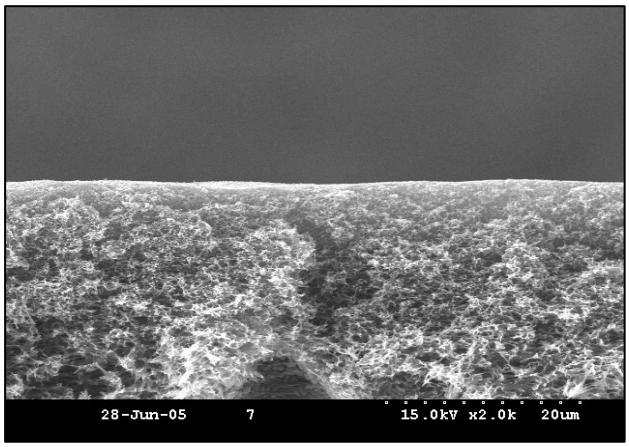

(j) TM820 2000X

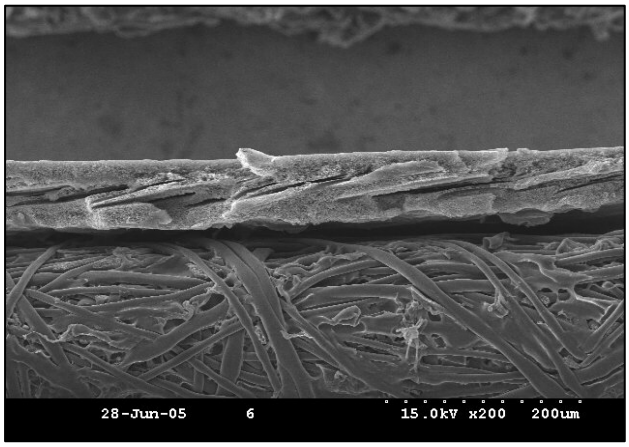

(k) TM820A 200X

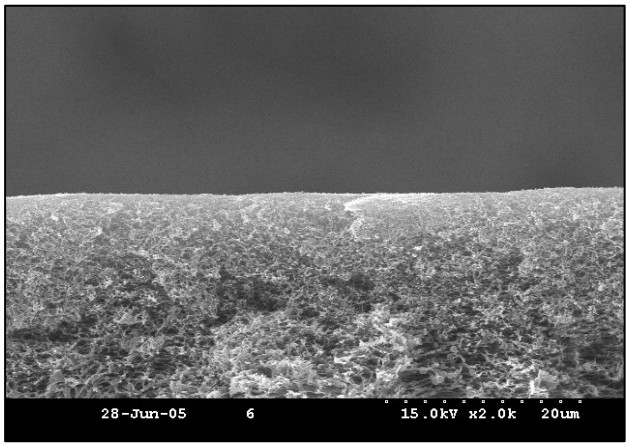

(l) TM820A 2,000X

Figure 3.7 Microscopic cross-section images of the SWRO membranes analyzed by SEM (continued).

3.4.2 Result of Filtration Experiment: pH Effect

Results of membrane filtration experiments followed an orthogonal experimental matrix of various pHs (6.5 to 9.5), and operating pressures (600 to 1,000 psi) are shown in figures 3.8 to 3.14 (later in this section). The effect of pH and pressure on membrane flux is shown in figure 3.8. For each membrane, flux was proportional to the operating pressure, but unrelated to pH. As pressure increased, the water flux increased in a nearly linear fashion for all membranes tested. This pressure dependence is consistent with equation (3) from the Spiegler-Kedem model. According to the equation, water flux increases proportionally to the difference between the applied pressure (P) and osmotic pressure (π). Osmotic pressure increases as pressure increases due to the increased degree of concentration polarization. However, the osmotic pressure increase might be small relative to the increase in applied pressure. It would be possible to calculate specific hydraulic permeability (p_h) by accounting for the osmotic pressure change (i.e., by combining equations (3), (5), and (13)). But such calculations were not performed since they did not serve the objectives of this project.

Figure 3.9 shows the effect of pressure and pH on the passage of boron. In contrast to other ionic species, which are discussed below, the passage of boron was highly dependent on solution pH. Boron passage decreased significantly as pH increased. For example, at an operating pressure of 600 psi, boron passage through SR membrane reduced from 21 to 7% when pH was increased from 6.2 to 9.5. At an operating pressure of 1,000 psi, boron passage decreased from 14 to 5% for the same pH change. The reduced boron passage at higher pH is likely explained by the increased charge repulsion between solute and membrane surface (Magara et al., 1998; Prats et al., 2000).

Boric acid is a weak acid with pK_{a1}' of 8.68 at 25 ^{o}C in high ionic strength solutions such as seawater (Stumm and Morgan, 1981). Note that K_{a1}' is the apparent first acid constant of boric acid and is defined as

$$K_{a1}' = \frac{[H_2BO_3^-]\{H^+\}}{[H_3BO_3]} \tag{17}$$

where, $[H_2BO_3^-]$ = borate concentration (ML^{-3}); $[H_3BO_3]$ = boric acid concentration (ML^{-3}), and $\{H^+\}$= activity of proton (ML^{-3}). Note that this equilibrium constant is defined using the *concentration* of a boron species and the *activity* of proton. Since boric acid is weak, the majority of boric acids exist as uncharged boric acid (H_3BO_3) in the natural pH range. However, as pH increases, the fraction of negatively-charged borates ($H_2BO_3^-$) increases, and when pH is above 8.68 (pK_{a1}'), borate ($H_2BO_3^-$) becomes the dominant species. As shown by the surface charge analysis presented above, membrane surface is negatively

charged over the whole pH range. Therefore, as pH increases, a charge repulsion between borate and a given membrane surface plays a critical role in hindering the transport of boron. The reduced passage of boron at higher pHs was quantitatively analyzed using the membrane transport model, which is described later in this report.

Boron passage was inversely proportional to operating pressure, which can be explained by the Spiegler-Kedem model and concentration polarization effect. The solute passage (or rejection) is determined by the ratio of solute transport rate and solvent transport rate across the membrane. As shown in figure 3.8 and as described by equation 3 of the Spiegler-Kedem model, increased operating pressure increases water flux. On the other hand, there is no explicit expression of pressure in equation 4 of the Spiegler-Kedem model, which explains the transport of solutes. However, increased pressure increases solute concentration in the concentration polarization layer, and the increased wall concentration (C_m) is expected to expedite the transport of solutes. A tradeoff between these two effects is likely to determine the effect of pressure on the rate of solute passage. Based on the experimental results, enhanced solvent flux might overwhelm increased solute transport, thereby decreasing boron passage (i.e., increasing boron rejection).

The effect of pH and pressure on the passage of sodium and chloride is shown in figures 3.10 and 3.11, respectively. pH did not appreciably affect the passage of sodium and chloride, which is likely explained by the fact that their charge is unaffected by pH. However, the sodium and chloride passage was reduced as operating pressure increased and appeared to follow a transport mechanism similar to that of boron.

Figures 3.12, 3.13, and 3.14 show the effect of pH and pressure on the passage of the divalent ions such as calcium, magnesium, and sulfate, respectively. Again, there was little change in solute passage with pH variation, which was also likely due to the fact that pH does not impact the charge of calcium, magnesium, or sulfate. Increased operating pressure caused a slight decrease or no change in the passage of ionic species. As described above, the effect of pressure on the transport of solutes could be decided by the tradeoff between increased solvent flux caused by increased pressure and enhanced solute transport caused by the increased ionic concentration at the membrane surface from concentration polarization. The slight or negligible pressure dependency of divalent ion transport might suggest that concentration polarization of divalent ions would be more significant than that of monovalent ion.

pH and pressure affected calcium, magnesium, and sulfate passage in a similar manner. The passage of ionic species is influenced by several factors, including water flux, concentration polarization, water-solute coupling, and ion paring.

Among them, ion paring might be mostly responsible for the observed similarity in the transport of divalent ions. When ionic species transport through a membrane, they move together with counter-ions (i.e., ions of opposite charge) to maintain electroneutrality (Marinas and Selleck, 1992). For instance, when sulfate passes through a membrane, it would associate and transport together with calcium or magnesium. Since ion paring effect is largely dependent on charge interaction, it is more pronounced in divalent or trivalent ions compared to monovalent ions.

TDS passage was not a function of pH (figure 3.15). Consistent with the above observations, TDS passage was inversely proportional to operating pressure for all membranes tested. Comparison of figure 3.11 and figure 3.15 suggests that the passage of chloride was very similar to that of TDS. This is reasonable given that chloride was the dominant ionic species in the synthetic seawater feed. Furthermore, lower rejection of chloride compared to other ionic species in the feed water also made chloride a major species in the permeate solution. Since chloride comprised the largest fraction of ionic species in both feed and permeate solutions, chloride passage would mirror TDS passage under various operating conditions. This implies that chloride passage can be estimated by TDS measurements without introducing significant error, and vice versa.

An effort was made to elucidate the apparent relationship between boron passage and the passage of other ions by plotting passage of boron versus passage of any one or all ions at different operating conditions for different membranes. However, no reasonable correlation was established (results not shown). Only portions of data that were obtained from the experiments performed at the same pH with different pressures showed an apparent linear relationship. The lack of a correlation suggests that no estimate of boron rejection by salt rejection can be made with confidence. This also suggests that transport of boron follows transport mechanism, which is different from those of the other ions. For example, even though TM820A membrane showed the lowest boron passage among the membranes, passage of the other salts such as sodium, calcium, magnesium, sulfate, and chloride through TM820A membrane was generally higher than TM820, SWC4+, and LE.

3.4.3 Result of Filtration Experiment: Temperature Effect

The results of membrane filtration experiments performed at 15, 25, and 35 ^{o}C at pH 6.2 and pH 9.5 are shown in figures 3.16 to 3.29. For each membrane except the SR and XLE membranes, the same coupons were used for all experiments. Different SR and XLE coupons were used for tests at different pHs and some deviations in the results obtained with these membranes might have resulted from the membrane to membrane variations. For figures 3.17 to 3.22, different vertical scales were used for better presentation.

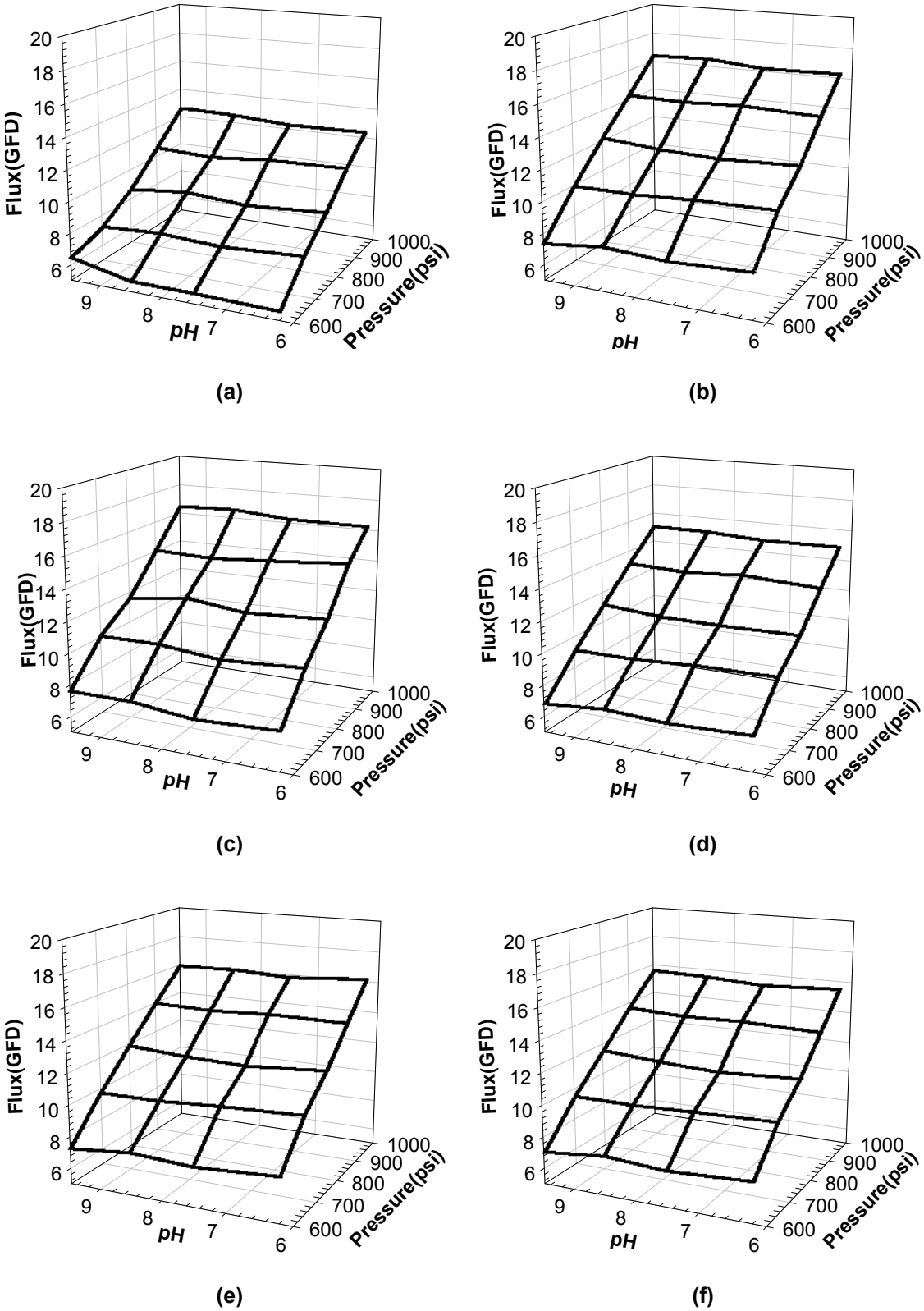

Figure 3.8 Effect of pH on membrane flux: (a)SR (b)SWC4+ (c)XLE (d)LE (e)TM820 (f)TM820A.

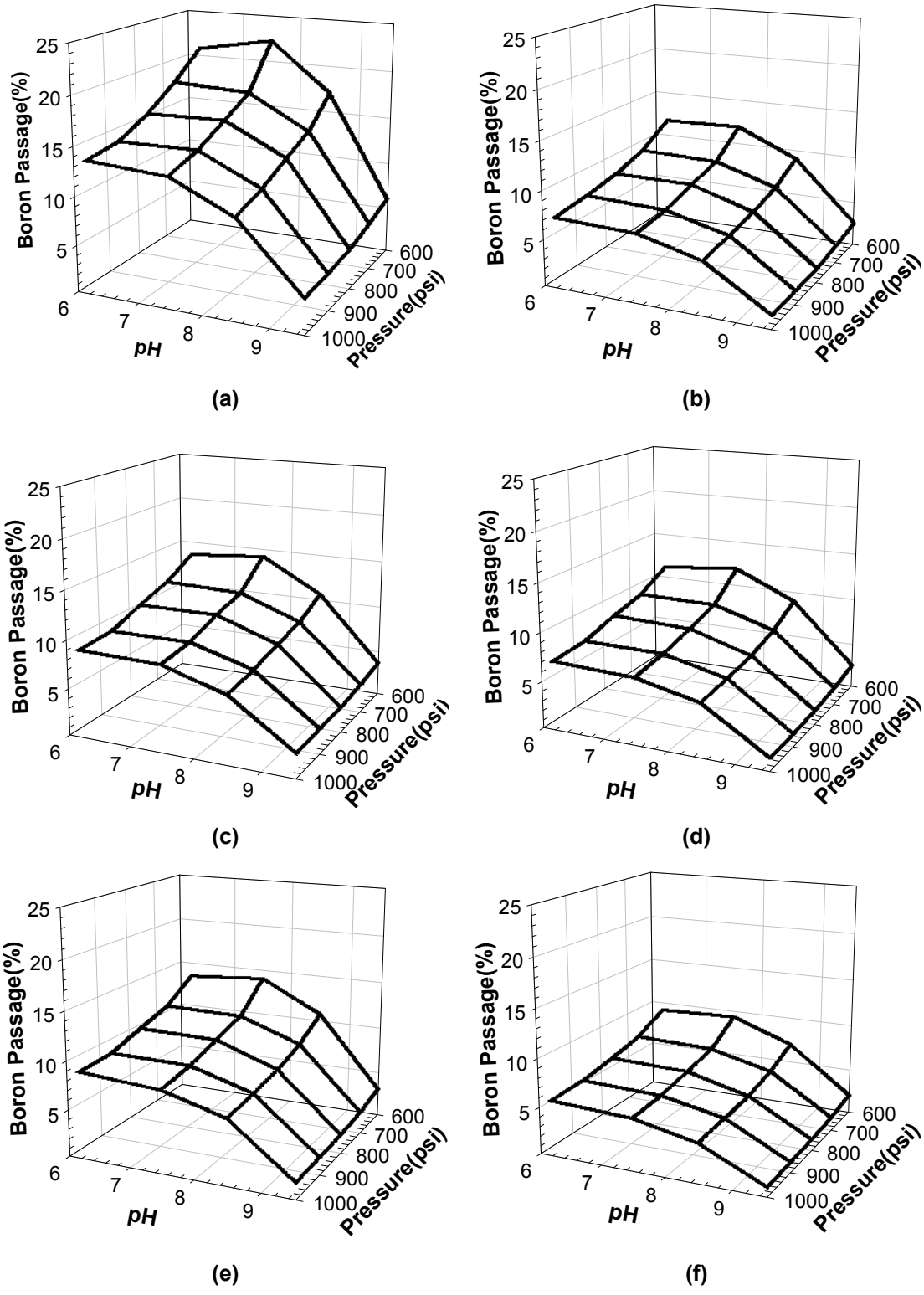

Figure 3.9 Effect of pH on boron passage: (a)SR (b)SWC4+ (c)XLE (d)LE (e)TM820 (f)TM820A.

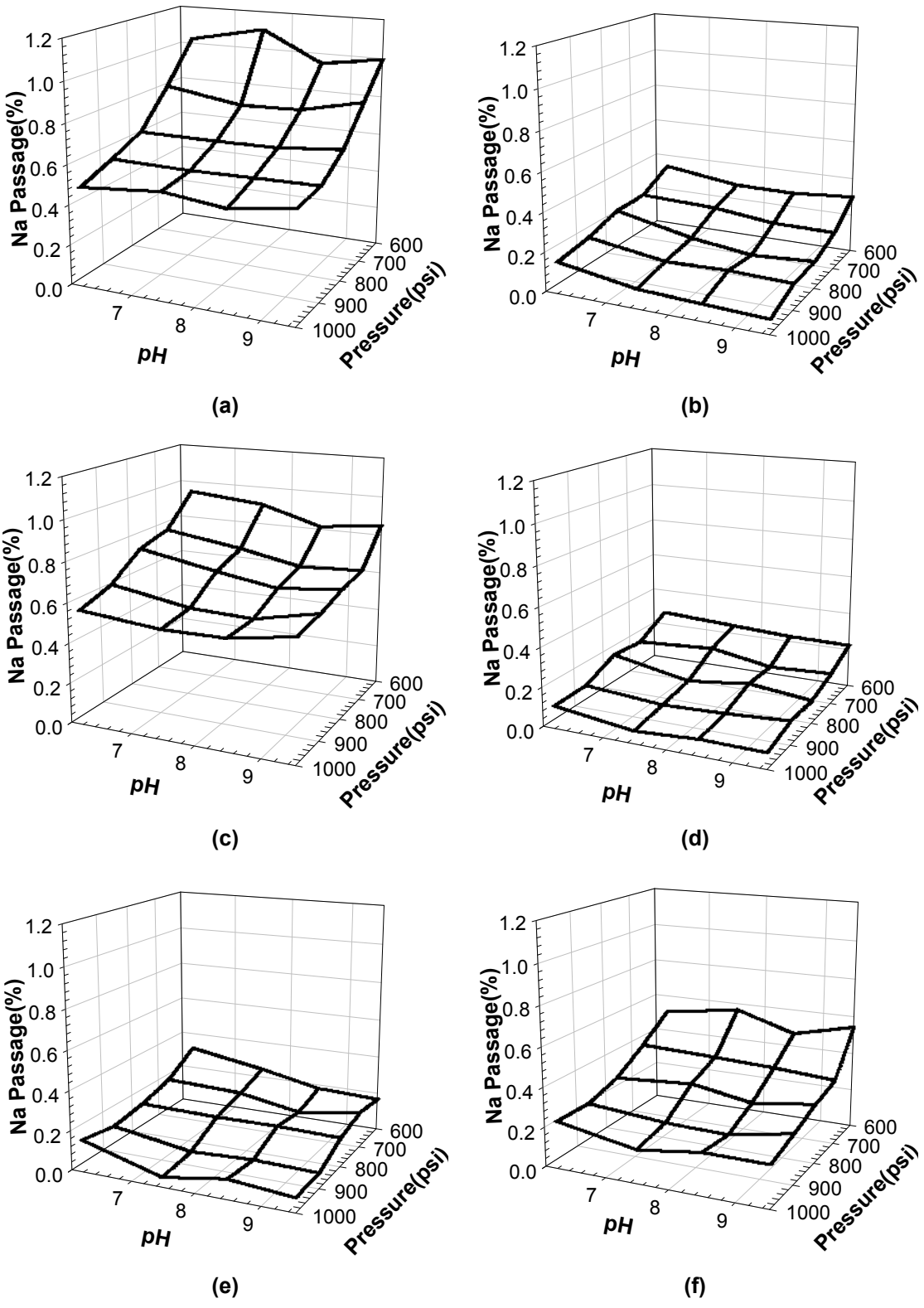

Figure 3.10 Effect of pH on Na passage: (a)SR (b)SWC4+ (c)XLE (d)LE (e)TM820 (f)TM820A.

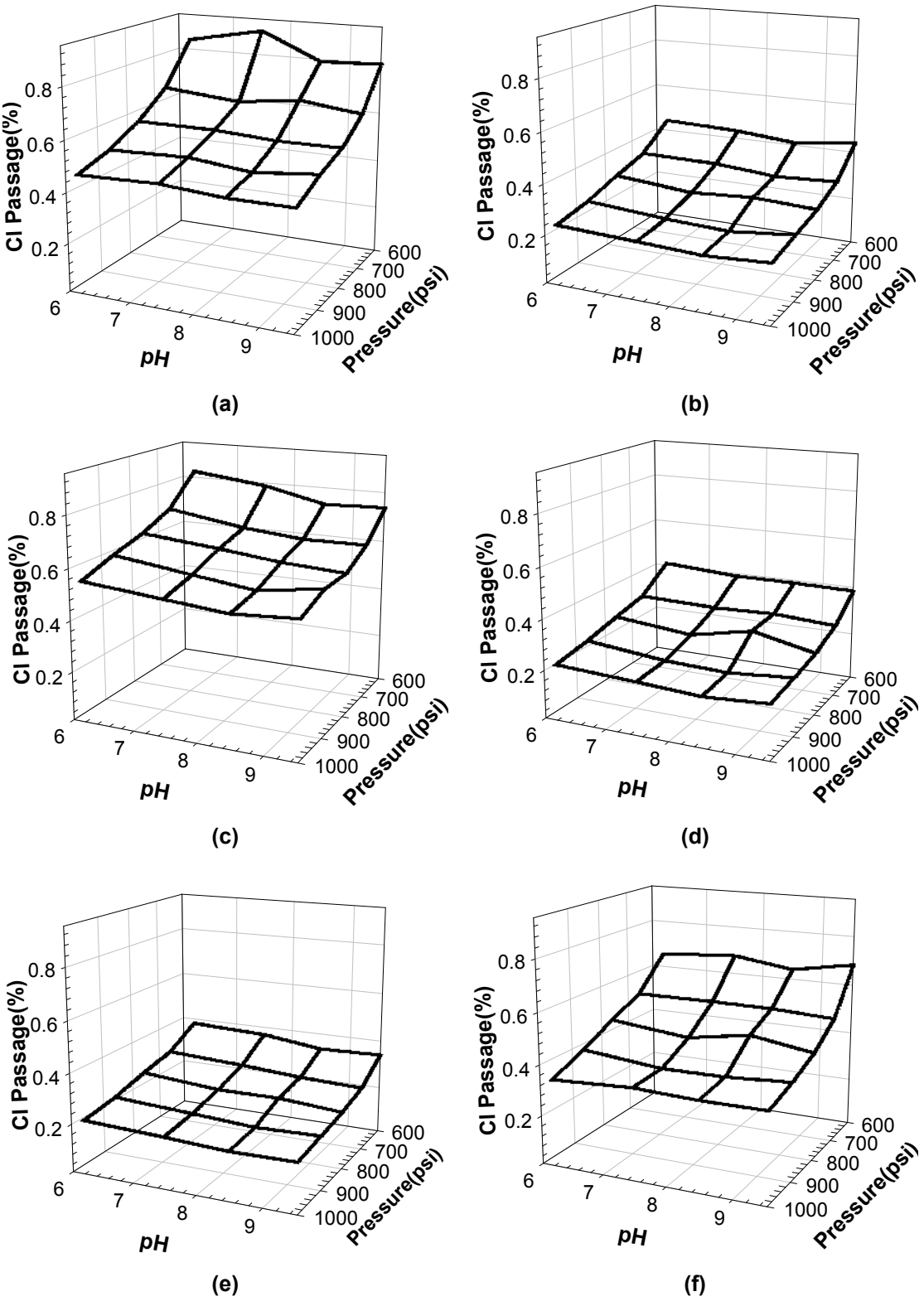

Figure 3.11 Effect of pH on Cl passage: (a)SR (b)SWC4+ (c)XLE (d)LE (e)TM820 (f)TM820A.

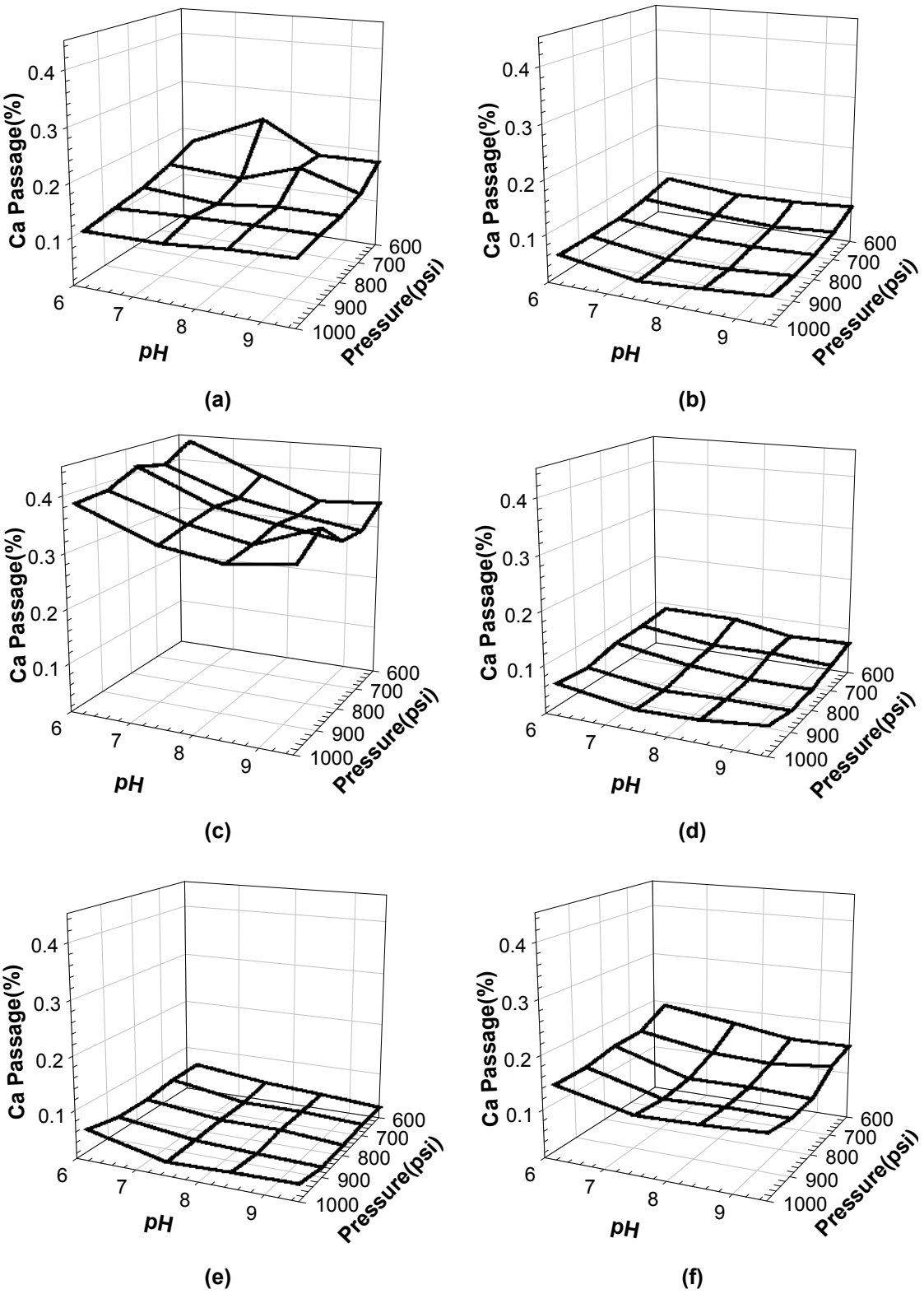

Figure 3.12 Effect of pH on Ca passage: (a)SR (b)SWC4+ (c)XLE (d)LE (e)TM820 (f)TM820A.

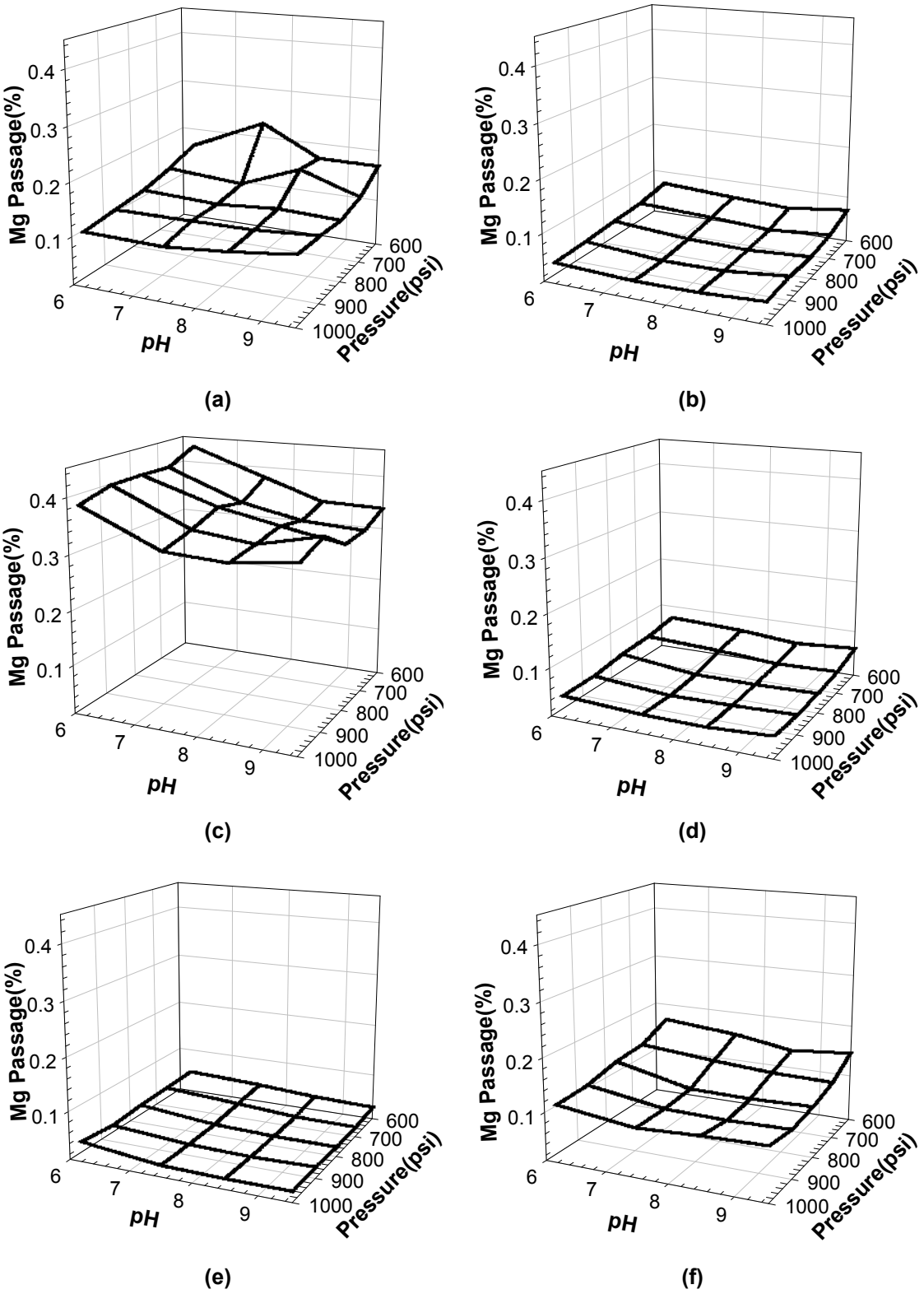

Figure 3.13 Effect of pH on Mg passage: (a)SR (b)SWC4+ (c)XLE (d)LE (e)TM820 (f)TM820A.

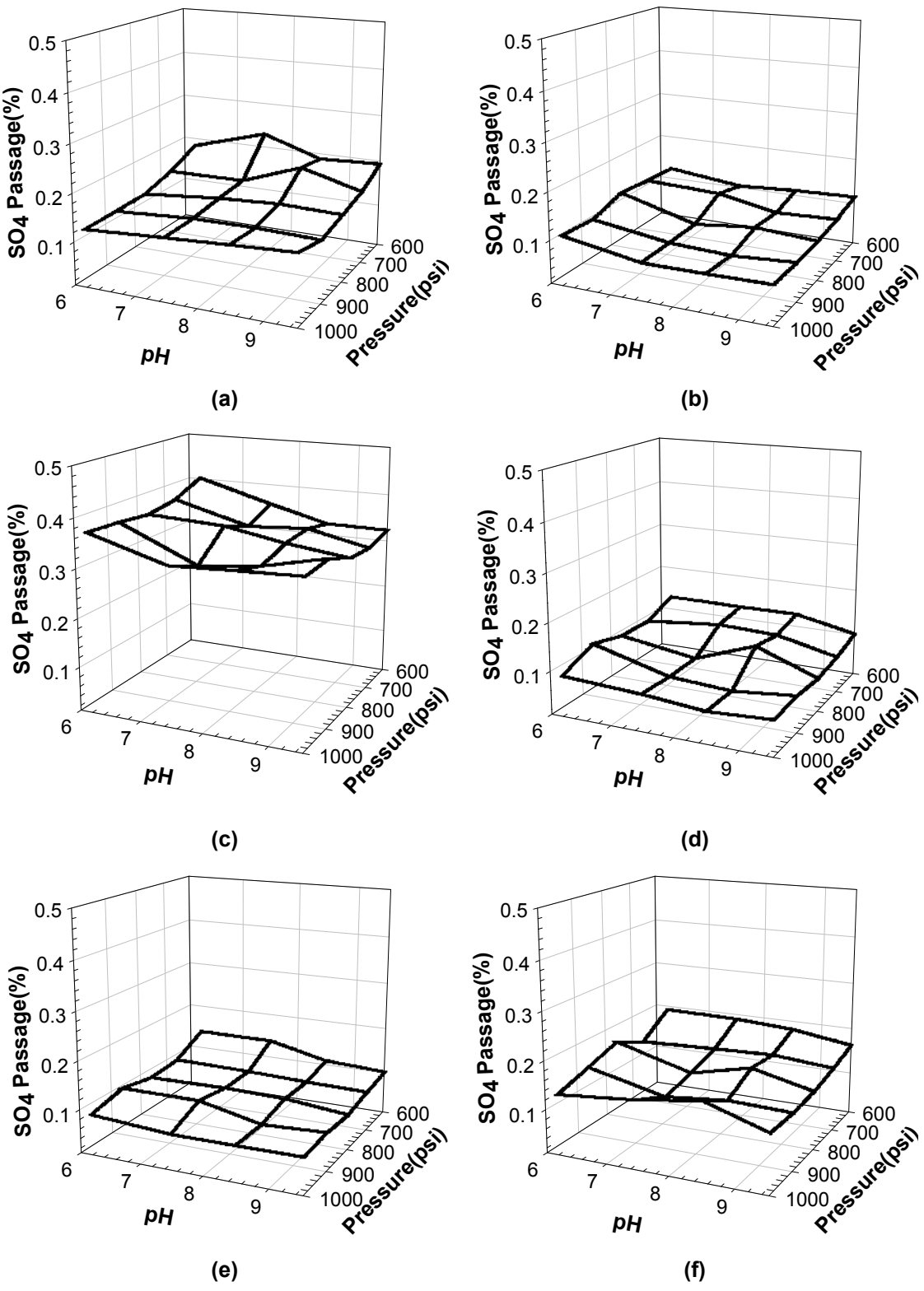

Figure 3.14 Effect of pH on SO4 passage: (a)SR (b)SWC4+ (c)XLE (d)LE (e)TM820 (f)TM820A.

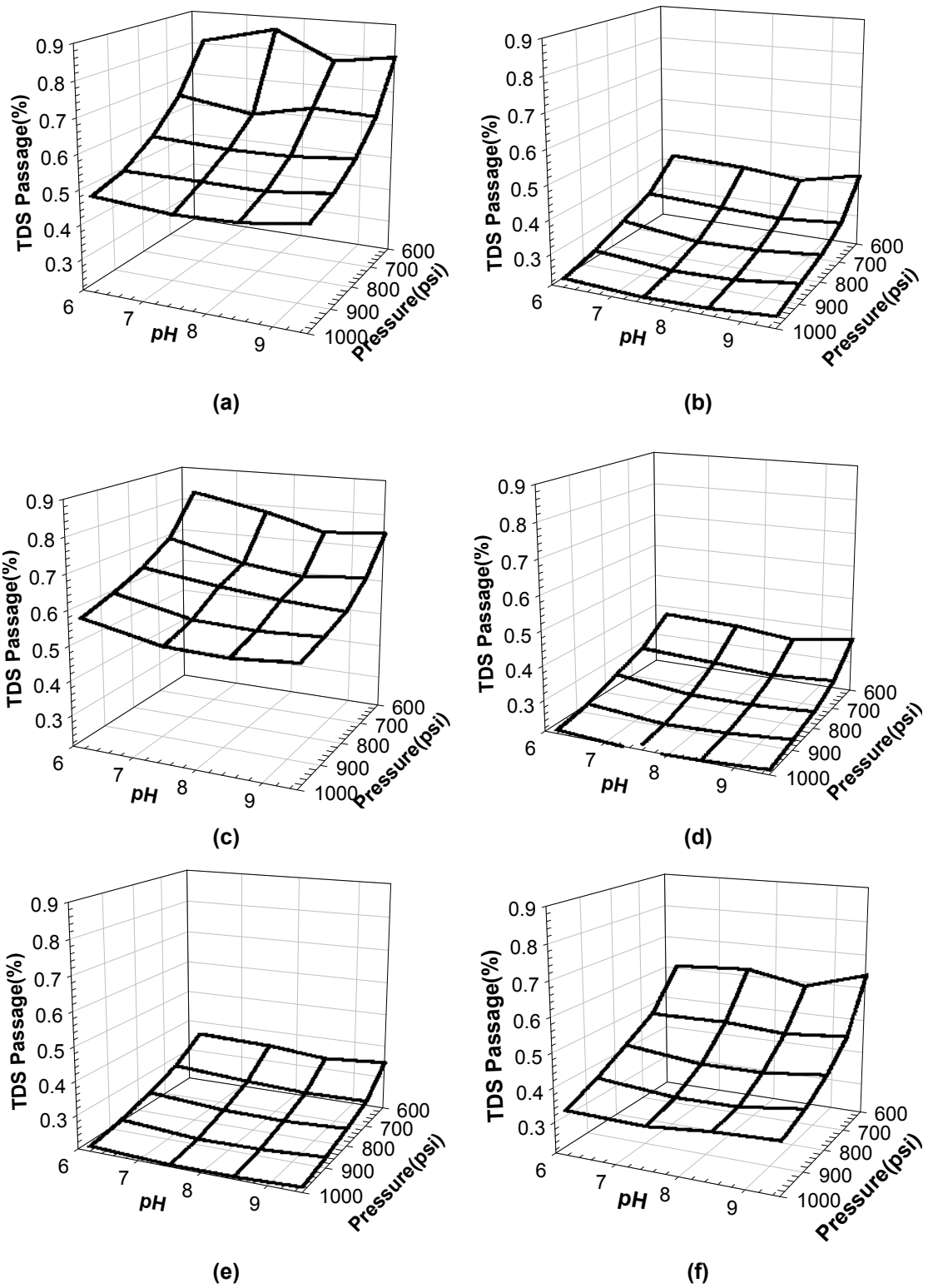

Figure 3.15 Effect of pH on TDS passage: (a)SR (b)SWC4+ (c)XLE (d)LE (e)TM820 (f)TM820A.

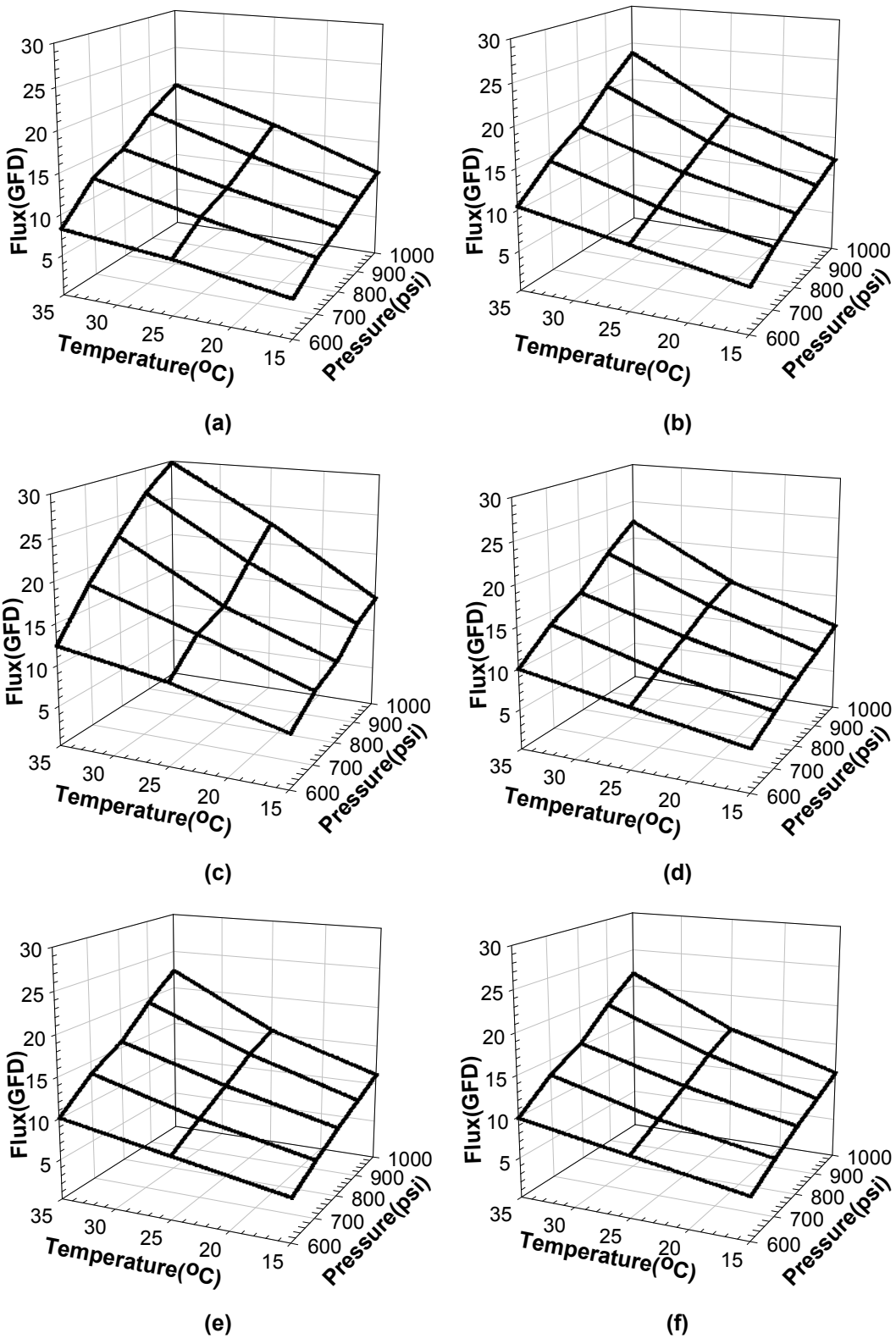

Figure 3.16 Effect of temperature on membrane flux at pH 6.2: (a)SR (b)SWC4+ (c)XLE (d)LE (e)TM820 (f)TM820A.

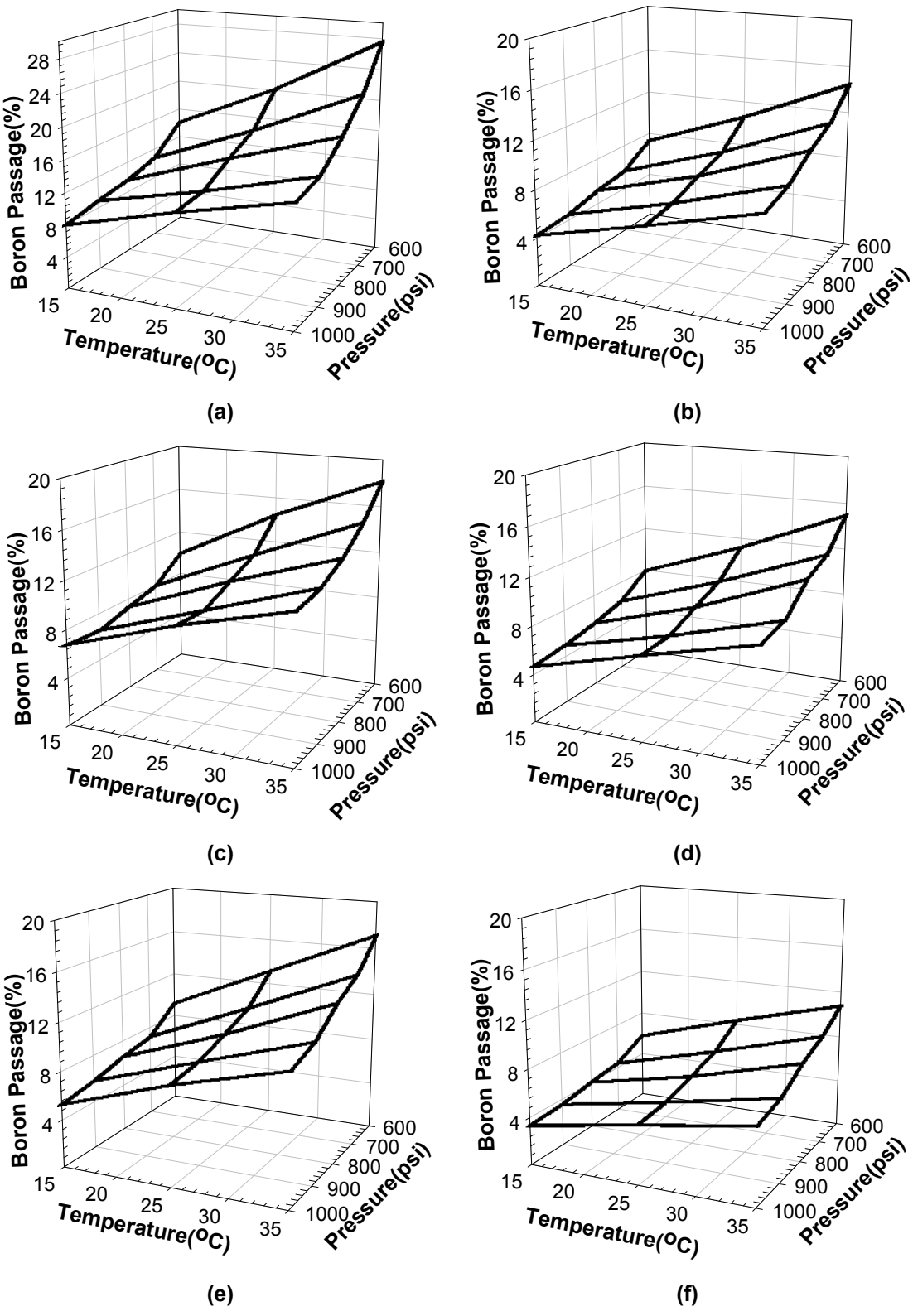

Figure 3.17 Effect of temperature on boron passage at pH 6.2: (a)SR (b)SWC4+ (c)XLE (d)LE (e)TM820 (f)TM820A.

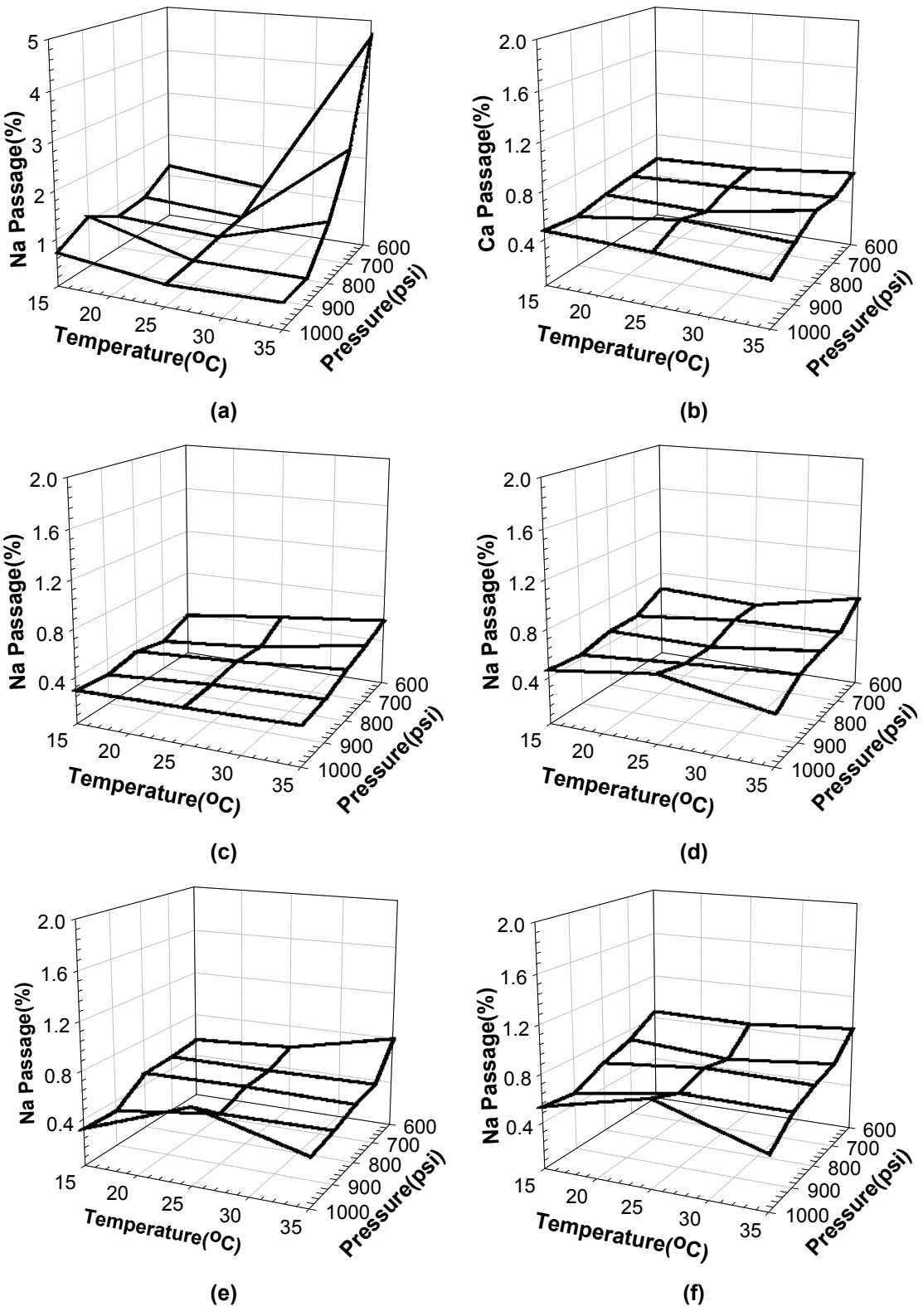

Figure 3.18 Effect of temperature on Na passage at pH 6.2: (a)SR (b)SWC4+ (c)XLE (d) LE (e)TM820 (f)TM820A.

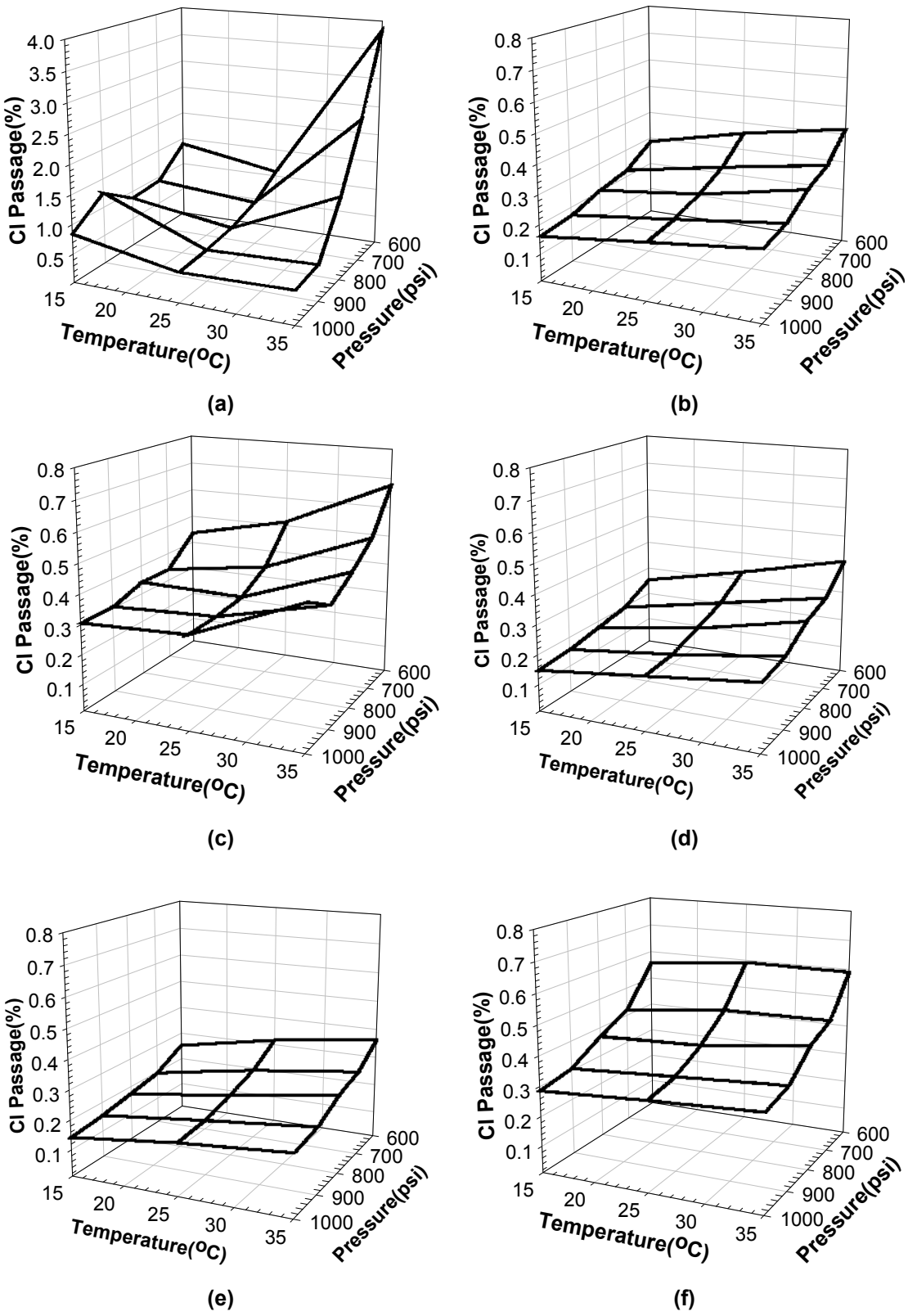

Figure 3.19 Effect of temperature on Cl passage at pH 6.2: (a)SR (b)SWC4+ (c)XLE (d)LE (e)TM820 (f)TM820A.

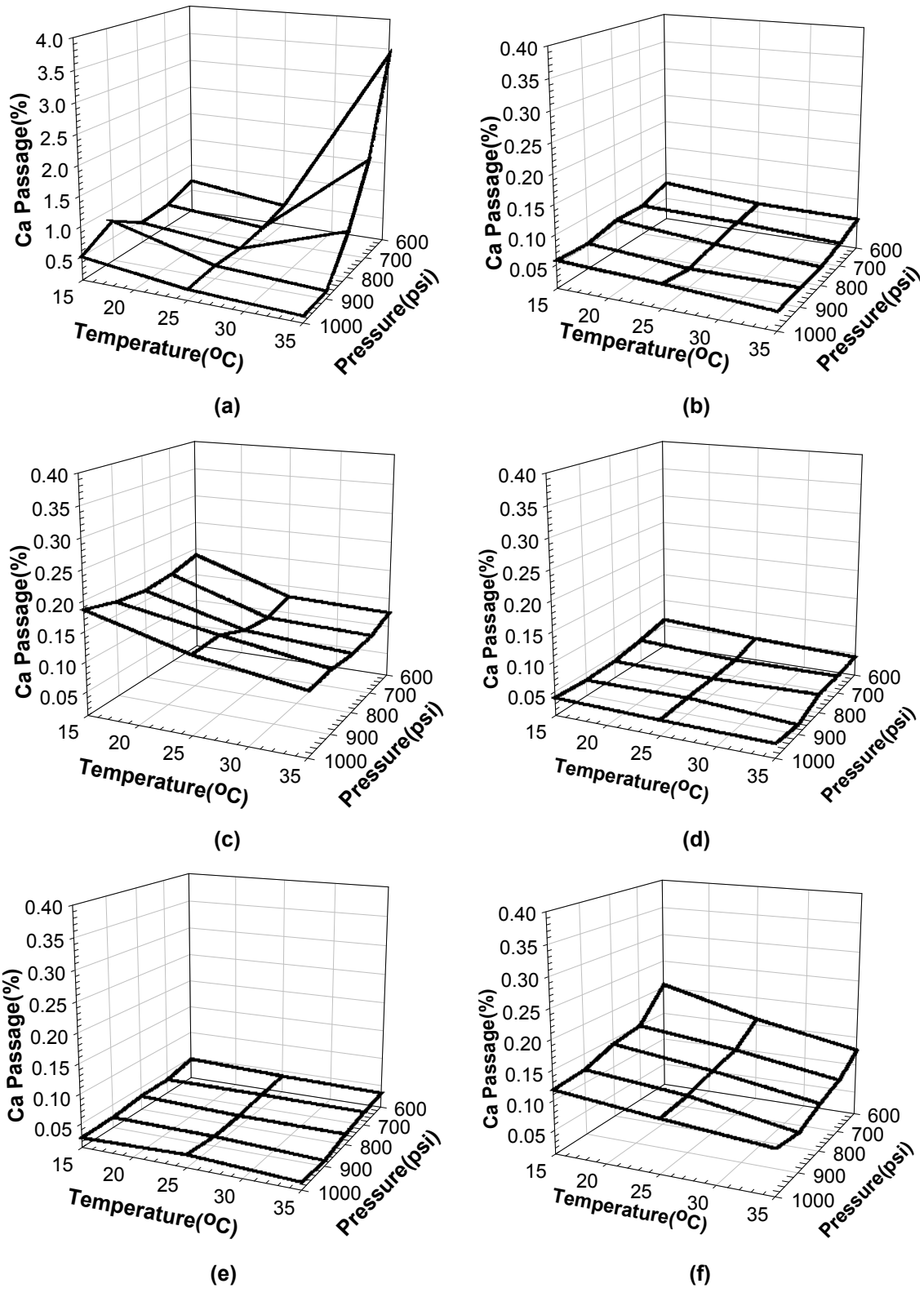

Figure 3.20 Effect of temperature on Ca passage at pH 6.2: (a)SR (b)SWC4+ (c)XLE (d)LE (e)TM820 (f)TM820A.

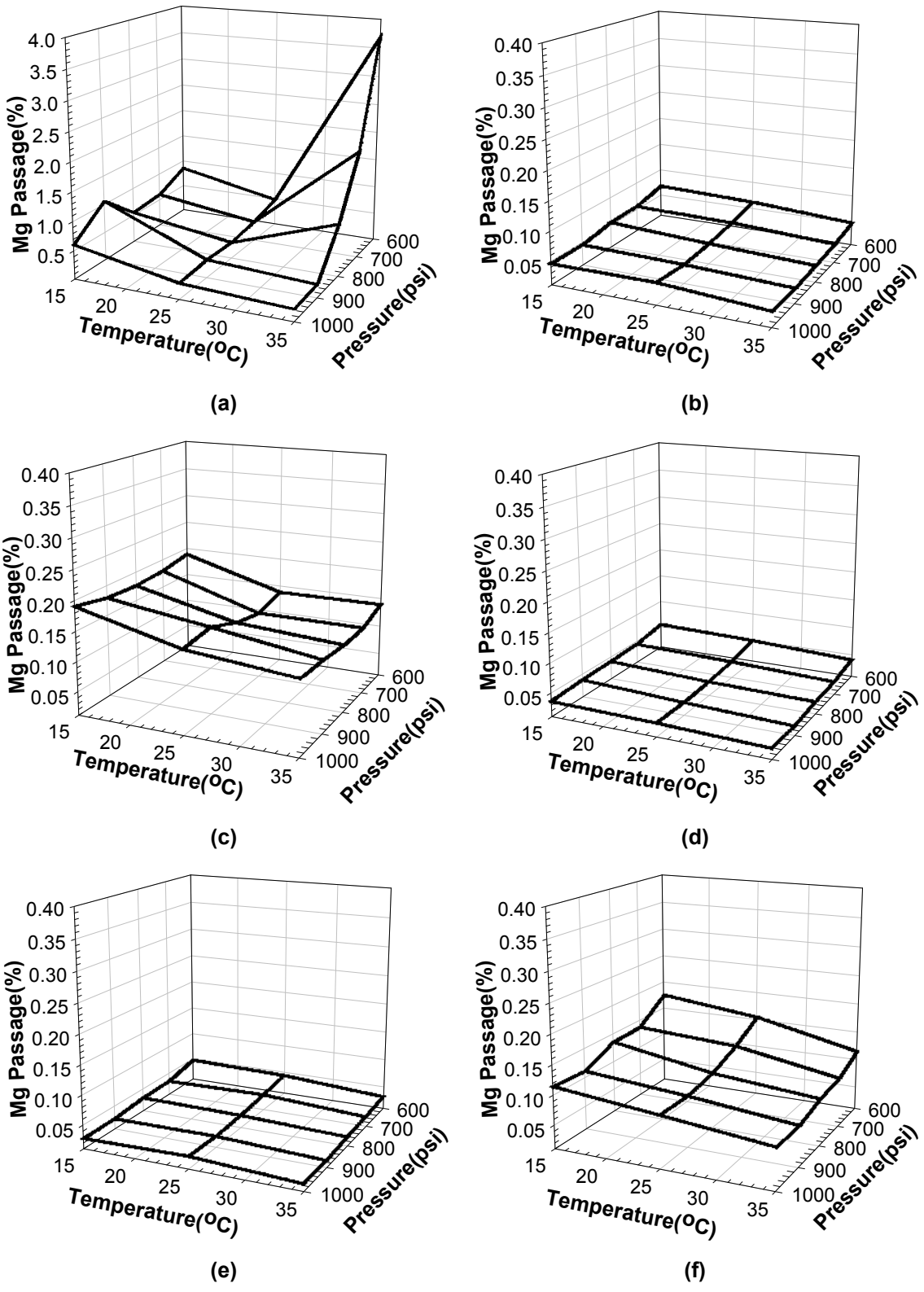

Figure 3.21 Effect of temperature on Mg passage at pH 6.2: (a)SR (b)SWC4+ (c)XLE (d)LE (e)TM820 (f)TM820A.

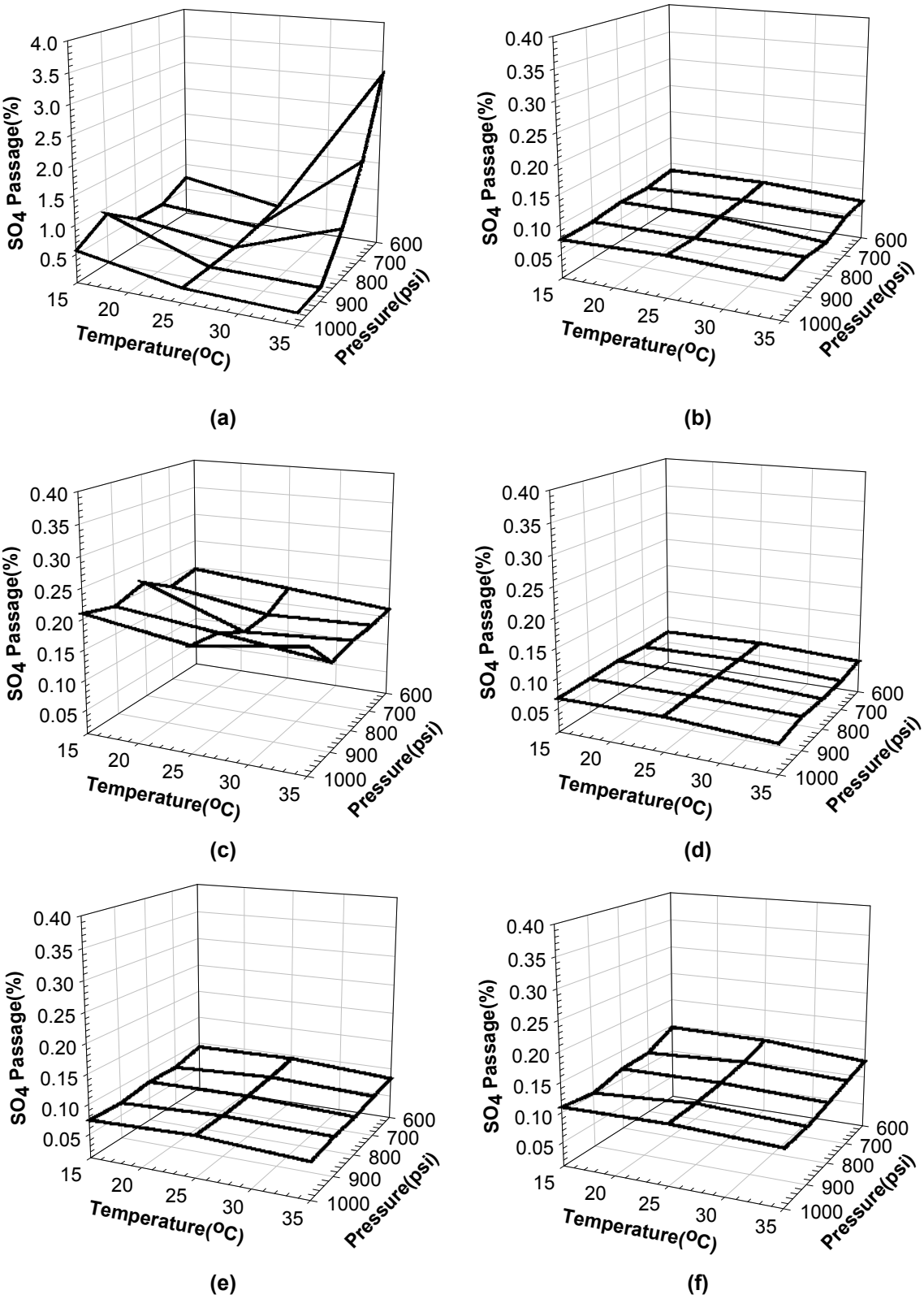

Figure 3.22 Effect of temperature on SO_4 passage at pH 6.2: (a)SR (b)SWC4+ (c)XLE (d)LE (e)TM820 (f)TM820A.

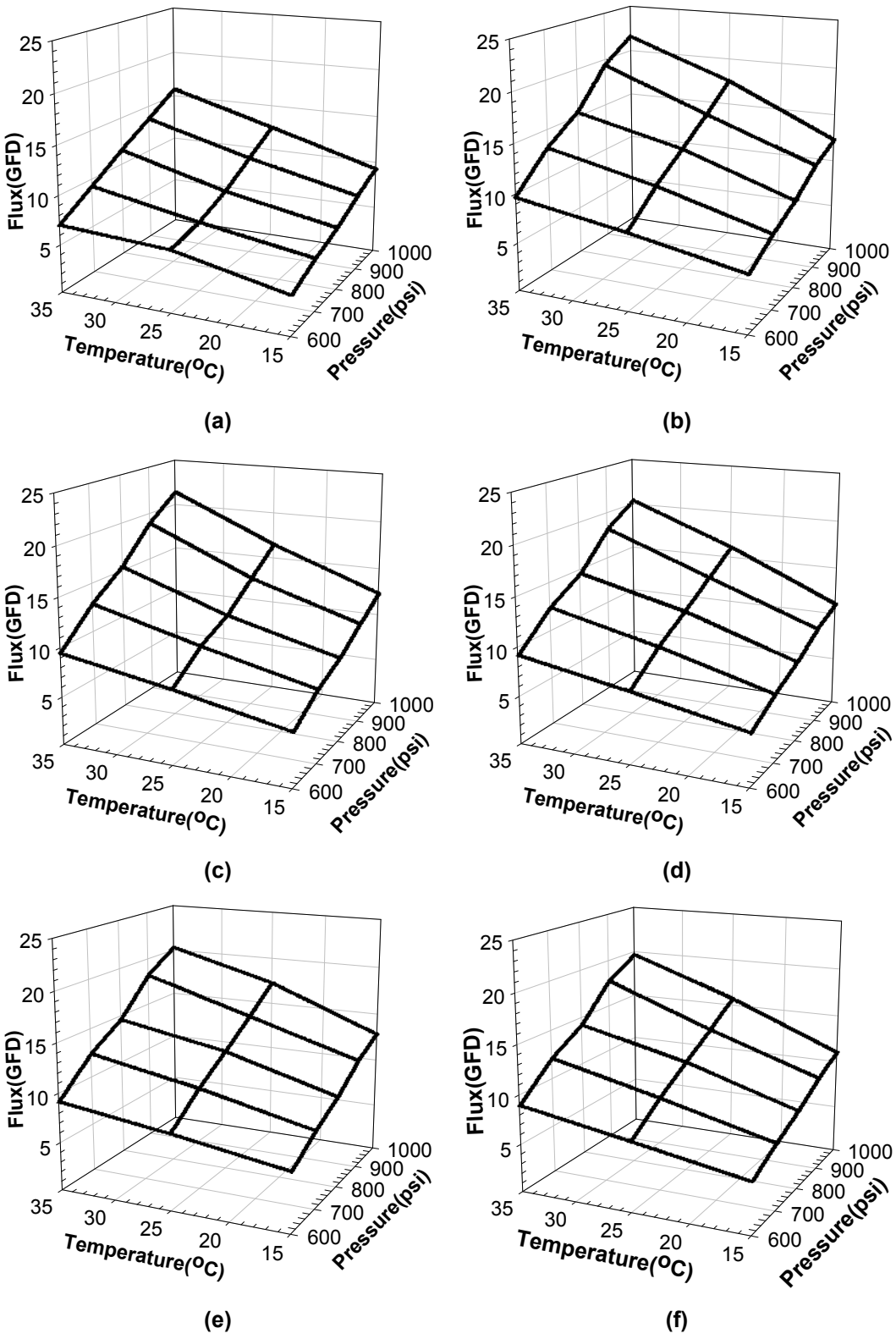

Figure 3.23 Effect of temperature on membrane flux at pH 9.5: (a)SR (b)SWC4+ (c)XLE (d)LE (e)TM820 (f)TM820A.

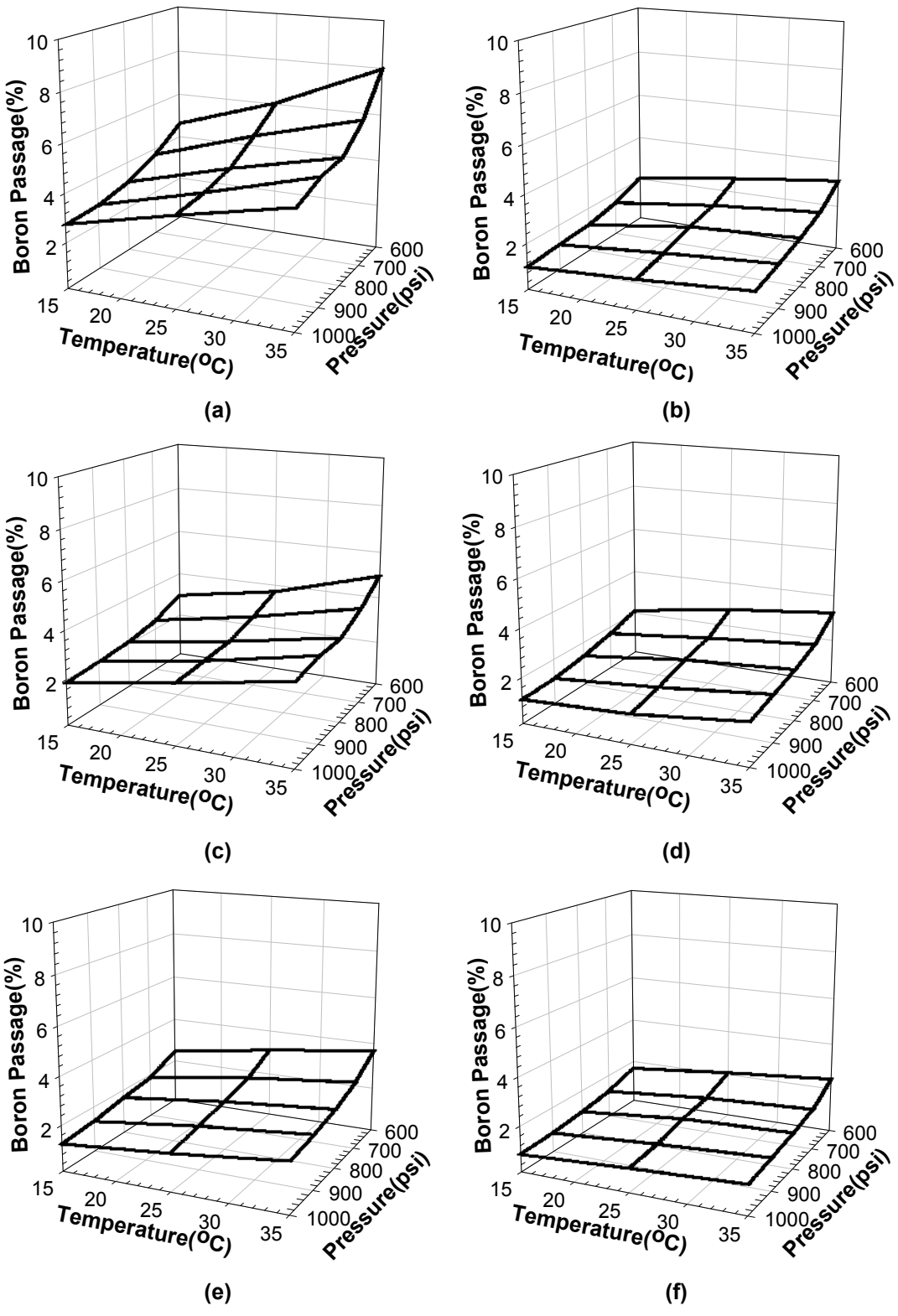

Figure 3.24 Effect of temperature on boron passage at pH 9.5: (a)SR (b)SWC4+ (c)XLE (d)LE (e)TM820 (f)TM820A.

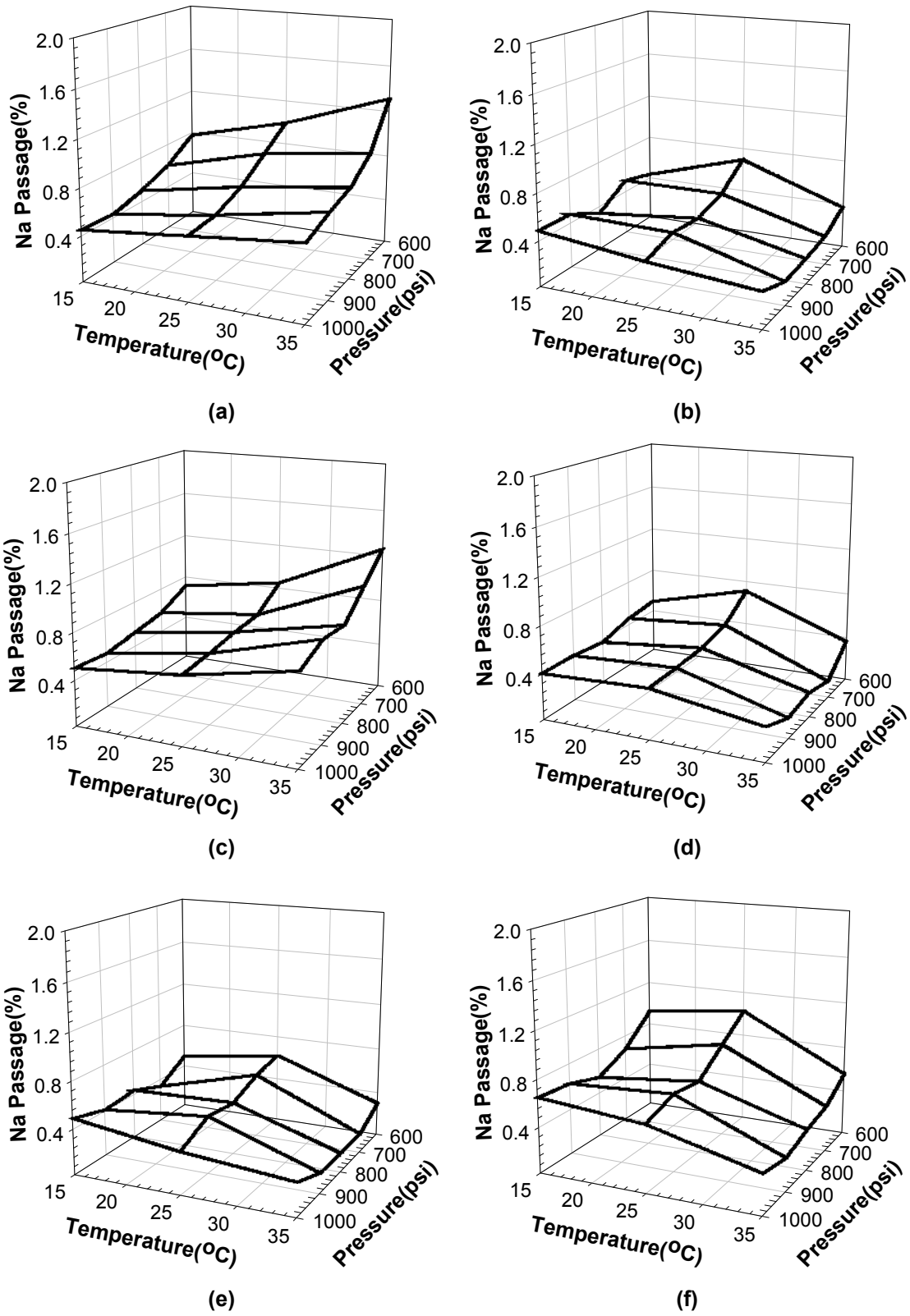

Figure 3.25 Effect of temperature on Na passage at pH 9.5: (a)SR (b)SWC4+ (c)XLE (d)LE (e)TM820 (f)TM820A.

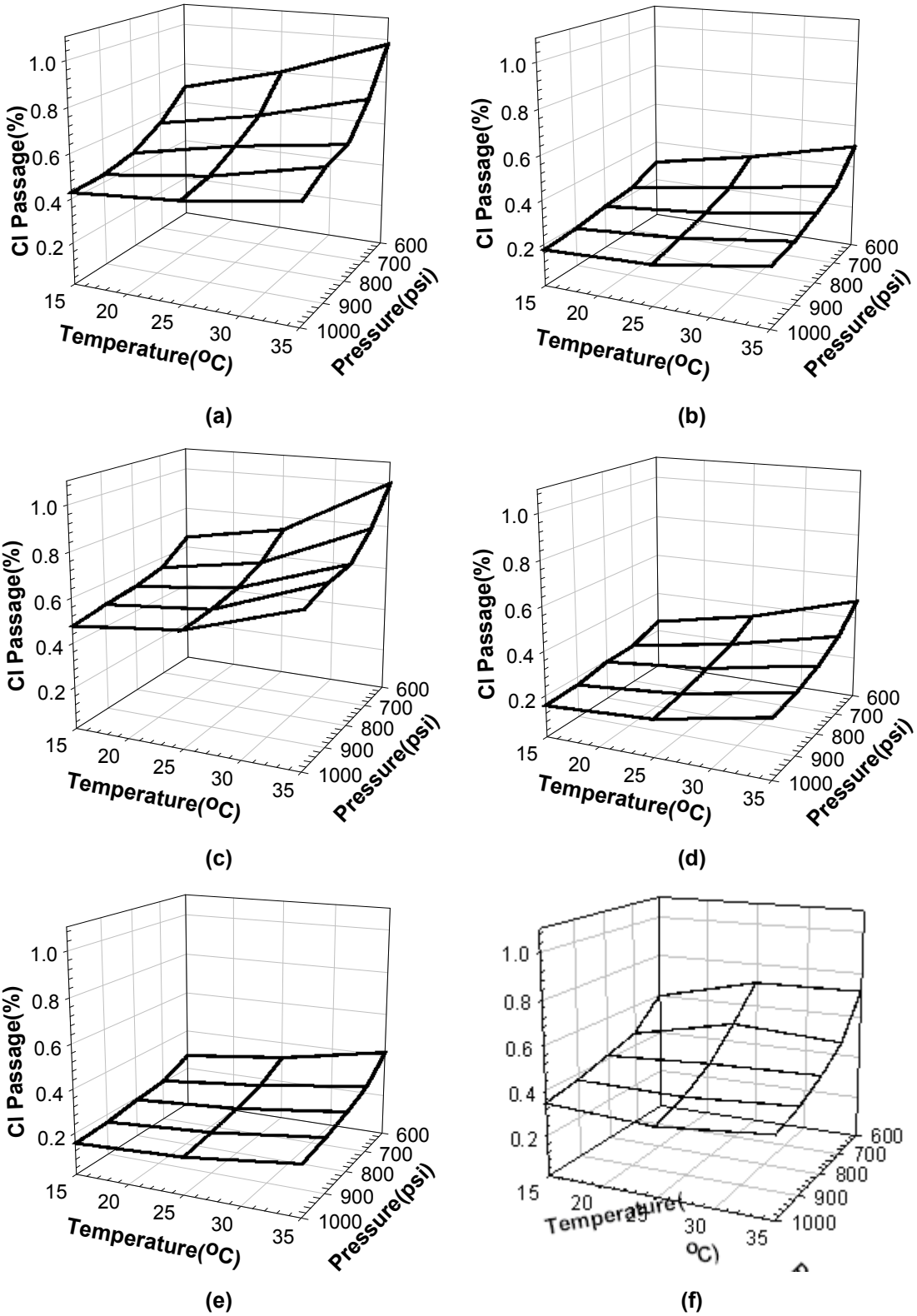

Figure 3.26 Effect of temperature on Cl passage at pH 9.5: (a)SR (b)SWC4+ (c)XLE (d)LE (e)TM820 (f)TM820A.

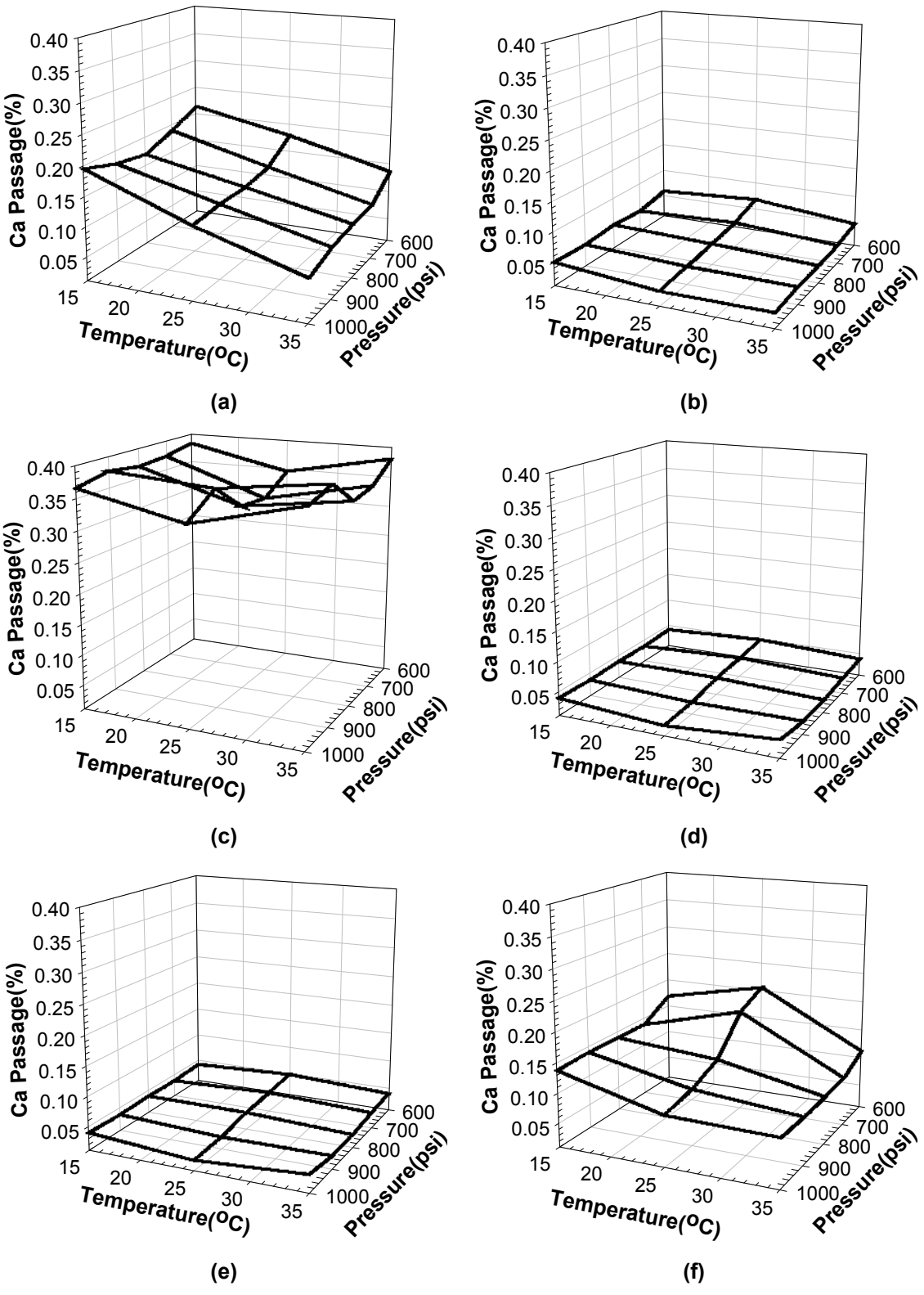

Figure 3.27 Effect of temperature on Ca passage at pH 9.5: (a)SR (b)SWC4+ (c)XLE (d)LE (e)TM820 (f)TM820A.

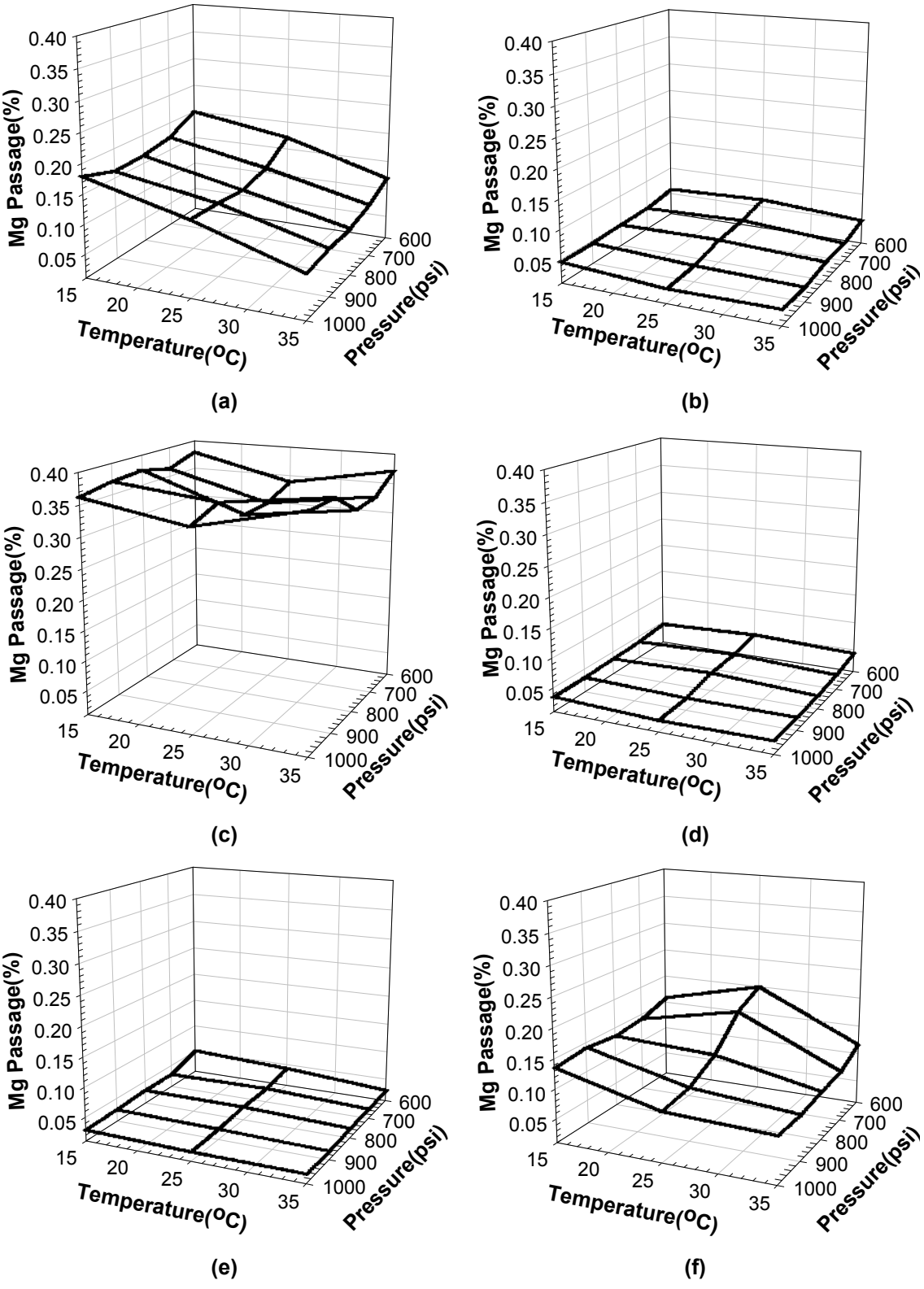

Figure 3.28 Effect of temperature on Mg passage at pH 9.5: (a)SR (b)SWC4+ (c)XLE (d)LE (e)TM820 (f)TM820A.

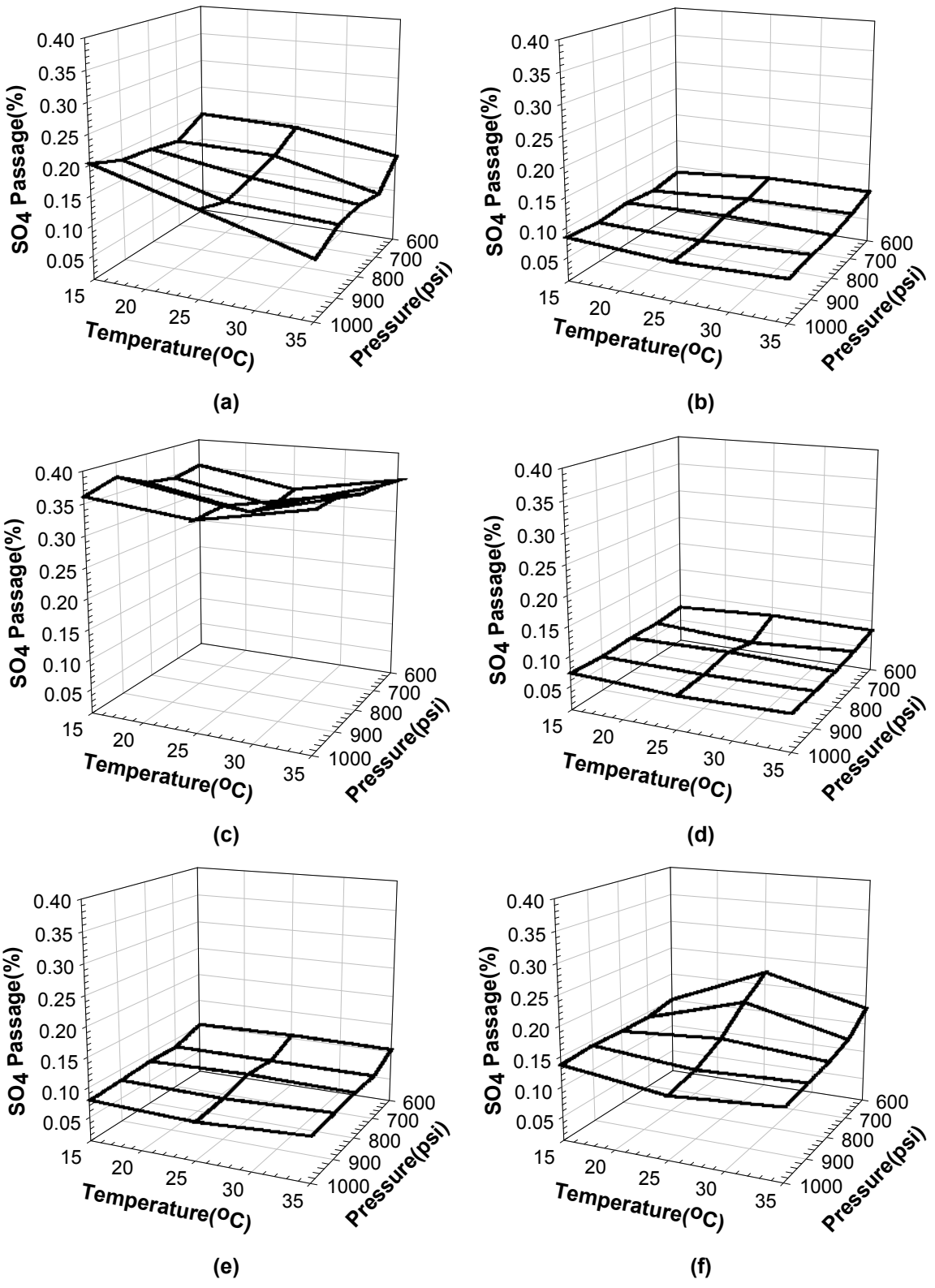

Figure 3.29 Effect of temperature on SO4 passage at pH 9.5: (a)SR (b)SWC4+ (c)XLE (d)LE (e)TM820 (f)TM820A.

The effect of temperature on flux is shown in figure 3.16 for pH 6.2 and in figure 3.23 for pH 9.5. Regardless of operating pressure and pH, flux increased as temperature increased, thereby confirming the temperature dependence of specific hydraulic permeability (p_h) in the Spiegler-Kedem model. The local hydraulic permeability (p_h) in the Spiegler-Kedem model could have been quantified further to include the temperature effect, but this was not done for this study.

The effect of temperature on boron removal at pH 6.2 and 9.5 is presented in figures 3.17 and 3.24, respectively. The passage of boron increased proportionally with temperature. As both local solute permeability (p_s) of boric acid and specific hydraulic permeability (p_h) increase with temperature, the temperature-dependence of solute passage will be determined by the balance between increases in the solute transport rate and water transport rate. Given the enhanced boron passage at higher temperature, it appears that local boric acid permeability is more affected by temperature than local hydraulic permeability.

Figures 3.18 and 3.25 show the effect of temperature and pressure on the passage of sodium across the membranes at pH 6.2 and 9.5, respectively. Temperature dependence of sodium transport was influenced by pH. At pH 6.2, sodium passage shows increasing tendency in proportion to the temperature for all membranes. At pH 9.5, sodium passage through the SR and XLE membranes also increased as temperature increased. However, passage through the rest of the membranes decreased with increasing temperature. Variable temperature dependence as a function of pH was not expected and is not well understood. These results might have resulted in part from experimental errors (i.e., for SR membranes, different coupons were used for different pHs).

Figures 3.19 and 3.26 show the effect of temperature on chloride passage across the membranes. In general, chloride transport increased as temperature increased. Again, this is likely due to a higher dependency of local solute permeability on temperature than that of specific hydraulic permeability. No further attempt was made to quantitatively model the temperature dependence of solutes other than boron.

The effects of temperature change on the passage of calcium, magnesium, and sulfate at pH 6.2 are shown in figures 3.20, 3.21, and 3.22, respectively, and at pH 9.5 are shown in figures 3.27, 3.28, and 3.29, respectively. With a few exceptions, the passage of divalent ions decreased as temperature increased. The extent of temperature dependence varied among the membranes tested. The balance between increased specific hydraulic permeability (p_h) and increased local solute permeability (p_s) with temperature might account for the reduced or increased passage of divalent ions at higher temperatures. Increasing temperature can also increase the mass transfer coefficient (k), which would decrease the

solute concentrations at the membrane surface, thereby also partially accounting for the diminished divalent ion passage with temperature.

3.4.4 Modeling of Experimental Results: pH Effect

(1) Estimation of Mass Transfer Coefficients

Mass transfer coefficients (k) of salts were calculated using the previously mentioned methods (section 3.3.3) and are presented in table 3.6. These evaluations were performed using the experimental pH dependence data presented previously. Mass transfer coefficients calculated using the "flux variation method from film theory" resulted in negative values. This was likely due to the dependence of $\ln[(1-R)/R]$ on J_v, which invalidates the assumption behind this method that intrinsic rejection (R) does not significantly depend on solute flux (J_v). This assumption might be valid for dilute solutions but not for concentrated solutions such as seawater. Mass transfer coefficients calculated from the second method, "flux variation method from Spiegler-Kedem model combined with film theory," varied widely with pH. This was problematic because the mass transfer coefficient should be governed largely by the hydrodynamic conditions of a given experimental system, not by the pH of a solution. These results indicate that this method might not be appropriate for the experimental conditions tested.

Table 3.6 Evaluation of Salt Mass Transfer Coefficients for pH Effect Experiment (cm/s)

	pH	SR	SWC4	XLE	LE	TM820	TM820A
Flux variation method with film theory	6.2	-0.00064	-0.00128	-0.00074	-0.00071	-0.00081	-0.00068
	7.5	-0.00058	-0.00123	-0.00072	-0.00066	-0.00077	-0.00063
	8.5	-0.00065	-0.00138	-0.00083	-0.00079	-0.00088	-0.00075
	9.5	-0.00069	-0.00141	-0.00082	-0.00081	-0.00094	-0.00074
Flux variation method from S-K model with film theory	6.2	0.00122	0.00099	0.00256	0.00199	0.00190	0.00283
	7.5	0.00157	0.00100	0.00267	0.00232	0.00197	0.00346
	8.5	0.00123	0.00097	0.00190	0.00155	0.00155	0.00197
	9.5	0.00131	0.00095	0.00175	0.00142	0.00131	0.00193
Osmotic pressure method	6.2	0.00183	0.00243	0.00258	0.00220	0.00197	0.00275
	7.5	0.00161	0.00219	0.00247	0.00215	0.00186	0.00271
	8.5	0.00177	0.00254	0.00228	0.00199	0.00174	0.00240
	9.5	0.00161	0.00252	0.00226	0.00200	0.00173	0.00240
Flux decline induced by salinity method	6.2	0.00195	0.00258	0.00275	0.00234	0.00208	0.00294
	7.5	0.00171	0.00233	0.00263	0.00228	0.00197	0.00274
	8.5	0.00188	0.00271	0.00242	0.00211	0.00184	0.00256
	9.5	0.00171	0.00268	0.00240	0.00212	0.00182	0.00256

Values for mass transfer coefficients estimated from the "osmotic pressure method" and the "flux decline induced by salinity method" were similar. This was expected considering these two methods are based on the same equations (i.e., equations (3) and (5)). The mass transfer coefficients calculated from these two methods were essentially independent of pH and were within the range of the mass transfer coefficient values reported in the literature for RO membranes

(Murthy and Gupta, 1997). The nonlinear parameter estimation method, described later in this report, showed that the transport parameters obtained using these mass transfer coefficients had relatively high correlation coefficients (R^2), which further supported the validity of these methods. Using equation (7), boron mass transfer coefficients were obtained from the salt mass transfer coefficients calculated by the "flux decline induced by salinity method" and are presented in table 3.7.

Table 3.7 Evaluation of Boron Mass Transfer Coefficients for pH Effect Experiment (cm/s)

pH	SR	SWC4+	XLE	LE	TM820	TM820A
6.2	0.00184	0.00238	0.00265	0.00207	0.00182	0.0025
7.5	0.00168	0.00236	0.00262	0.00208	0.0018	0.0025
8.5	0.00203	0.00286	0.00269	0.00244	0.00217	0.00307
9.5	0.00178	0.00274	0.00242	0.00238	0.00205	0.00285

(2) Nonlinear Parameter Estimation

Reflection coefficients (σ_B) and boron permeability constants ($P_{s,B}$) of six membranes at four different pHs were evaluated by nonlinear optimization and are presented in table 3.8 along with corresponding correlation coefficients (R^2). This method for parameter estimation appeared accurate, as most of the estimated correlation coefficients (R^2) were higher than 0.98, regardless of pH condition and type of membrane. Reflection coefficients (σ) ranged from 0.962 to 0.9992, depending on the pH and membrane tested, and it decreased as pH decreased. This suggests that the extent of boron transport via solvent-coupling becomes more significant as boron speciation shifts toward neutral boric acid. The reflection coefficients increased proportionally with pH and became very close to unity at pH 9.5. On the other hand, permeability constants decreased as pH increased (i.e., higher rejection). As described previously, this result was likely due to the increased fraction of negatively charged borate as pH increased. Experimental data and predictions based on the Spiegler-Kedem model (equation (6)) using the parameters presented in table 3.8 are compared in figure 3.30. The model showed excellent agreement with the experimental data.

Table 3.8 Result of Nonlinear Parameter Estimation for pH Effect Experiment

	pH	6.2	7.5	8.5	9.5
SR	σ_B	0.9753	0.994	0.9905	0.9933
	P_s (cm/s)	5.47E-05	6.11E-05	4.65E-05	1.40E-05
	R^2	0.9877	0.9867	0.9951	0.9319
SWC4+	σ_B	0.9832	0.9918	0.9858	0.9957
	P_s (cm/s)	3.84E-05	3.92E-05	2.84E-05	7.24E-06
	R^2	0.9951	0.9971	0.9956	0.9701
XLE	σ_B	0.962	0.9696	0.9766	0.9878
	P_s (cm/s)	4.15E-05	4.21E-05	3.24E-05	9.48E-06
	R^2	0.9923	0.9949	0.9928	0.9836
LE	σ_B	0.9821	0.9931	0.9876	0.9976
	P_s (cm/s)	3.33E-05	3.61E-05	2.51E-05	6.82E-06
	R^2	0.9921	0.9942	0.9872	0.9747
TM820	σ_B	0.9812	0.9986	0.9935	0.9989
	P_s (cm/s)	4.36E-05	4.74E-05	3.40E-05	8.93E-06
	R^2	0.9847	0.9971	0.9956	0.9943
TM820A	σ_B	0.9819	0.9912	0.9928	0.9992
	P_s (cm/s)	2.76E-05	2.85E-05	2.11E-05	6.07E-06
	R^2	0.9904	0.9917	0.9846	0.9922

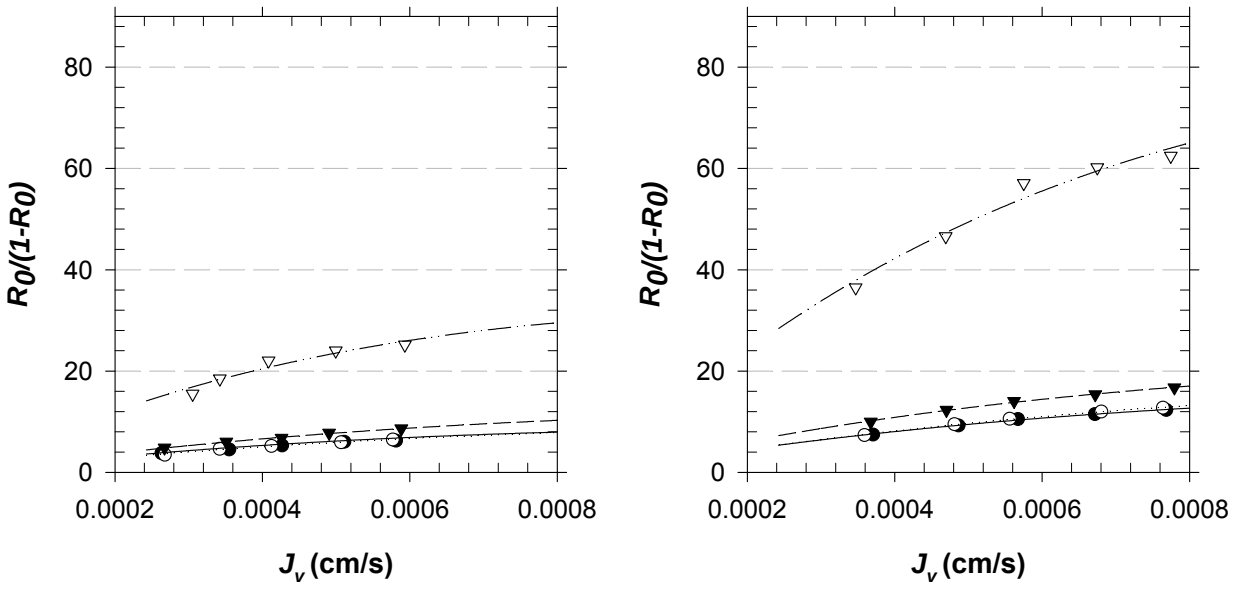

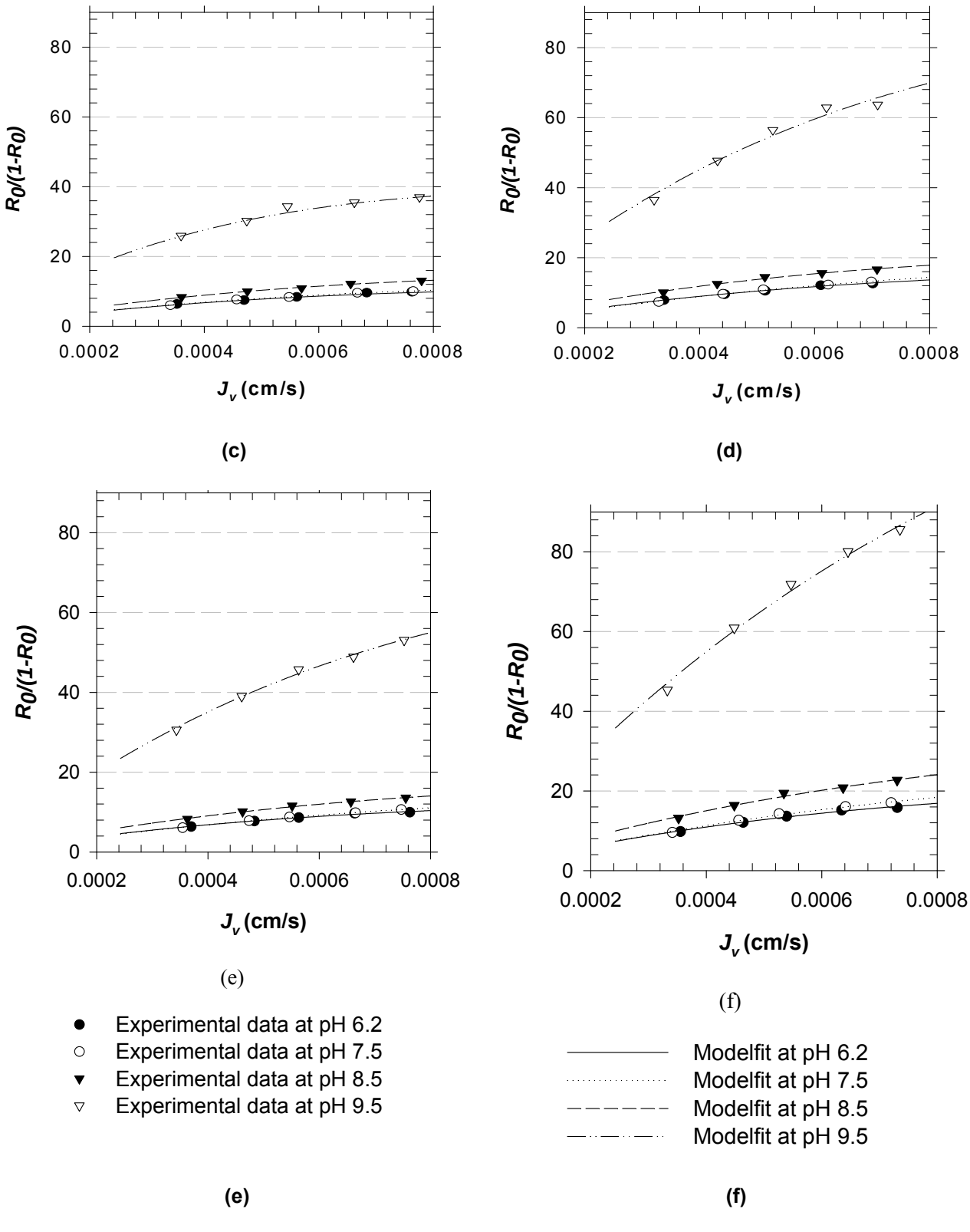

Figure 3.30 Experimental data and curve-fit from Spiegler-Kedem model for boron transport in pH effect experiment (a)SR (b)SWC4+ (c)XLE (d)LE (e)TM820 (f)TM820A (continued).

(3) The Apparent Acid Constant

Since boric acid and borate ions have different permeability constants and reflection coefficients, it is possible to predict the overall transport of boron based on the fraction of boric acid and borate in the feed water under specific conditions. Fractions of boric acid (α_0) and borate (α_1) at a specific pH could be calculated from the following correlations, assuming the second and third acid constants (K_{a2} and K_{a3}) of boric acid are negligible in the pH range tested during this work:

$$\alpha_0 = \frac{[H^+]}{[H^+] + K_{a1}} = \frac{[H_3BO_3]}{C_{T,B}} \tag{18}$$

$$\alpha_1 = \frac{K_{a1}}{[H^+] + K_{a1}} = \frac{[H_2BO_3^-]}{C_{T,B}} \tag{19}$$

$$K_{a1} = \frac{\{H_2BO_3^-\}\{H^+\}}{\{H_3BO_3\}} \tag{20}$$

where, α_0 = fraction of boric acid [dimensionless]; α_1 = fraction of borate [dimensionless]; $C_{T,B}$ = total concentration of boron species (ML^{-3}); $[H_2BO_3^-]$ = concentration of borate (ML^{-3}); $[H_3BO_3]$ = concentration of boric acid (ML^{-3}); $[H^+]$= concentration of proton (ML^{-3}); $\{H_2BO_3^-\}$ = activity of borate (ML^{-3}); $\{H_3BO_3\}$ = activity of boric acid (ML^{-3}); $\{H^+\}$ = activity of proton (ML^{-3}); and K_{a1} = the first acid constant of boric acid (ML^{-3}). This equation is only valid in dilute solutions where ionic strength effects are negligible. In case of high ionic strength solutions such as seawater, different definitions of α_0 and α_1 are generally adopted that incorporate an apparent acid constant (Riley and Skirrow, 1975).

$$\alpha_0 = \frac{\{H^+\}}{\{H^+\} + K_{a1}'} = \frac{[H_3BO_3]}{C_{T,B}} \tag{21}$$

$$\alpha_1 = \frac{K_{a1}}{\{H^+\} + K_{a1}'} = \frac{[H_2BO_3^-]}{C_{T,B}} = 1 - \alpha_0 \tag{22}$$

where, K_{a1}' = apparent first acid constant of boric acid [ML^{-3}], defined by equation (17). In high ionic strength solutions, if pH is measured by the potentiometric method and calibrated using an NBS standard buffer, the pH can be considered to be -log{H+} (Riley and Skirrow, 1975). Therefore, the above equation can be used when proton activity deviates significantly from the proton concentration, as is the case in the seawater.

To predict α_0 and α_1 from the above equations, it is necessary to accurately estimate the value of the apparent acid constant at various experimental conditions. The apparent first acid constant of boric acid (K_{a1}') is dependent on the temperature and salinity of water. An empirical equation for estimating the constant at different temperatures and chlorinity (chlorinity = salinity/1.80655) conditions was provided by Gieskes (1974).

$$-\log K_{a1}' = \frac{2291.9}{T} + 0.01756 - 3.385 - 0.32051 \times Cl^{1/3} \quad (23)$$

where, T=Temperature [K]; Cl = chlorinity, [dimensionless; ‰]. Using this equation, the apparent first acid constant was plotted as a function of temperature and salinity (figure 3.31). Note that the salinity was expressed in terms of chlorinity. K_{a1}' decreased significantly as temperature and salinity increased. The value of 8.68 was calculated using representative seawater salinity (19 ‰ chlorinity) and 25 ^{o}C.

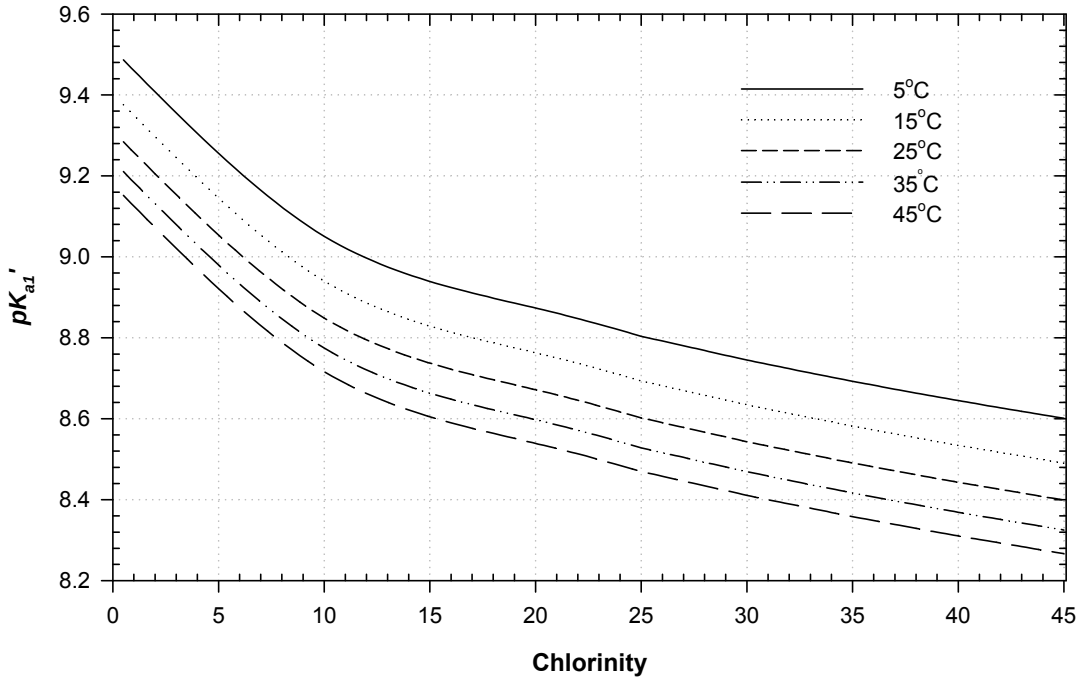

Figure 3.31 Change of apparent first acid constant (K_{a1}') with temperature and chlorinity.

From the apparent first acid constant (K_{a1}') calculated from equation (23), the fraction of boric acid (α_0) at different pHs and three different salinities (0.5, 19, and 38 ‰) was estimated and the results are presented in figure 3.32. Note that the three chlorinities in the figure represent low-salinity water, seawater, and seawater concentrate. The distribution curve shifted left as ionic strength increased, which implies that more boric acid would dissociate in higher strength

solutions at a given pH. The distribution of boric acid species (α_0) at three different temperatures of 15, 25, and 35 ^{o}C was also estimated and is presented in figure 3.33. The distribution curve also shifted left as temperature increased.

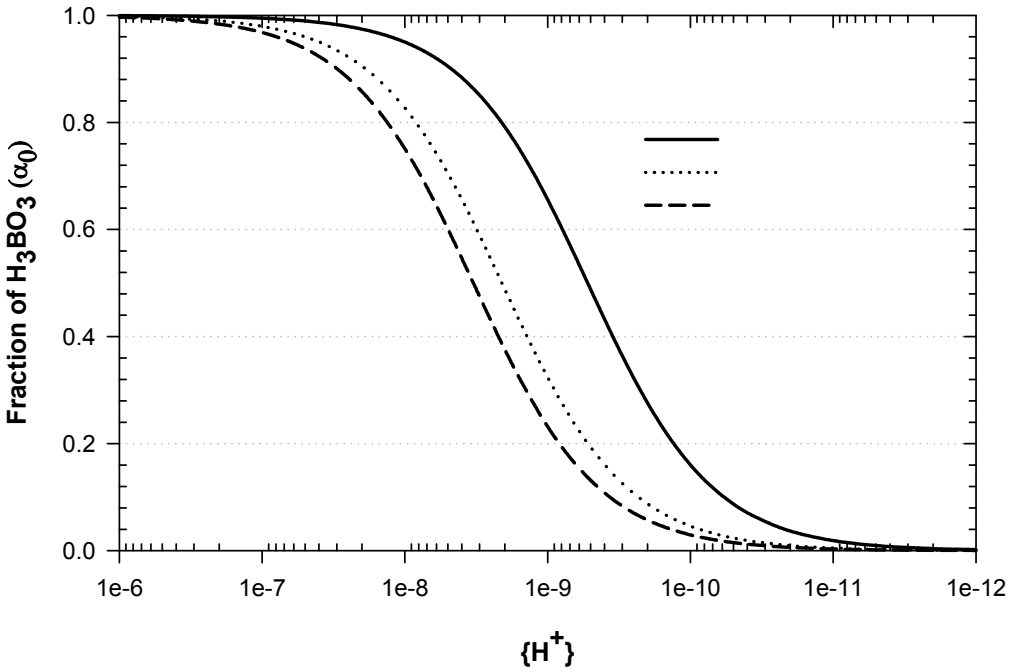

Figure 3.32 Effect of salinity on the distribution of boric acid.

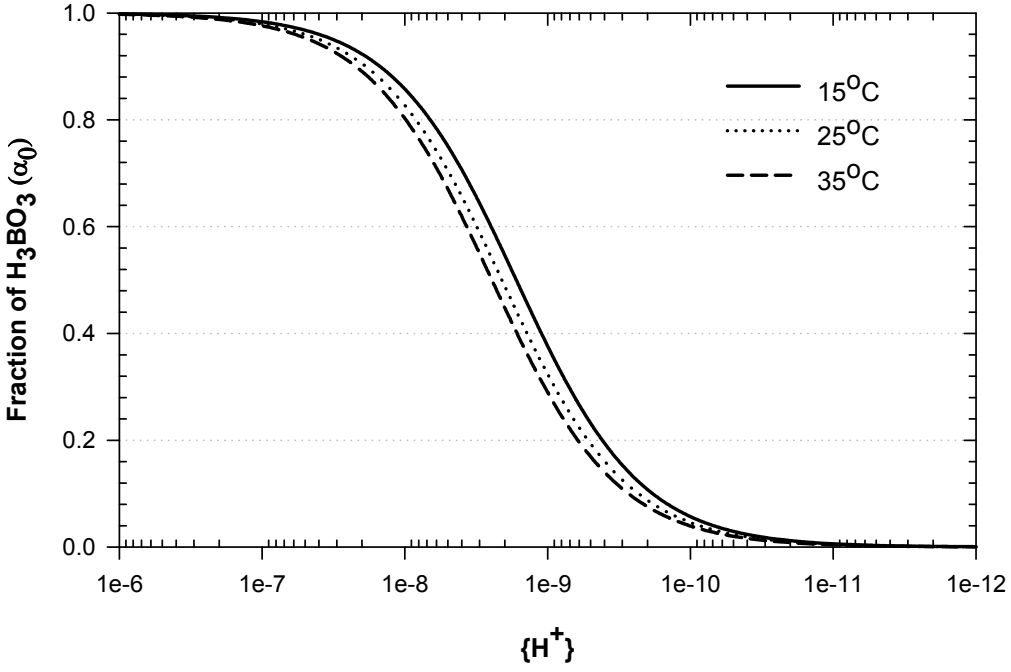

Figure 3.33 Effect of temperature on the distribution of boric acid.

To calculate apparent first acid constants (K_{a1}') from experimental data, concentration polarization effects necessitated that the concentration of salts at the membrane wall (C_m) be considered instead of the bulk salt concentration. In addition, salt concentration in the concentration polarization layer was expected to be different for each membrane due to variable rejection performances. Therefore, apparent first acid constants (K_{a1}') at pH 6.2, 7.5, 8.5, and 9.5 for each membrane were separately calculated from equation (23) using the wall concentration (C_m) of salt estimated from equation (5) (table 3.9). The resulting apparent first acid constants (K_{a1}') varied only slightly with membranes and pHs and ranged from 8.59 to 8.63.

Table 3.9 Calculation of the Apparent First Acid Constants of Boric Acid (at 25 °C)

	pH	*k* of salt (cm/sec)	C_m of salt (mg/L)	Chlorinity of C_m (‰)	pK_{a1}'
SR	6.2	0.00195	43,558	23.65	8.62
	7.5	0.00171	44,545	24.18	8.61
	8.5	0.00188	43,906	23.83	8.62
	9.5	0.00171	44,441	24.12	8.61
SWC4+	6.2	0.00258	43,602	23.67	8.62
	7.5	0.00233	44,432	24.12	8.61
	8.5	0.00271	43,064	23.38	8.62
	9.5	0.00268	43,379	23.55	8.62
XLE	6.2	0.00275	42,930	23.30	8.62
	7.5	0.00263	43,108	23.40	8.62
	8.5	0.00242	44,299	24.05	8.61
	9.5	0.0024	43,929	23.85	8.62
LE	6.2	0.00234	43,600	23.67	8.62
	7.5	0.00228	43,786	23.77	8.62
	8.5	0.00211	44,645	24.24	8.61
	9.5	0.00212	44,887	24.37	8.61
TM820	6.2	0.00208	45,887	24.91	8.60
	7.5	0.00197	46,190	25.07	8.60
	8.5	0.00184	47,231	25.64	8.59
	9.5	0.00182	47,690	25.89	8.59
TM820A	6.2	0.00294	42,041	22.82	8.63
	7.5	0.00274	42,410	23.02	8.63
	8.5	0.00256	43,124	23.41	8.62
	9.5	0.00256	43,334	23.52	8.62

(4) Prediction of Transport Parameters

Since the overall passage of boron across a given membrane was expected to be equal to the sum of boric acid and borate passage, the following

equation was developed to predict the overall permeability constant of boron at any given condition:

$$P_{s,B} = \alpha_0 \times P_{s(H_3BO_3)} + \alpha_1 \times P_{s(H_2BO_3^-)} \quad (24)$$

where, $P_{s,B}$ = overall permeability constant of boron (LT^{-1}); $P_{s(H3BO3)}$ = permeability constant of boric acid (LT^{-1}); and $P_{s(H2BO3-)}$ = permeability constant of borate (LT^{-1}). Using this equation, the permeability constant of boric acid ($P_{s(H3BO3)}$) and that of borate ($P_{s(H2BO3-)}$) were obtained from fitting the equation to P_s, α_0, and α_1 at pHs 6.2 and 9.5. The values of α_0, and α_1 were estimated from equations (21) and (22) using the apparent acid constant (K_{a1}') for each membrane in table 3.9. Calculated permeability constants for boric acid ($P_{s(H3BO3)}$) and borate ($P_{s(H2BO3-)}$) are presented in table 3.10.

Table 3.10 Calculation of Permeability Constants of Boric Acid and Borate

	pH	P_s (cm/s)	α_0	α_1	$P_{s(H3BO3)}$ (cm/s)	$P_{s(H2BO3-)}$ (cm/s)
SR	6.2	5.47E-05	0.9962	0.0038	5.47E-05	8.76E-06
	9.5	1.40E-05	0.1141	0.8859		
SWC4+	6.2	3.84E-05	0.9962	0.0038	3.84E-05	3.13E-06
	9.5	7.24E-06	0.1165	0.8835		
XLE	6.2	4.15E-05	0.9962	0.0038	4.15E-05	5.26E-06
	9.5	9.48E-06	0.1165	0.8835		
LE	6.2	3.33E-05	0.9962	0.0038	3.33E-05	3.41E-06
	9.5	6.82E-06	0.1141	0.8859		
TM820	6.2	4.36E-05	0.9960	0.0040	4.36E-05	4.66E-06
	9.5	8.93E-06	0.1095	0.8905		
TM820A	6.2	2.76E-05	0.9963	0.0037	2.76E-05	3.23E-06
	9.5	6.07E-06	0.1165	0.8835		

These data suggest that boric acid permeability is approximately 6 to 12 times higher than borate permeability for the membranes tested. This is consistent with current understanding that charge repulsion dominates the rejection of charged species by RO membranes. Once permeability constants of boric acid ($P_{s(H3BO3)}$) and borate ($P_{s(H2BO3-)}$) were determined, $P_{s,B}$ at any pH could be estimated using equation (24). Figure 3.34 compares estimated overall boron permeability constant ($P_{s,B}$) with the value obtained from a nonlinear optimization of experimental data. This comparison suggests that the overall boron permeability constant ($P_{s,B}$) can be predicted confidently based on the approach developed in this study.

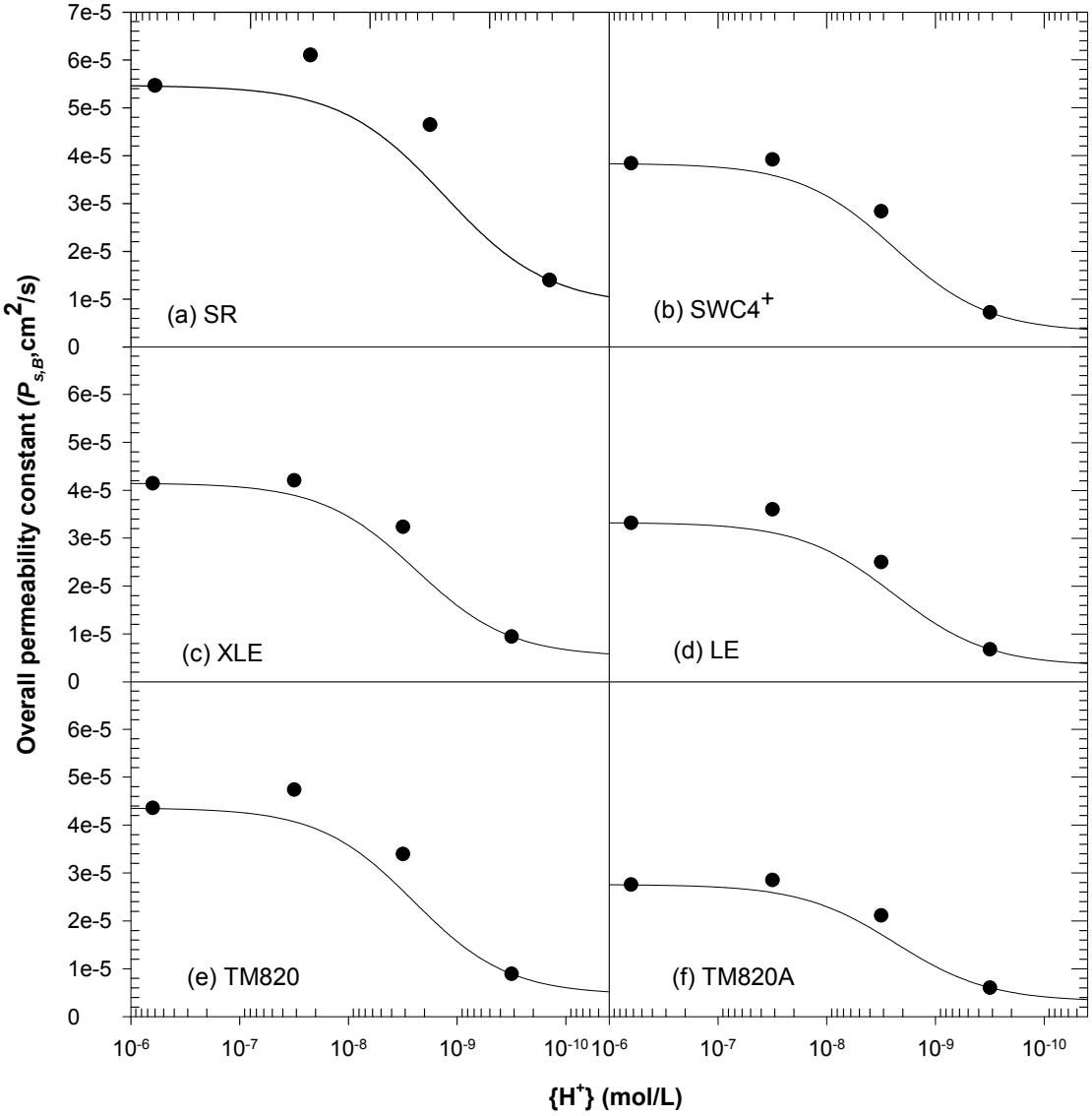

Figure 3.34 Prediction of change of overall permeability coefficient of boron by pH.

A similar predictive approach could be applied to estimate the reflection coefficient of boron (σ_B) at any pH (i.e., by calculating $\sigma_{(H3BO3)}$ and $\sigma_{(H2BO3-)}$ and multiplying it by α_0 and α_1, respectively):

$$\sigma_B = \alpha_0 \times \sigma_{(H_3BO_3)} + \alpha_1 \times \sigma_{(H_2BO_3^-)} \quad (25)$$

where, σ_B = reflection coefficient of boron (dimensionless); $\sigma_{(H3BO3)}$ = reflection coefficient of boric acid (dimensionless); and $\sigma_{(H2BO3-)}$ = reflection coefficient of boric acid (dimensionless). Figure 3.35 compares boron reflection coefficient values (σ_B) predicted using equation (25) to those determined using nonlinear

parameter estimation from experimental data. The reflection coefficient of boron increased slightly as pH increased. However, due to the relatively small change in reflection coefficient with pH, the prediction was not as accurate as the overall permeability constant prediction. Note that since the overall transport of boron is more dependent on diffusive transport (i.e., permeation), small variations in solvent coupling would have a negligible effect on the overall estimate of boron transport using equations (24) and (25).

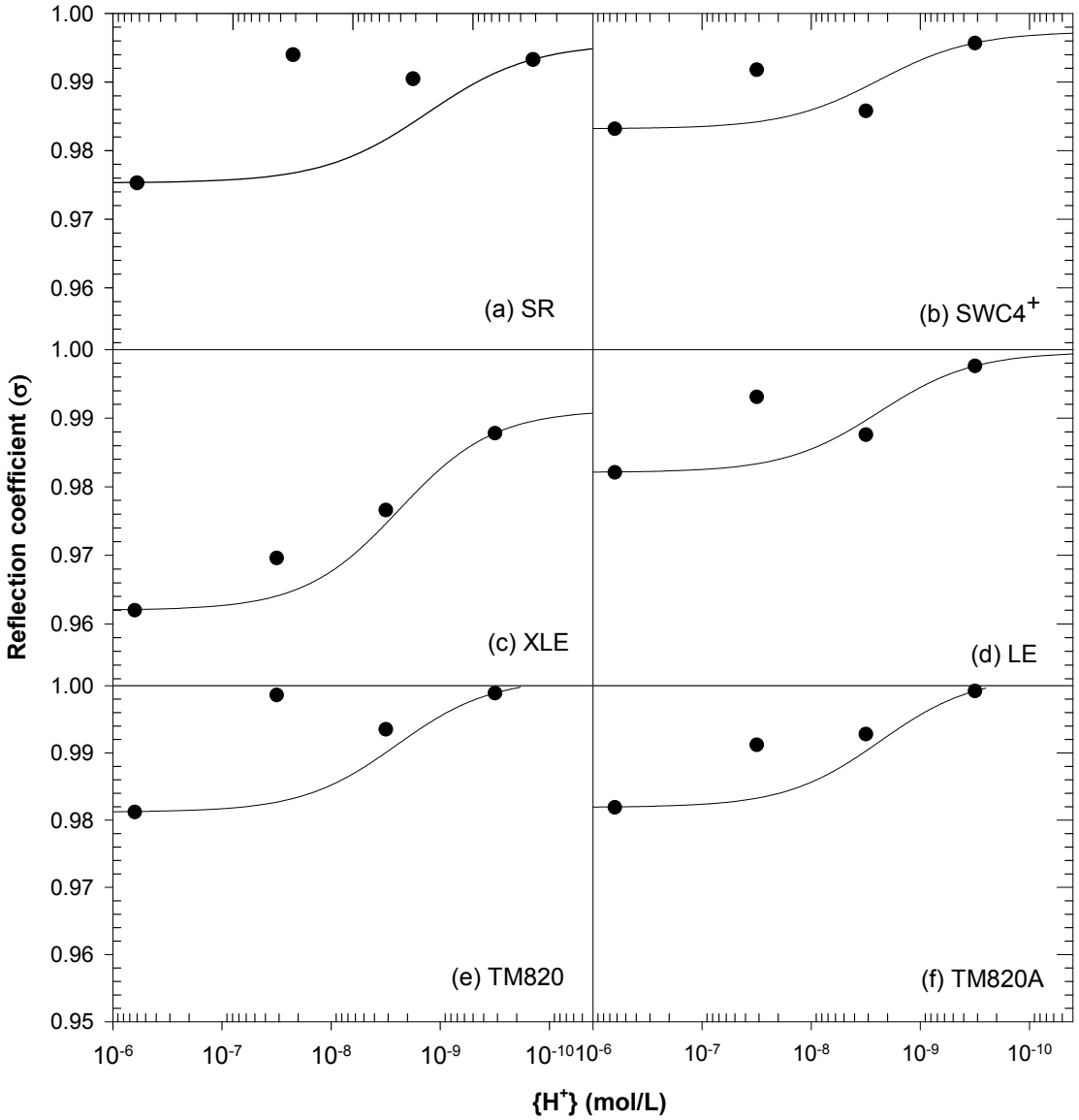

Figure 3.35 Prediction of change of reflection coefficient by pH.

3.4.5 Modeling of Experimental Results: Temperature Effect

(1) Mass Transfer Coefficients Estimation

Boron transport parameters were evaluated following the same method used for the pH effect experiments. In brief, mass transfer coefficients (k) were first calculated using the "flux decline induced by salinity method" and overall permeability constants ($P_{s,B}$) and reflection coefficients (σ_B) were then estimated using nonlinear parameter estimation method. The results are presented in table 3.11.

Table 3.11 Result of Parameter Estimation for Temperature Effect Experiment

		pH 6.2			pH 9.5		
		15 °C	**25 °C**	**35 °C**	**15 °C**	**25 °C**	**35 °C**
SR	k (cm/s)	0.00129	0.00195	0.00288	0.00113	0.00171	0.00252
	σ_B	0.999	0.999	0.999	0.9963	0.9933	0.9854
	$P_{s,B}$ (cm/s)	3.08E-05	6.63E-05	1.22E-04	7.35E-06	1.40E-05	2.15E-05
SWC4	k (cm/s)	0.00170	0.00258	0.00381	0.00177	0.00268	0.00396
	σ_B	0.9997	0.9943	0.9826	0.999	0.999	0.9974
	$P_{s,B}$ (cm/s)	1.77E-05	3.69E-05	6.97E-05	4.19E-06	8.29E-06	1.24E-05
XLE	k (cm/s)	0.00181	0.00275	0.00406	0.00158	0.00240	0.00355
	σ_B	0.9771	0.9718	0.959	0.994	0.9878	0.9812
	$P_{s,B}$ (cm/s)	2.35E-05	5.62E-05	9.96E-05	5.80E-06	9.48E-06	1.52E-05
LE	k (cm/s)	0.00154	0.00234	0.00346	0.00140	0.00212	0.00313
	σ_B	0.9968	0.9917	0.9861	0.999	0.999	0.996
	$P_{s,B}$ (cm/s)	1.73E-05	3.63E-05	7.00E-05	4.00E-06	7.60E-06	1.16E-05
TM820	k (cm/s)	0.00137	0.00208	0.00308	0.00120	0.00182	0.00269
	σ_B	0.999	0.9967	0.9953	0.999	0.999	0.9971
	$P_{s,B}$ (cm/s)	2.23E-05	4.75E-05	8.93E-05	4.72E-06	9.04E-06	1.35E-05
TM820A	k (cm/s)	0.00194	0.00294	0.00435	0.00169	0.00256	0.00378
	σ_B	0.9956	0.9956	0.9934	0.999	0.999	0.998
	$P_{s,B}$ (cm/s)	1.26E-05	2.73E-05	5.14E-05	3.05E-06	5.97E-06	8.76E-06

For all membranes tested, both mass transfer coefficients and permeability constants increased as temperature increased. Alternatively, reflection coefficients generally decreased as temperature increased, while the temperature dependency varied largely from membrane to membrane. Consistent with the previous results, the mass transfer coefficient (k) was not affected by pH, but the overall boron permeability constants ($P_{s,B}$) were significantly affected by pH. Experimental data and model predictions using transport parameters in table 3.11 are presented in figures 3.36 and 3.37. The model matched experimental data very well.

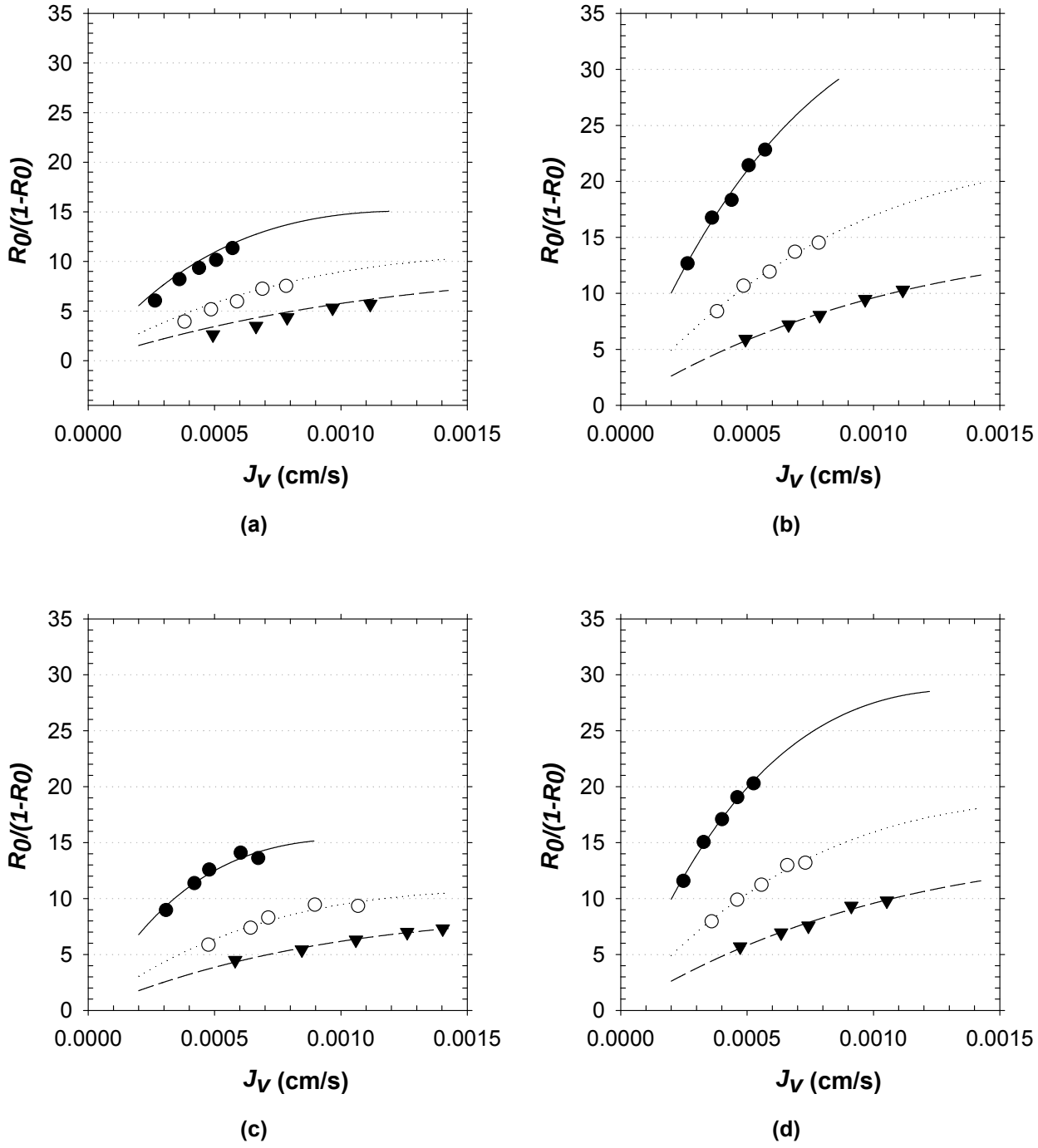

Figure 3.36 Experimental data and curve-fit from Spiegler-Kedem model for boron transport in temperature effect experiment at pH 6.2: (a)SR (b)SWC4+ (c)XLE (d)LE (e)TM820 (f)TM820A.

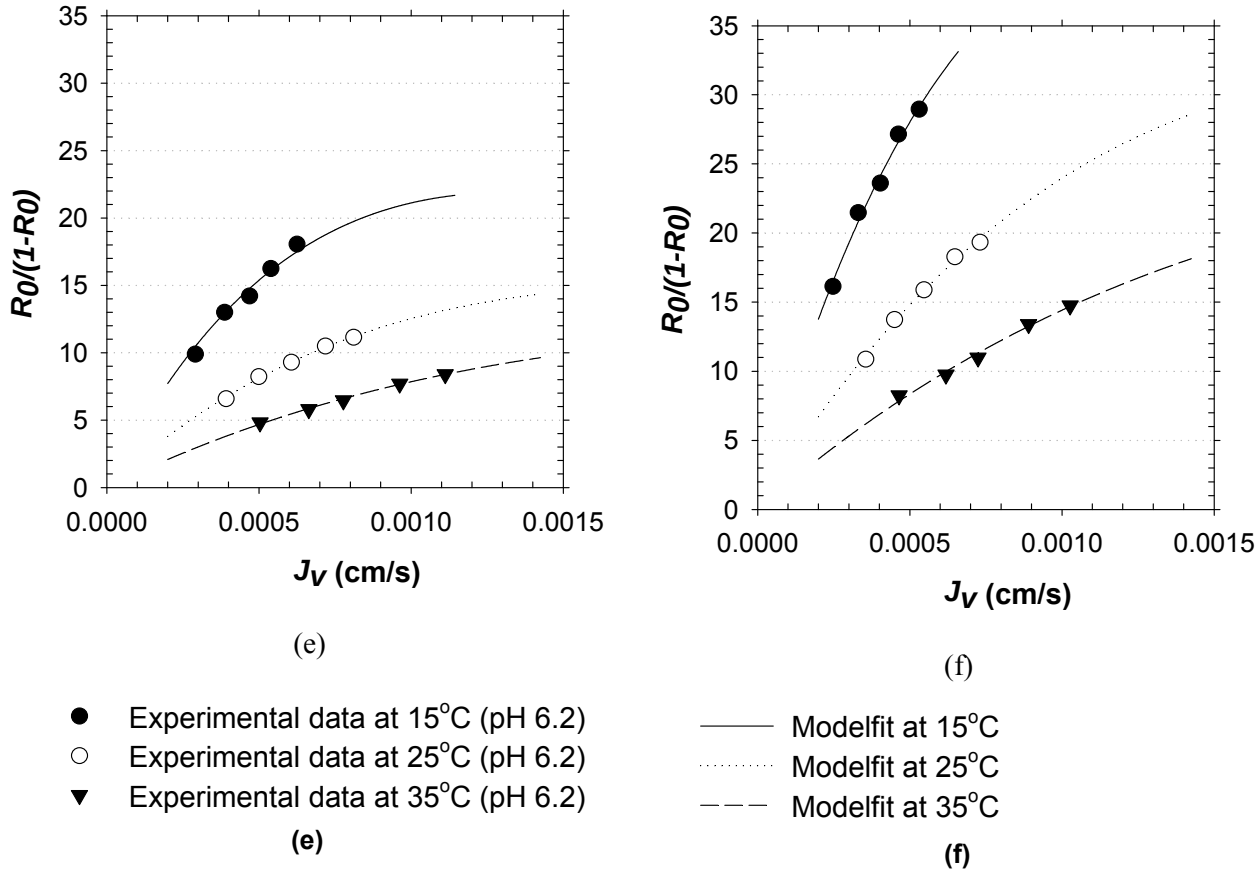

Figure 3.36 Experimental data and curve-fit from Spiegler-Kedem model for boron transport in temperature effect experiment at pH 6.2: (a)SR (b)SWC4+ (c)XLE (d)LE (e)TM820 (f)TM820A (continued).

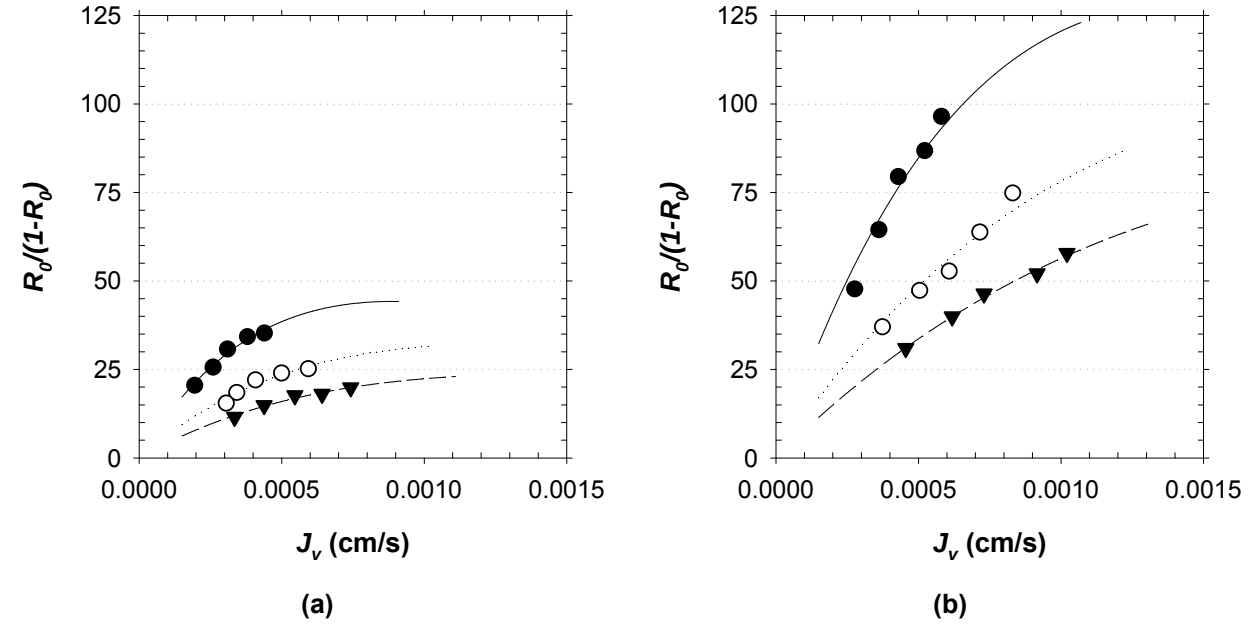

Figure 3.37 Experimental data and curve-fit from Spiegler-Kedem model for boron transport in temperature effect experiment at pH 9.5: (a)SR (b)SWC4+ (c)XLE (d)LE (e)TM820 (f)TM820A.

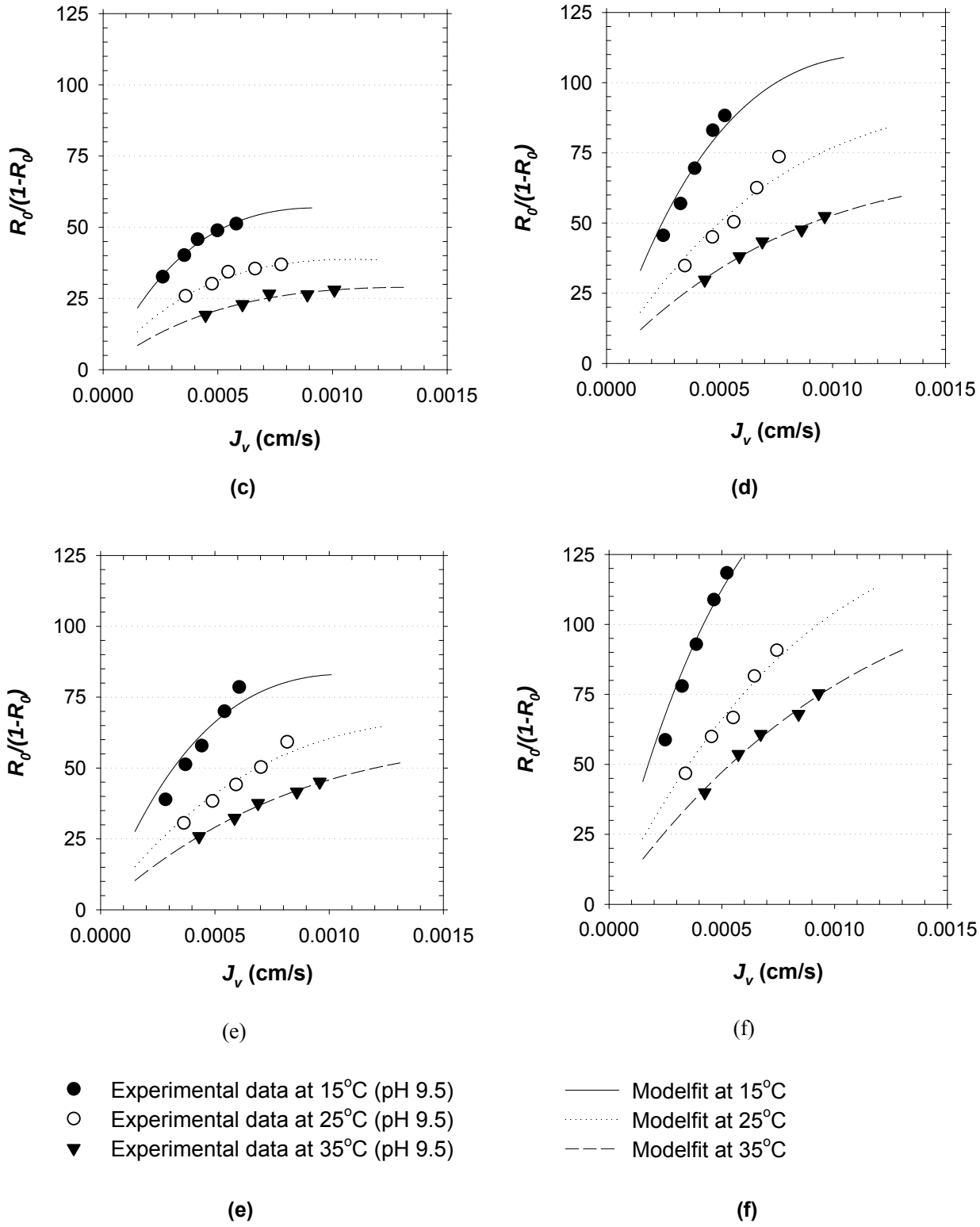

Figure 3.37 Experimental data and curve-fit from Spiegler-Kedem model for boron transport in temperature effect experiment at pH 9.5: (a)SR (b)SWC4+ (c)XLE (d)LE (e)TM820 (f)TM820A (continued).

An earlier study (Sourirajan, 1970) suggested the following correlations for describing the temperature-dependence of mass transfer coefficients and solute transport parameters in a sodium chloride – water system:

$$k \propto \exp(0.005T) \tag{26}$$

$$\left(\frac{D_{AM}K}{\Delta x}\right) \propto \exp(0.005T) \tag{27}$$

where, $(D_{AM}K/\Delta x)$ = solute transport parameter (LT^{-1}); D_{AM} = diffusion coefficient of solute in the membrane (L^2T^{-1}); K = partition coefficient between solvent (water) and membrane (dimensionless) and Δx = thickness of membrane (L). Considering the similarity between the permeability constant and the solute transport parameter, the correlations might be applicable to our experimental results for predicting the temperature dependency of permeability constants. However, due to the differences in solute concentration and other experimental conditions, the value of the exponent (0.005) in both equations might not be applicable to this work, so nonlinear regression for both mass transfer coefficients and permeability constants was performed assuming the pre-exponent value was unknown.

Figure 3.38 shows the result of nonlinear regression and compares the experimentally obtained mass transfer coefficients (k) and those predicted using equation (26) with the fitted exponent. The exponential function precisely predicted the change of mass transfer coefficient, with most of the correlation coefficients (R^2) over 0.99. It was noteworthy that a pre-exponent value of 0.04 was predicted for every membrane even at different pH conditions. Therefore, the temperature dependence of the boron mass transfer coefficient could be expressed by the following equation:

$$k = k_0 \exp(0.04T) \tag{28}$$

where, k_0 = a constant that has a different experimentally determined value for each membrane. Once the mass transfer coefficient at 25 ^oC is estimated, mass transfer coefficients at any temperatures can be predicted using the following equation:

$$k_t = k_{25} \exp 0.04(T - 298) \tag{29}$$

where, k_t = mass transfer coefficient of boron at t ^oC (LT^{-1}); k_{25} = mass transfer coefficient of boron at 25 ^oC (LT^{-1}) and T = absolute temperature (K). This correlation might be applicable to calculate k_t with known value of mass transfer coefficient at any temperature not only at 25 ^oC.

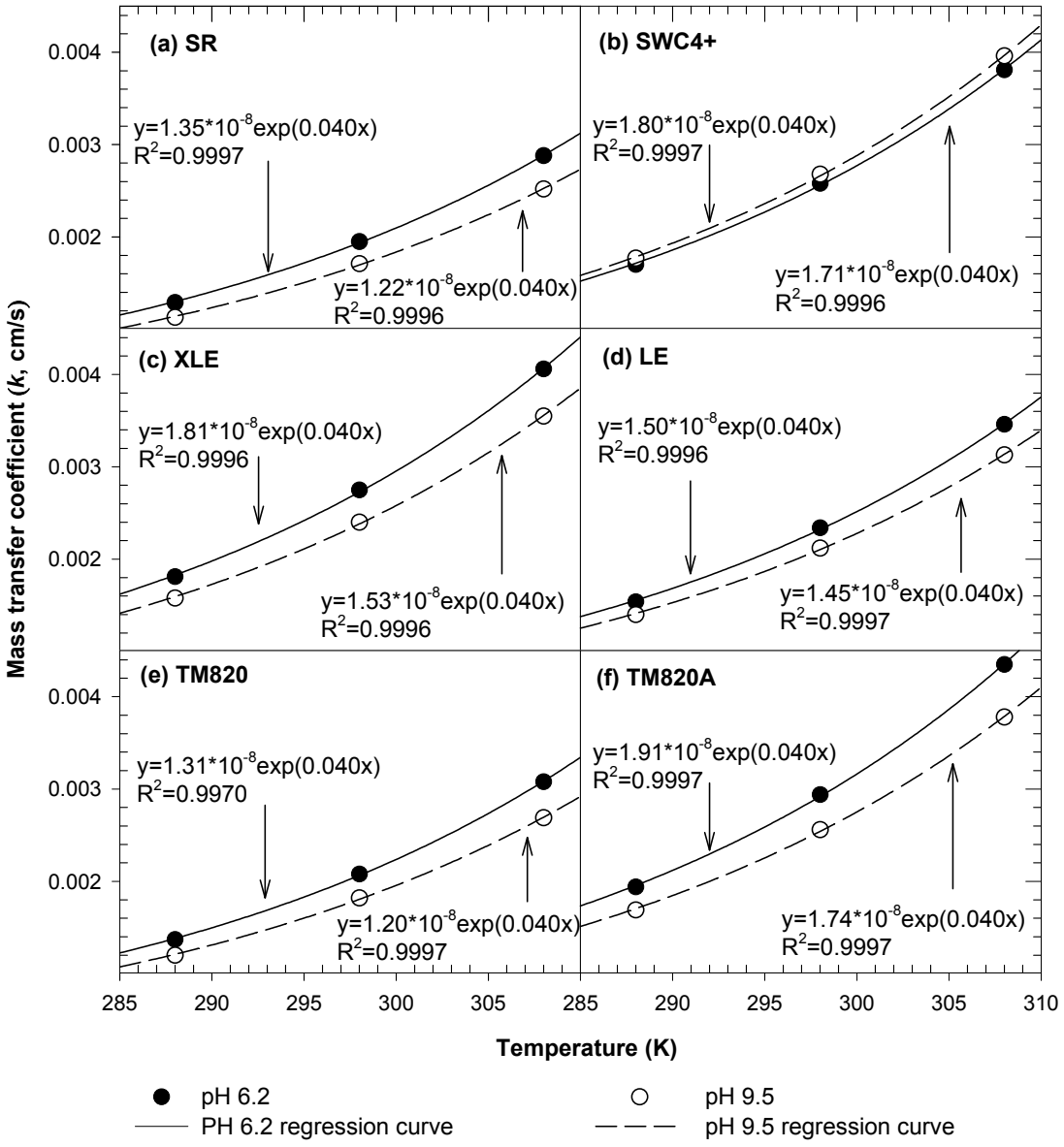

Figure 3.38 Prediction of mass transfer coefficients by temperature change.

(2) Permeability Constants Estimation

The permeability constants of boric acid ($P_{s(H3BO3)}$) and borate ($P_{s(H2BO3-)}$) at 15, 25, and 35 ^{o}C were estimated from the experimental data at pHs 6.2 and 9.5 using the same method used during the pH effect experiment. Due to the possible errors originating from the use of different membrane sheets at pH 6.2 and pH 9.5, the SR and XLE membranes were not included in this estimation.

First, salt concentrations at the membrane wall (C_m) were estimated from the mass transfer coefficient and the experimental data using equation (23). Using temperature and the estimated wall concentration of salt, the boric acid apparent acid constant (K_{a1}') was calculated (table 3.12). In spite of the decreased salt concentrations at the membrane wall (C_m), the boric acid apparent acid constant (K_{a1}') was reduced as temperature increased due to the dominant effect of temperature in equation (23). The K_{a1}' was not dependent on pH or temperature. The fractions of boric acid (α0) and borate (α1) were estimated from equations (20) and (21) using the K_{a1}' calculated above. Finally, using equation (24), boric acid and borate permeability constants for each membrane at 15, 25, and 35 °C were obtained from the overall permeability constants of boron (Ps,B) at two different pH of 6.2 and 9.5 and α0 and α1 at each pH. The resulting permeability constants are presented in table 3.13. This analysis suggested that permeability constants of boric acid and borate increased in proportion to temperature.

Using the data in table 3.13, the permeability constants of boric acid and borate at different temperatures were predicted from nonlinear parameter estimation and compared with experimental data (figure 3.39). Boric acid permeability matched well with the model predictions, while some minor deviations were observed with borate. In contrast to the mass transfer coefficient, pre-exponent values of the permeability constant were dependent on the type of membrane, though the dependency was slight. It was notable that boric acid and borate had similar pre-exponent values. For the tested membranes, the pre-exponent values ranged from 0.066 to 0.070, depending on the boron species and membrane.

Table 3.12 Calculation of the Apparent First Acid Constants for Temperature Effect Experiment

		pH 6.2				pH 9.5			
		***k* of salt (cm/s)**	**C_m of salt (mg/L)**	**Chlor-inity (‰)**	**pK_{a1}'**	***k* of salt (cm/s)**	**C_m of salt (mg/L)**	**Chlor-inity (‰)**	**pK_{a1}'**
SWC4+	15 °C	0.00163	45,786	24.86	8.69	0.00170	45,060	24.46	8.70
	25 °C	0.00248	44,387	24.10	8.61	0.00258	44,308	24.05	8.61
	35 °C	0.00366	43,401	23.56	8.55	0.00381	42,399	23.02	8.55
LE	15 °C	0.00148	45,865	24.90	8.69	0.00134	46,811	25.41	8.69
	25 °C	0.00225	44,836	24.34	8.61	0.00203	46,160	25.06	8.60
	35 °C	0.00332	43,778	23.77	8.54	0.00300	44,033	23.90	8.54
TM820	15 °C	0.00132	49,963	27.12	8.67	0.00115	51,364	27.88	8.66
	25 °C	0.00200	47,399	25.73	8.59	0.00175	49,100	26.65	8.58
	35 °C	0.00295	45,542	24.72	8.53	0.00259	45,689	24.80	8.53
TM820A	15 °C	0.00186	43,456	23.59	8.71	0.00162	44,439	24.12	8.70
	25 °C	0.00283	42,460	23.05	8.63	0.00246	43,784	23.77	8.62
	35 °C	0.00418	41,629	22.60	8.56	0.00363	42,134	22.87	8.55

Table 3.13 Calculation of Permeability Constants of Boric Acid and Borate at Different Temperature

	Temperature	pH	$P_{s,B}$ (cm/s)	α_0	α_1	$P_{s(H3BO3)}$ (cm/s)	$P_{s(H2BO3-)}$ (cm/s)
SWC4+	15 °C	6.2	1.77E-05	0.9967	0.0033	1.77E-05	2.10E-06
		9.5	4.19E-06	0.1341	0.8659		
	25 °C	6.2	3.69E-05	0.9961	0.0039	3.69E-05	7.08E-06
		9.5	8.29E-06	0.1141	0.8859		
	35 °C	6.2	6.97E-05	0.9956	0.0044	6.97E-05	1.18E-05
		9.5	1.24E-05	0.1009	0.8991		
LE	15 °C	6.2	1.73E-05	0.9968	0.0032	1.73E-05	1.94E-06
		9.5	4.00E-06	0.1341	0.8659		
	25 °C	6.2	3.63E-05	0.9961	0.0039	3.63E-05	6.38E-06
		9.5	7.60E-06	0.1118	0.8882		
	35°C	6.2	7.00E-05	0.9954	0.0046	7.00E-05	1.10E-05
		9.5	1.16E-05	0.0988	0.9012		
TM820	15 °C	6.2	2.23E-05	0.9966	0.0034	2.23E-05	2.18E-06
		9.5	4.72E-06	0.1263	0.8737		
	25 °C	6.2	4.75E-05	0.9968	0.0032	4.75E-05	7.45E-06
		9.5	9.04E-06	0.1073	0.8927		
	35 °C	6.2	8.93E-05	0.9953	0.0047	8.93E-05	1.26E-05
		9.5	1.35E-05	0.0968	0.9032		
TM820A	15 °C	6.2	1.26E-05	0.9969	0.0031	1.26E-05	1.54E-06
		9.5	3.05E-06	0.1368	0.8632		
	25 °C	6.2	2.73E-05	0.9963	0.0037	2.73E-05	5.10E-06
		9.5	5.97E-06	0.1165	0.8835		
	35 °C	6.2	5.14E-05	0.9957	0.0043	5.14E-05	8.33E-06
		9.5	8.76E-06	0.1009	0.8991		

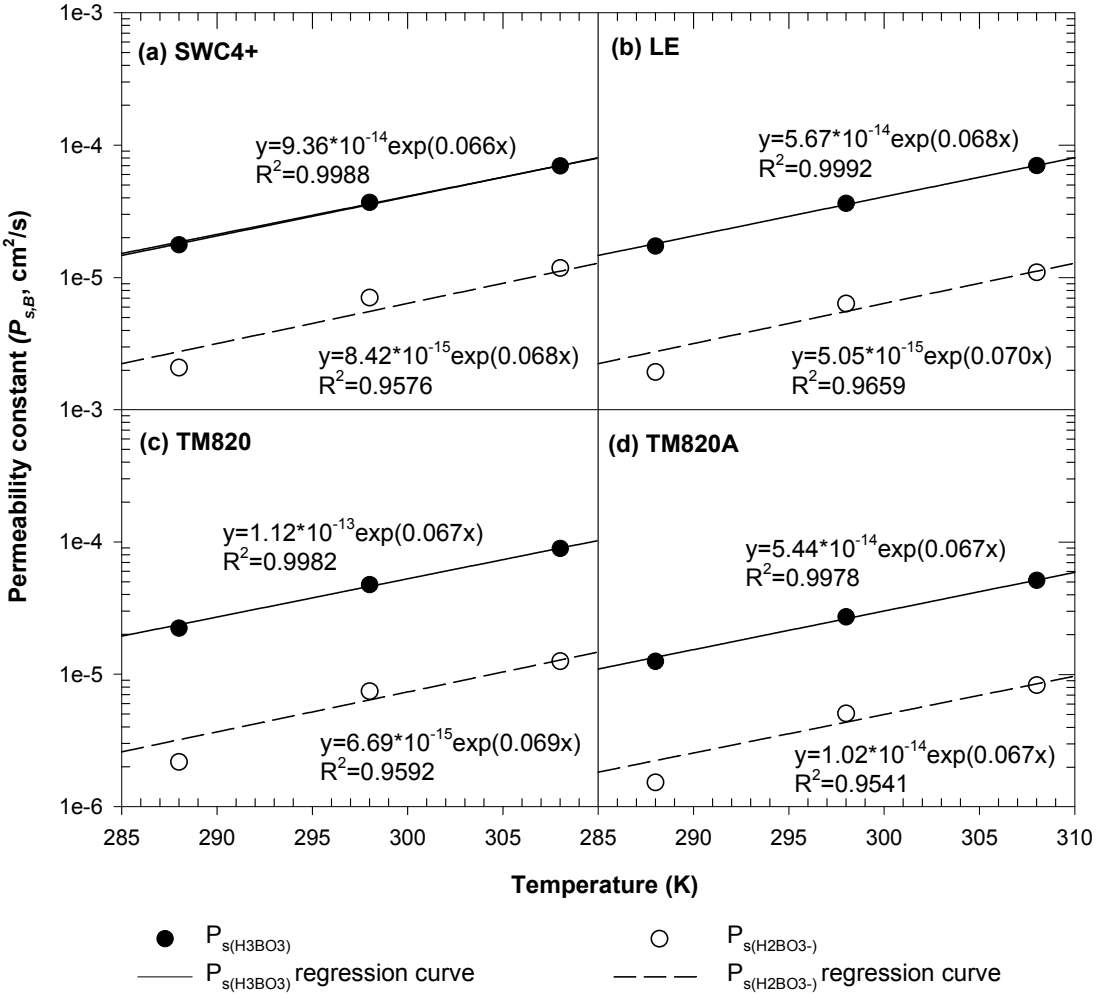

Figure 3.39 Prediction of permeability constants of boric acid and borate by temperature change.

Based on the results, the following equations are proposed to predict the temperature effect on the permeability constants of boric acid ($P_{s(H3BO3)}$) and borate ($P_{s(H2BO3-)}$):

$$P_{s(H_3BO_3)} = P_{s(H_3BO_3)0} \exp(a \times T) \tag{29}$$

$$P_{s(H_2BO_3^-)} = P_{s(H_2BO_3^-)0} \exp(b \times T) \tag{30}$$

where, $P_{s(H3BO3)0}$ = pre-exponential value of boric acid [LT^{-1}]; $P_{s(H2BO3-)0}$ = pre-exponential value of borate [LT^{-1}]; a = pre-exponent value of boric acid [T^{-1}]; and b = pre-exponent value of borate [T^{-1}]. $P_{s(H3BO3)0}$, $P_{s(H2BO3-)0}$, a, and b are constants having different values depending on the type of membrane. From equations

(24), (29), and (30), the following equation was derived to predict the effect of pH and temperature on the overall boron permeability constant ($P_{s,B}$).

$$P_{s,B} = \alpha_0 \times P_{s(H_3BO_3)25} \exp(a(T-298)) + \alpha_1 \times P_{s(H_2BO_3^-)25} \exp(b(T-298)) \quad (31)$$

where, $P_{s,B}$ = overall permeability constant of boron (LT^{-1}); $P_{s(H3BO3)25}$ = permeability constant of boric acid estimated at 25 °C (LT^{-1}); $P_{s(H2BO3-)25}$ = permeability constant of borate estimated at 25 °C (LT^{-1}); α_0 = fraction of boric acid (dimensionless); α_1=fraction of borate (dimensionless); and T = absolute temperature (K). Values of a and b for the membranes tested in this experiment were provided in table 3.14.

Table 3.14 Constants *a* and *b* for the Permeability Constants Estimation

	SWC4+	LE	TM820	TM820A
a (K^{-1})	0.066	0.068	0.067	0.067
b (K^{-1})	0.068	0.068	0.069	0.067

Boric acid and borate reflection coefficients were estimated using the same method as that used for permeability constant estimation, and the results are shown in table 3.15. Figure 3.40 shows the change in reflection coefficient (σ) with temperature. Temperature did not appear to affect the reflection coefficient significantly. Since the difference in values of reflection coefficients is very small, some deviations might have resulted from experimental errors. As previously described, this slight change could be neglected since contribution of boron transport by coupling is very small compared to diffusive transport.

The parameter estimation method used for this work (i.e., using modeling equations to predict parameters at different pH and temperature conditions) would likely be applicable for the prediction of pilot- or full-scale boron removal performance.

Table 3.15 Calculation of Reflection Coefficients of Boric Acid and Borate at Different Temperature

	Temperature	pH	σ	α_0	α_1	$\sigma_{(H3BO3)}$	$\sigma_{(H2BO3-)}$
SWC4+	15 °C	6.2	0.9997	0.9967	0.0033	0.9997	0.9989
		9.5	0.9990	0.1341	0.8659		
	25 °C	6.2	0.9943	0.9961	0.0039	0.9826	0.9971
		9.5	0.9990	0.1141	0.8859		
	35 °C	6.2	0.9826	0.9956	0.0044	0.9917	0.9993
		9.5	0.9974	0.1009	0.8991		
LE	15 °C	6.2	0.9968	0.9968	0.0032	0.9990	0.9990
		9.5	0.9990	0.1341	0.8659		
	25 °C	6.2	0.9917	0.9961	0.0039	0.9953	0.9969
		9.5	0.9990	0.1118	0.8882		
	35 °C	6.2	0.9861	0.9954	0.0046	0.9956	0.9994
		9.5	0.9960	0.0988	0.9012		
TM820	15 °C	6.2	0.9990	0.9966	0.0034	0.9990	0.9990
		9.5	0.9990	0.1263	0.8737		
	25 °C	6.2	0.9967	0.9968	0.0032	0.9967	0.9990
		9.5	0.9990	0.1073	0.8927		
	35 °C	6.2	0.9953	0.9953	0.0047	0.9953	0.9969
		9.5	0.9971	0.0968	0.9032		
TM820A	15 °C	6.2	0.9956	0.9969	0.0031	0.9956	0.9995
		9.5	0.9990	0.1368	0.8632		
	25 °C	6.2	0.9956	0.9963	0.0037	0.9956	0.9994
		9.5	0.9990	0.1165	0.8835		
	35 °C	6.2	0.9934	0.9957	0.0043	0.9934	0.9983
		9.5	0.9980	0.1009	0.8991		

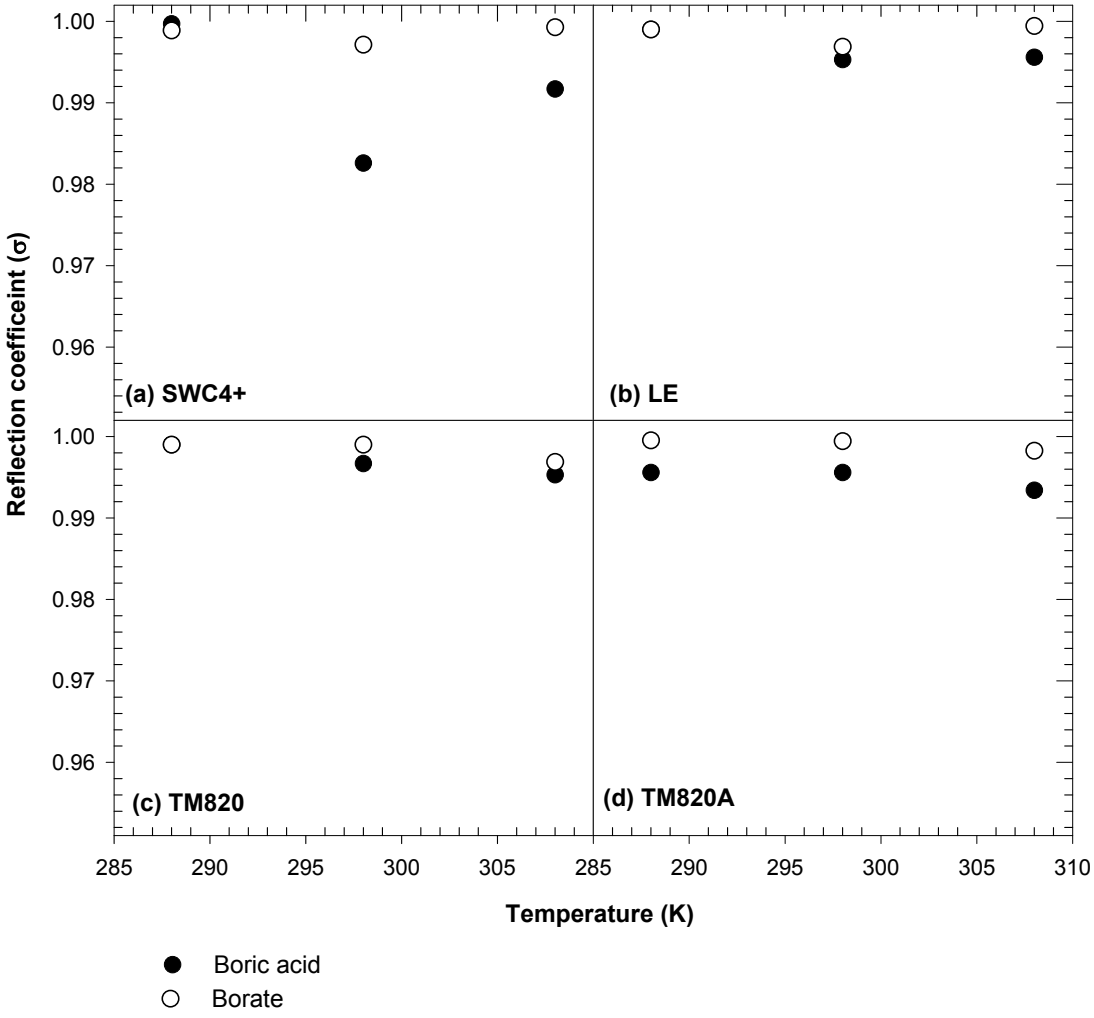

Figure 3.40 Change of reflection coefficients by temperature.

4. National Reconnaissance Study

4.1 Overview

Concentrations of major ionic species in the feed, concentrate, and permeate samples from six SWRO plants (designated as plants A, B, C, D1, D2, and D3) and three brackish water RO plants (designated as plants E, F, and G) identified in table 4.1 were analyzed. This set of selected treatment plants represented a wide spectrum of different treatment options. Among six seawater plants, plants A, B and C use the Pacific Ocean as feed and plants D1, D2, and D3 use the Atlantic Ocean. Water samples from plant A and plant C were obtained from pilot-scale units, and those from plants B, D1, D2, and D3 were obtained from full-scale systems. Seawater treatment plants recovery varied from 40 to 50%, and brackish water treatment plants recovery varied from 20 to 85%. Seawater treatment plants were equipped with either single-pass or double-pass SWRO membrane units with operating pressures ranging from 545 to 966 psi. Some of the membranes in these plants were the same models that were used in the bench-scale experiments performed at Georgia Tech. The target brackish water treatment plants were equipped with either single-pass or double-pass brackish water RO membrane units with operating pressures ranging from 125 to 245 psi. Plants C and G consisted of multiple trains, and samples from each train were analyzed and compared. Detailed information on the location, system configuration, and operating condition of all the plants investigated are summarized in table 4.1.

4.2 Material and Methods

Samples representing a cold season (February – March) and a hot season (August–September) were separately collected from participating utilities during the project. For quality assurance/quality control (QA/QC) purposes, *Sampling Instruction* and *Sample Information* forms were developed by Georgia Institute of Technology and distributed to participating utilities prior to sampling. All sampling was performed following the instructions specified in these forms, which are attached in the appendix. Concentrations of several ionic species including boron, sodium, calcium, magnesium, chloride, and sulfate were measured at different stages along the treatment trains. All measurements were duplicated. The concentrations of boron, sodium, magnesium, and calcium were determined by Inductively Coupled Plasma-Atomic Emission Spectroscopy and chloride and sulfate were analyzed by Ion Chromatography. An Ion 5 conductivity meter (Hach, Loveland, CO) was used to measure the sample conductivity. Detailed descriptions of equipment, experimental conditions, and detection limits of these analyses were provided in section 3.

Table 4.1 Operating Condition of Water Treatment Plants

Plant	Location	Train	Feed water	Array of the membrane	Model of the membrane, manufacturer	Operating pressure	Permeate flow rate	Reco-very
A	Carlsbad, California	-	Seawater (Pacific)	Single pass	SWC3, Hydranautics	810 psi	17.2 gpm	50%
B	Abila Beach, California	-	Seawater (Pacific)	Double pass	FT30, Dow (Filmtec)	880 psi	225 gpm	45%
C	Corte Madera, California	#1	Seawater (Pacific)	Single pass	TM820A-400, Toray	560 psi	2.5 gpm	40%
		#2			SW30HR LE-400, Dow(Filmtec)	660 psi	2.9 gpm	40%
		#3			SWC4+, Hydranautics	545 psi	2.2 gpm	40%
D1	Cayman island		Seawater (Atlantic)	Double pass (Sampling performed after the first pass)	SWHR30-380, Dow (Filmtec)	802 psi	574gpm	38%
D2					SWHR30-380, Dow (Filmtec)	966psi	455 gpm	40%
D3					SWHR30-380, Dow (Filmtec)	945 psi	321 gpm	42%
E	El Segundo, California	-	Brackish water	Single pass	ESPA2 (Hydranautics)	245 psi	1,450 gpm	85%
F	Venice, Florida	-	Brackish groundwater	Single pass	8821 TFC HR, Fluid systems	161 psi	750 gpm	50%
G	Mountain Pleasant, South Carolina	#1	Brackish groundwater	Double pass	ESPA1&2, Hydranautics	125 psi	400 gpm	80%
		#2		Double pass	ESPA1&2, Hydranautics	145 psi	350 gpm	80%
		#3		Double pass	ESPA1&2, Hydranautics	125 psi	500 gpm	80%
		#4		Double pass	ESPA1&2, Hydranautics	125 psi	486 gpm	80%

4.3 Results and Discussions

Results obtained from the National Reconnaissance Study are summarized in tables 4.2 and 4.3. In general, rejection of boron was significantly lower than that of other species in all the samples tested. Boron rejection in seawater treatment plants ranged from 65 to 85%, while boron rejection in the brackish water treatment plants (plants E, F, and G) ranged from 0 to 68%. Note that percent rejection (*R (%)*) was calculated as follows:

$$R\ (\%) = \left(1 - \frac{C_p}{C_f}\right) \times 100 \qquad (32)$$

where C_p = concentration in the permeate; C_f = concentration in the feed (not concentrate). The following is a summary of the observations made during this study:

Plant A. During both cold and hot seasons, relatively high rejection of all measured ionic species (99.35 to 99.95%) was observed. However, the rejection of boron (~70%) was much lower than those of ionic species. This boron rejection was much lower than that shown in the bench-scale experiments detailed in the previous section. It was partly due to the

Table 4.2 Analysis of Cold Season Water Samples from Four Water Facilities

Plant		pH	Conductivity	B	Na	Mg	Ca	Cl	SO_4
A	Feed	6.69	56,400	4.46	11,462	1140	378	16,856	2,104
	Concentrate	-	106,600	7.32	26,295	2339	769	35,269	4,612
	Permeate	5.33	387	1.36	75.02	0.54	0.18	92.56	1.65
	Rejection	-	99.31	**69.54**	99.35	99.95	99.95	99.45	99.92
E	Feed	6.24	1,186	0.48	640	23.5	60.28	112.1	224.7
	Concentrate	-	6,900	1.47	1,492	177.5	461	724.4	1936
	Permeate	6.32	23.10	0.24	12.81	0.025	0.022	ND	ND
	Rejection	-	98.05	**49.17**	98	99.89	99.96	100	-
F	Feed	7.10	3,570	0.11	669	159.5	412.6	407.2	1,556
	Concentrate	-	6,290	0.15	1,492	311.5	806.4	781.6	3,011
	Permeate	6.04	38	0.051	25.52	0.17	0.44	2.97	3.15
	Rejection	-	98.94	**53.20**	96.19	99.89	99.89	99.27	99.80
G Train 1	Feed	8.31	1,713	2.88	688	0.44	1.44	112.6	ND
	Concentrate	-	7,420	2.04	2,802	1.25	4.32	502.1	ND
	Permeate	8.13	89.10	3.39	45.36	0.024	0.028	ND	ND
	Rejection	-	94.80	**-17.76**	93.41	94.47	98.03	100	-
G Train 2	Feed	8.55	1,615	2.66	707	0.32	1.19	98.84	ND
	Concentrate	-	6,070	2.91	2513	0.96	3.68	378.2	ND
	Permeate	8.35	120.80	3.16	33.42	0.019	0.011	ND	ND
	Rejection	-	92.52	**-18.88**	95.28	94.09	99.07	100	-
G Train 3	Feed	8.4	1,760	3.01	900	0.38	1.46	118.8	ND
	Concentrate	-	7,420	2.31	2552	1.20	4.56	521.7	ND
	Permeate	8.16	98.10	2.56	33.23	0.025	0.022	ND	ND
	Rejection	-	94.43	**15.17**	96.31	93.37	98.48	100	-
G Train 4	Feed	8.35	1,827	3.37	842	0.49	1.56	119.3	ND
	Concentrate	-	7,580	2.83	2,552	1.50	4.91	506.7	ND
	Permeate	8.06	184.90	3.00	25.91	0.025	0.029	ND	ND
	Rejection	-	89.88	**10.99**	96.93	94.90	98.11	100	-

Table 4.3 Analysis of Hot Season Water Samples from Six Water Facilities (mg/L, except conductivity in μS)

Plant		pH	Conductivity	B	Na	Mg	Ca	Cl	SO_4
A	Feed	8.03	50,700	4.00	9,780	609.5	1,182	18,968	2,569
	Concentrate	-	91,500	7.05	19,597	806.1	1,767	32,644	4603
	Permeate	6.58	510	1.17	70.23	0.51	1.50	142.26	4.94
	Rejection	-	98.99	**70.55**	99.28	99.92	99.87	99.25	99.81
B	Feed	8.2	49,740	4.19	10,434	614.4	1,190	19,183	2606
	Concentrate	-	76,000	7.18	27,384	791.0	1,745	32,123	4773
	Permeate	7.4	570	0.82	85.23	1.38	4.60	158.47	10.61
	Rejection	-	98.85	**80.43**	99.18	99.78	99.61	99.17	99.59
C (Conventional Pretreatment)	Feed	8.01	42,580	3.62	7,864	567.20	1,049	15,970	2112
	Concentrate	-	-	-	-	-	-	-	-
	TM820A Permeate	7.73	320	1.13	49.30	0.44	1.78	92.94	5.40
	LE Permeate	7.56	220	0.61	32.34	0.21	1.05	65.98	4.04
	SWC4+ Permeate	7.74	100	0.52	29.12	ND	0.12	33.19	2.28
	TM820A Rejection	-	99.47	**68.81**	99.37	99.92	99.83	99.42	99.74
	LE Rejection	-	99.64	**82.93**	99.59	99.96	99.90	99.59	99.81
	SWC4+ Rejection	-	99.83	**85.42**	99.63	100.00	99.99	99.79	99.89
C (Membrane Pretreatment)	Feed	7.5	43,054	3.64	8,340	573.90	1,053	15,884	2115
	Concentrate	-	-	-	-	-	-	-	-
	TM820A Permeate	6.00	240	0.99	45.82	0.21	1.08	68	5
	LE Permeate	6.02	180	0.54	39.43	ND	0.43	50.13	2.63
	SWC4+ Permeate	6.06	150	0.70	19.88	ND	0.09	41.99	2.28
	TM820A Rejection	-	99.60	**72.74**	99.45	99.96	99.90	99.57	99.77
	LE Rejection	-	99.70	**85.16**	99.53	100.00	99.96	99.68	99.88
	SWC4+ Rejection	-	99.75	**80.73**	99.76	100.00	99.99	99.74	99.89
D1	Feed	7.03	54,880	4.73	12,838	626.2	1,153	18,509	2551
	Concentrate	-	81,580	7.32	29,592	733.7	1,478	25,882	3859
	Feed End Permeate	5.80	375	0.78	60.32	0.44	1.63	100.25	5.76
	Brine End Permeate	5.97	886	1.55	157.4	1.18	3.74	255.31	9.22
	Feed End Rejection	-	99.55	**83.52**	99.53	99.93	99.86	99.46	99.77
	Brine End Rejection	-	98.94	**67.19**	98.77	99.81	99.68	98.62	99.64
D2	Feed	7.18	52,410	4.51	11,004	641.6	1197	18,996	2563
	Concentrate	-	83,550	7.07	28,304	830.5	1735	32,440	4479
	Feed End Permeate	6.42	464	0.85	47.48	0.91	2.79	124.03	16.48
	Brine End Permeate	6.39	2,198	1.56	301.3	8.93	29.43	657.64	75.13
	Feed End Rejection	-	99.48	**81.01**	99.57	99.86	99.77	99.35	99.36
	Brine End Rejection	-	97.55	**65.27**	97.26	98.61	97.54	96.54	97.07
D3	Feed	7.19	50,380	4.67	12,304	615.4	1,173	18,869	2598
	Concentrate	-	83,390	6.97	30,302	747.6	1,575	28,359	3928
	Feed End Permeate	6.56	334	0.94	45.39	0.23	1.11	87.18	11.41
	Brine End Permeate	6.27	2,651	1.59	402.3	10.87	37.20	783.17	87.58
	Feed End Rejection	-	99.64	**79.87**	99.63	99.96	99.91	99.54	99.56
	Brine End Rejection	-	97.11	**65.95**	96.73	98.23	96.83	95.85	96.63
E	Feed	6.32	1,429	0.71	537	96.95	86.90	168	213
	Concentrate	-	8,805	2.11	1,104	248.9	155.5	780	1445
	Permeate	5.27	38.05	0.35	9.34	ND	ND	2.33	0.24
	Rejection	-	97.34	**50.43**	98.26	100.00	100.00	98.61	99.89
F	Feed	7.06	4,775	0.12	901	326.2	173.6	320	1430
	Concentrate	-	10,380	0.19	1,932	535.8	256.5	566	2853
	Permeate	6.09	40.05	0.04	12.01	0.36	0.10	3.79	6.70
	Rejection	-	99.16	**67.83**	98.67	99.89	99.94	98.82	99.53

difference in operational mode and the rejection calculation method. In the lab-scale experiments, all the concentrate was recirculated to the feed, and the rejection was calculated based on the concentration in the feed, which was virtually identical to that in the concentrate. In contrast, the rejection for the plant data was calculated based on the concentration in the feed, which was lower than that in the concentrate. If rejection was based on the average concentration in the RO module (for example, arithmetic mean of the feed and the concentrate), the boron rejection would be 76.9% and 78% for cold and hot seasons, respectively. However, these values were still lower than those observed in the lab-scale experiments, primarily due to high recovery of the plant compared to the lab-scale experiments.

Rejections of ionic species and boron at plant A showed slight seasonal variation and the boron concentration in the permeate was 1.36 mg/L for the hot season and 1.18 mg/L for the cold season, which were higher than the World Health Organization's current water quality guideline value of 0.5 mg/L. However, these levels were within the current regulatory level of 1 mg/L (when one significant number is considered) established by the California Department of Health Services which were applicable to plant A.

As discussed in section 3, the rejection of boron was largely dependent on pH. In this plant, feed pH changed from 6.69 for cold season to 8.03 for hot season. However, there was only slight change in boron rejection from the pH change since the pH in the hot season was still much lower than the pK_{a1}' of seawater (8.68 at 25 ^{o}C)

Plant B. Only hot season samples were analyzed for plant B. While the rejection of ionic species was comparable to that from plant A, higher rejection of boron (approximately 80%) was observed, resulting in lower product water boron concentration (0.82 mg/L). The permeate boron concentration was in between the WHO guideline and the CDHS regulatory level. The higher boron rejection might be attributed to different membrane modules, higher operating pressure, and/or lower system recovery utilized in plant B.

Plant C. Plant C consisted of two trains with different pretreatment options: one with conventional pretreatment and the other with low-pressure membrane pretreatment. Each train consists of three vessels using membranes from three different manufacturers, which were the same models (i.e., TM820A, LE, and SWC4+) tested in bench-scale experiments. As shown in table 4.3, permeate with membrane pretreatment generally showed better salt rejection than that with

conventional pretreatment. For both pretreatment scenarios, rejection of boron was around 70% for the TM820A membrane and 80 to 85% for LE and SWC4+ membranes. Permeate boron concentrations were 0.61 and 0.54 mg/L for the LE membrane, 0.52 and 0.70 mg/L for the SWC4+ membrane, 1.13 and 0.99 mg/L for the TM820A membrane, after conventional and membrane pretreatments, respectively. There was a large difference in the boron rejection and permeate concentration between the bench-scale experiments and the full- or pilot-scale system. This discrepancy appeared to be due to the higher recovery and lower operating pressure of the full- or pilot-scale system. Contrary to the results of bench-scale experiments, the TM820A membrane had the lowest rejection among the three membranes. This might be because the bench-scale experiments represented only a small flat-sheet portion of the membrane unit not the entire spiral-wound module, which includes a spacer, glue, sealing, etc. It is also possible that bench-scale membranes did not truly represent the average performance of a given membrane due to lot-to-lot variability produced during the membrane manufacturing process. It was notable that the rejection of boron was largely dependent on the membranes, even though there was not much difference in the rejection of ionic species among the membranes tested.

Plants D1, D2, and D3. Plants D1, D2, and D3 were different double-pass systems adopting the same RO membranes, which are located in the Cayman Islands. Permeate samples were collected during the hot season from the brine side and feed side of permeate lines in each train. Because the retentates become concentrated as they move from the feed side to the brine side, permeates from the brine side contained higher salts and boron concentrations. Among the three plants, plant D3 showed the highest rejection of salts and boron, though the differences among plants were relatively small. There existed a large difference in boron rejection between permeates from the feed end and those from the brine end. Boron rejection of the feed side was approximately 80%, while that of the brine side was only about 65%. This observation is consistent with the arguments previously given for the differences between lab-scale and full- or pilot-scale data. For an accurate prediction in full- or pilot-scale processes, an increase in boron concentration in the retentate as membrane filtration proceeds should be factored.

Plant E and F. In both plants E and F, rejection of ionic species was relatively high, but boron rejections were less than 70%. Low overall boron rejection might be due to low feed concentration, single-pass configuration, or characteristics of the BWRO membranes installed in these plants. Since the feed water contained low boron concentrations

(0.48 for plant E and 0.11 mg/L for plant F for cold season and 0.71 for plant E and 0.12 mg/L for plant F for hot season), the product water contained less than 0.5 mg/L of boron and could meet projected regulatory level of the WHO.

Plant G. This plant consisted of double-pass RO processes in which a portion of permeate from the first-pass RO was further treated by second-pass RO. It was notable that the feed contained a significant amount of boron (i.e., approximately 3 mg/L). Recovery of the overall system was 80%, which was much higher than that in plants E and F. This plants showed very low rejection of the boron for every trains, even though it was operated with the pH higher than 8.3. Trains 1 and 2 appeared ineffective in removing boron, and concentration of boron in the product water was even higher that that in the feed water, which might have resulted from the combined effect of errors in sampling, time gaps between sampling, and/or errors in instrumental analysis. Poor boron removal may have resulted from the high percent recovery, but further investigation is required.

As previously discussed in section 3, pH is one of the most important factors that determine boron transport through the RO membranes. However, all the plants in this study operated at the pH lower than *pKa1'* of boron (8.68 for seawater at 25 °C). Therefore, the rejections of boron in the systems could be improved by optimization of the feed pH, if necessary

Generally, boron rejection of the field samples was much lower than that observed during the laboratory experiments, which was mainly due to higher recovery of the full- or pilot-scale systems. The laboratory experiment employed membrane coupons, which have relatively low area and system recovery, so change in feed concentration along the membrane surface was assumed to be negligible. However, in the full- or pilot-scale systems, high recoveries mean that feed water is gradually concentrated as it flows along the membrane surface. Hence, downstream membranes treat feed containing much higher boron concentrations, which results in lower overall boron rejections. This suggests that extrapolation of bench-scale rejection performance to full-scale systems would require mathematical models that account for nonhomogenous conditions along the membrane element. One approach (Mi et al., 2005) was to divide a spiral wound element into many smaller control volumes in which the water quality parameters could be assumed homogenous. Then the mass balances could be established based on sub-elements, resulting in a set of equations to describe the overall permeation of boron. It is noteworthy that equations developed in this study (such as equations (25) and (31)) serve as a basis for

such models that are specifically aimed toward accurate estimation of boron rejection in full-scale processes.

In summary, rejection of boron in the seawater desalination plants ranged from 65 to 85% and was dependent on membrane type, operating conditions, and sampling location in the membrane vessel (brine end versus feed end). Consequently, boron concentrations in the permeates from these plants were in compliance with a currently applicable regulation in the United States (CDHS action level of 1 mg/L) but higher than the current WHO guideline of 0.5 mg/L. Brackish water treatment plants also showed low rejection of boron. However, boron concentrations in the brackish water were generally low and the rejection of the BWRO is not likely to pose a concern.

5. Economic Evaluation of Boron Removal Processes

5.1 Overview

Several system configurations have been studied to reduce boron concentrations in the permeate from SWRO desalination plants. As previously discussed in this report, boron rejection was greatly enhanced as pH increased. However, due to possible scale formation at relatively high pH (i.e., primarily due to hardness and alkalinity), increasing the feed pH for a single-pass RO process has been primarily practiced with lower salinity waters such as brackish waters (Mukhopdyay and Whipple, 1997). In a typical double-pass process, which might be able to meet the regulatory level of boron, permeate of an SWRO system operating at a low or neutral feed pH is further treated by a brackish RO unit operating at an elevated feed pH. Unfortunately, a simple double-pass configuration might incur high operating costs mainly due to low system recovery. A stringent boron regulation and high operating costs of simple double-pass configurations necessitate alternative design options including multistage RO processes and the addition of boron specific ion exchange units. In this study, six representative RO desalination configurations were selected and their economics were compared.

5.2 Representative RO System Configurations for Boron Reduction

Six representative RO desalination process configurations currently practiced to control boron were selected for the cost analysis. Simplified schematics of these process options, of which costs will be analyzed in the following chapter, are presented in figure 5.1.

(1) Single-Pass RO System

Figure 5.1(a) shows the schematic of a conventional single-pass RO process. For the treatment of seawaters, a typical single-pass process would operate at a recovery from 40 to 50% and a permeate flux of 7 to 9 gfd (12 to 15 L/m^2-hr). For example, the target recovery of one of the plants tested in the National Reconnaissance study of this project, which operated in a single-pass mode (i.e., plant C in table 4.1), was 40%. Typical feed pH for these systems ranges from 6.0 to7.5 (acidified) or 7.8 to 8.2 (natural) (see tables 4.2 and 4.3). Under these conditions, the single-pass SWRO membrane unit generally produced permeate with salinity within the potable limits (i.e., less than 500 mg/L TDS) from the simulation data. However, boron concentrations in the permeate were likely to be

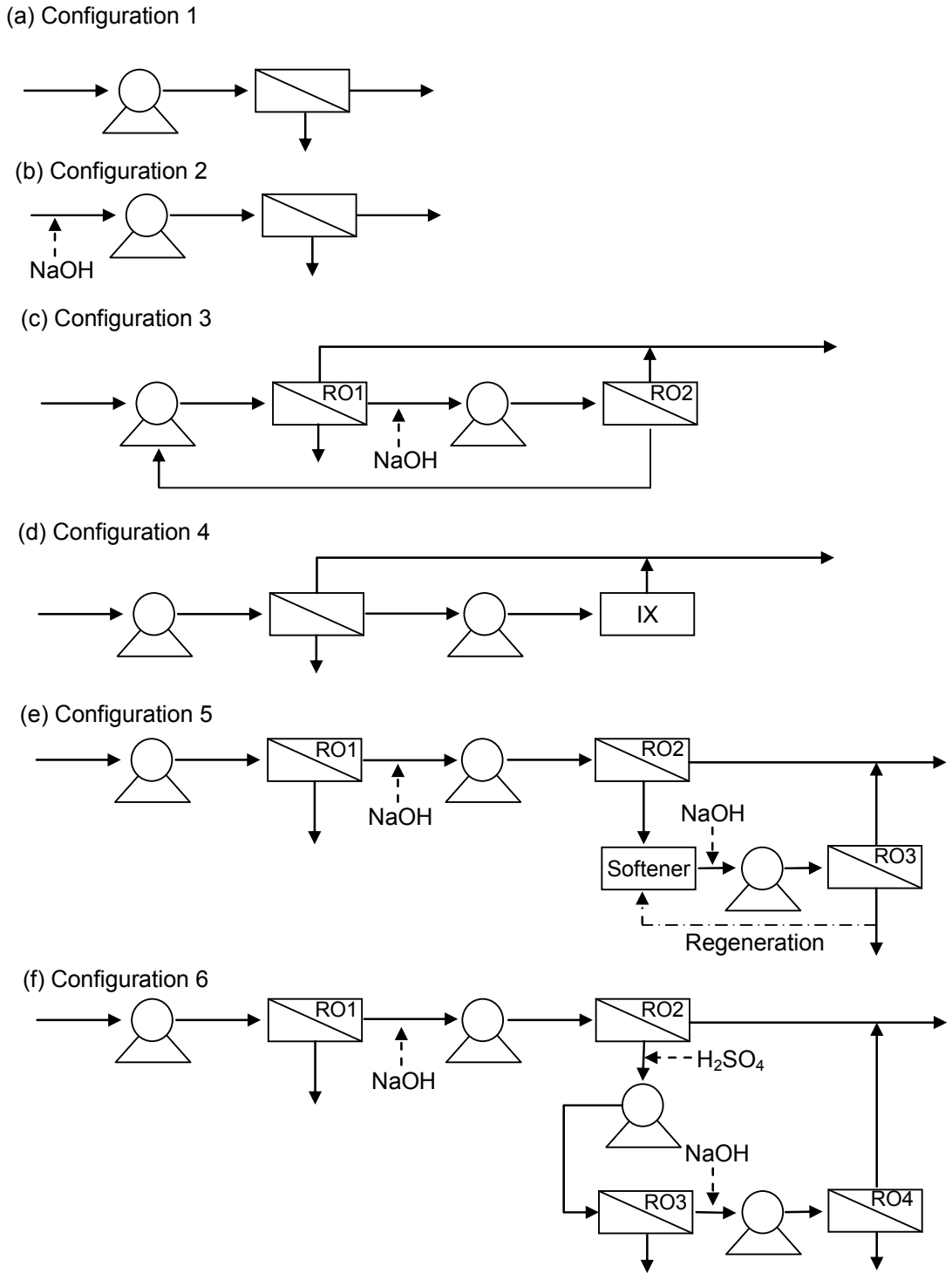

Figure 5.1 Configurations of different process options for boron removal.

much higher than 0.5 mg/L as evident from results presented in tables 4.2 and 4.3. Boron rejection becomes more challenging as the feed pH decreases and the temperature increases. As previously discussed in section 3, the rejection of boron in a single-pass configuration can be significantly enhanced by increasing the feed pH. Figure 5.1(b) shows a single-pass RO process with feed pH adjustment. In this configuration, an antiscalant must be used if the pH is increased above 9.5.

(2) Double-Pass RO System

A schematic of a double-pass RO system is shown in figure 5.1(c). The double-pass process typically consists of a leading SWRO unit (RO1) operating at a recovery of 40 to 50% followed by a brackish RO unit (RO2) operating at a recovery of 85 to 90%. Since the feed to the RO2 process is the RO1 permeate (i.e., RO2 feed has low salinity), the RO2 unit operates at a relatively high flux (typically 20 gfd). Therefore, the number of elements required in the RO2 unit would be relatively small, thereby lowering marginal capital costs. In addition, depending on the temperature of and boron concentration in the feed water, it is possible that only a portion of RO1 permeate would be treated by the RO2 to produce a combined permeate that meets the provisional boron standard. Increasing the pH of RO2 feed beyond 9.5 (and up to 10) by adding sodium hydroxide as shown in the figure 5.1(c) is commonly practiced to achieve 80 to 95% boron rejection by the brackish membranes. Consequently, a double-pass system generally achieves a much higher level of boron reduction when compared with a single-pass system. However, the samples obtained from two seawater plants during the National Reconnaissance study of the this project suggest that the overall boron rejection in two-pass systems might not be always as high as expected. Boron rejection by plant B was reached only 80%.

The operating costs of a double-pass system could be substantial. A portion of the RO1 permeate that feeds the RO2 unit is inevitably discharged as a concentrate. Therefore, when 85 to 90% recovery in the RO2 is assumed, 10 to 15% of RO1 permeate should be discarded as the concentrate of RO2 and operating cost will be proportionally increased.

Another complicating factor is the potential for scale formation in the RO2 unit since the RO1 permeate contains alkalinity, calcium, and magnesium. Even though the concentrations of these species are not high in the RO2 feed, scales of calcium carbonate and/or magnesium hydroxide could form under elevated pH conditions. Consequently, a scale inhibitor needs to be added to the RO2 feed or the recovery of the RO2 unit needs to be lowered. Alternatively, the upper limit of RO2 feed pH could be reduced, which would result in diminished boron rejection performance.

An additional consideration is the fact that overall boron reduction in the double-pass system depends on the fraction of RO1 permeate used to feed the RO2 unit. As the fraction of RO1 permeate feeding the RO2 unit increases, higher boron removal will be possible. However, increasing the fraction of RO1 permeate treated by the RO2 unit would increase the capital and operating costs due to the additionally required RO elements. For the cost analysis performed as part of this study, a system treating 16% of RO1 permeate was considered.

(3) Single-Pass RO with Boron Specific Ion Exchange Resin

In this configuration, a portion of permeate from a single-pass SWRO unit is treated by a boron specific ion exchange system (figure 5.1(d)). In contrast to the double-pass RO system, this configuration does not require a pH adjustment of the RO permeate. Recovery rates for ion exchange systems are typically very high (~98%). However, O&M costs of ion exchange systems tend to be high due to the expense of specialty resins required for removing boron and the need for resin regeneration. Due to the relatively small market size of boron-specific resins and the high cost of chemicals used in their production, no significant reduction in boron-specific resin costs is anticipated in the near future. For the cost analysis, it was assumed that the ion exchange unit treated 16% of RO permeate.

(4) Multistage RO Systems

The low recovery and scale formation potential problems associated with double-pass systems might be effectively avoided by multistage configurations without requiring the costly ion exchange process. Two multistage configurations (configuration 5 and 6), which have been used in full-scale SWRO systems, were considered in this study. In both configurations, additional RO units are employed to further treat the concentrate produced from the second pass RO unit. In the first design option, shown in figure 5.1-(e), the concentrate from the second-pass RO is treated by an ion exchange softening process to remove divalent cations. The effluent from the softener is further treated by RO (RO3). Since there is little calcium and magnesium present in the effluent from the softener, risk of scale formation in the RO3 unit is minimal, regardless of pH. In addition, the concentrate from the RO3 unit is essentially a pure NaCl solution. Therefore, it can be used to regenerate the softener, thereby reducing operation and maintenance costs. Another design option for the multistage process is shown in figure 5.1(f). In this configuration, the concentrate from the second-pass RO (RO2) is directly treated with another RO unit (RO3). To prevent scale formation, pH of the RO2 concentrate is reduced by acidification, prior to processing by the RO3 unit. The permeate from RO3, which has a very low concentration of divalent cations, is further processed with an additional RO unit (RO4) at an elevated pH.

5.3 Methods of Cost Estimation

To estimate the cost of water production by each configuration described previously, details of operating conditions and design parameters were first defined. Water production costs were then evaluated by separately estimating capital and operation costs. However, it is impossible to establish a universal formula to calculate costs of all the necessary components since the actual costs depend on many unquantifiable factors, including location and time, quality of equipment, labor and services, etc. A literature review (Diaz-caneja et al., 1991; Kiernan, 2005; Leitner, 1989; Vaarapeneni et al., 2003) suggested that related cost estimates are often based on numerous assumptions, and specific assumptions varied from reference to reference. Note that some assumptions and equations used in the cost estimation relied on the investigators' personal experience when no objective reference was available.

It should be noted that the cost analysis given in this report did not attempt to measure the actual costs of the above processes. The purpose of the cost analysis in this project was to compare the costs of the above six process options using the same assumptions under comparable conditions (for example, same membrane units, same capacity, etc.). The assumptions and operational conditions used in the calculations are discussed below along with the specific estimation methods.

5.3.1 Performance Prediction of Each Configuration

The cost analysis was based on the performance of one representative SWRO membrane, SWC5, and one representative BWRO membrane, ESPA2. The SWC5 membrane was recently developed to achieve high boron rejection. Thus, the results are biased toward higher boron rejection. The properties of these membranes are summarized in table 5.1. For all process options, the production capacity and overall system recovery were fixed at 10,000 m^3/day and around 50%, respectively. At this production rate and system recovery, the performance (i.e., rejection of ionic species including boron and associated system pressure) of the processes was predicted from IMS software using a Pacific seawater containing 5 mg/L boron as a feed. This software (available from www.membranes.com) was developed by Hydranautics to predict the field performance of its RO membranes in various configurations and operating conditions. In this software, boron rejection at different pHs was estimated using the dissociation constant of boric acid.

Table 5.1 Specifications of Representative BWRO and SWRO Membranes

Model	ESPA2	SWC5
Membrane material	Polyamide	Polyamide
Permeate flow (m^3/day)	34.1	34.1
Salt rejection (%)	99.5	99.8
Boron rejection (%)	75	93
Membrane area (ft^2)	400	400
Test condition	1,500 mg/L NaCl feed, 150 psi, 15% recovery, pH 6.5~7.0, 25°C	32,000 mg/L NaCl feed, 800 psi, 10% recovery, pH 6.5~7.0, 25°C

5.3.2 Capital Cost Estimation

Capital costs were divided into seven categories: RO equipment costs, other equipment costs, pretreatment equipment costs, site and construction costs, engineering costs, contingency costs, and other indirect costs. Further cost breakdowns for each item are summarized in table 5.2.

Table 5.2 Breakdown of Capital Cost

RO equipment cost	Pressure vessel, membrane element, trains
Other equipment cost	Pumps, MCC, controls, cleaning system, piping, permeate post treatment equipment
Pretreatment equipment cost	Chemical dosing system, filtration system
Site and construction cost	Raw water intake, feed storage tanks, site preparation, buildings and construction
Engineering cost	Construction supervision, process, and system design
Other indirect cost	Financing, Interest during construction

Table 5.3 shows the basis of calculation for the RO equipment, pretreatment, and ion exchanger cost. Unit prices of the pressure vessel, membrane elements, membrane trains, and ion exchange unit were obtained from manufacturer information. RO pretreatment cost of \$50/m^3 feed was assumed.

Table 5.3 Calculation Basis for the Equipment Cost

SWRO pressure vessel	\$2,400/each
SWRO membrane element	\$550/each
SWRO trains	\$4,440/Pressure vessel
BWRO pressure vessel	\$1,700/each
BWRO membrane element	\$550/each
BWRO trains	\$2,910/Pressure vessel
RO pretreatment cost	\$50/m^3 feed
Ion exchange unit	\$150,000 for 70 m^3/hr capacity

For comparative purposes, it was assumed that site and construction costs were \$1,500,000 for single-pass system, \$1,600,000 for partial double-pass system and single-pass system with ion exchanger, and \$1,700,000 for double-pass system

with concentrate recovery. These assumptions were based largely on the investigators' personal experience. Other equipment cost, engineering costs, indirect costs, and contingency costs were estimated from the estimated equipment costs and site and construction costs using the following equations:

Other equipment cost =
1 × (Pressure vessel cost + RO element cost + RO train cost) (33)

Engineering cost = 0.2 ×
(Pressure vessel cost + RO element cost + RO train cost +
RO pretreatment cost +site and construction cost) (34)

Indirect cost = 0.5 × (Pressure vessel cost + RO element cost +
RO train cost +RO pretreatment cost + site and construction cost) (35)

Contingency cost = 0.1 × (Pressure vessel cost + RO element cost +
RO train cost + RO pretreatment cost + site and construction cost) (36)

Total system costs were obtained from the summation of the above costs. From the total system costs, the capital costs were calculated using the following equations:

Capital cost = System cost ÷ Yearly capital cost factor
(Annuity factor) ÷ Time ÷ Plant capacity ÷ Loading factor (37)

$$\text{Yearly capital cost factor} = \frac{1}{i}\left(1 - \frac{1}{(1+i)^n}\right) \quad (38)$$

where, i = interest rate and n = system life. Calculations in this study used the following values: time = 365 days, plant capacity = 10,000 m^3/day and loading factor = 0.9 (i.e., 90% operation during the whole period (20 years) of operation). Using an interest rate of 6% and a system life of 20 years, a yearly capital cost factor (annuity factor) of 11.469 was obtained and used for equation (37).

5.3.3 Operation Cost Estimation

Operation costs include energy, chemicals, membrane replacement, maintenance, and labor cost. Because of the high pressure required for SWRO operation, power costs comprise the biggest portion of the total operation costs. Power used to operate pumps and power recovered from the energy recovery turbine were calculated from the following equations.

Pumping power = 0.027 × Feed flow × Pressure head ÷
Pump efficiency ÷ Motor efficiency (39)

Recovered power = 0.027 × Flow × Pressure head × Turbine efficiency (40)

For the above calculations, the assumptions were made: (1) pump efficiency of 86% and motor efficiency of 94% for high-pressure SWRO pumps; (2) pump efficiency of 84% and motor efficiency of 94% for BWRO pumps; (3) pump efficiency of 75% and motor efficiency of 90% for the pumps used for ion exchangers and softening; (4) energy recovery device efficiency of 86%. Total power requirements were calculated by subtracting recovered power from pumping power. Once pumping energy was calculated by dividing total power requirement by production rate, power cost could be calculated by using the assumed electricity cost of $0.05 per kilowatthour ($/kw-hr). Note that power cost also included additional pretreatment and auxiliary power consumption at 0.5 kilowatthour per cubic meter (kw-hr/m^3). The calculation basis for other operational costs is provided in table 5.4.

Table 5.4 Calculation Basis for the Operation Cost

Chemical cost	0.0225 $/$m^3$ treatment of feed
Electricity cost	0.05 $/kW-hr
Membrane replacement cost	15% replacement per year
Maintenance cost	3% of equipment cost
Labor cost	8 persons, $30,000/year/person

5.4 Results of Cost Analysis

Details of operating conditions, power consumption and feed, concentrate, and permeate water quality are summarized in the following tables and figures for each configuration (tables 5.5 to 5.22 and figures 5.2 to 5.7). From these calculations, water production costs were evaluated and summarized in table 5.23.

Configuration 1

Table 5.5 Operating Conditions of Configuration 1

Permeate recovery (%)	50	Feed flow (m^3/hr)	833.3 (20,000 m^3/day)
Feed pressure (bar)	57.3	Concentrate pressure (bar)	55.9
Number of vessels	100*	Feed pH	8.0

* 8 membrane element per pressure vessel

Table 5.6 Concentrations of Ionic Species in Configuration 1

Constituent	Feed (mg/L)	Permeate (mg/L)	Concentrate (mg/L
pH	8.0	6.4	8.3
Ca	356	0.7	879
Mg	1,200	2.4	2,398
Na	10,669	103	21,235
K	362	4.3	720
CO_3	0.3	0.0	0.6
HCO_3	133	2.1	264
SO_4	2,500	5.6	4,994
Cl	18,700	167	37,233
B	5.0	1.2	8.8
TDS	33,932	286	67,578

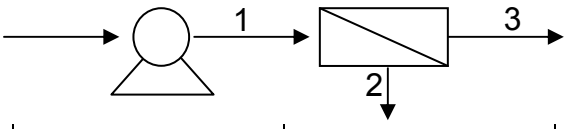

Location	1	2	3
Flow (m^3/hr)	833.3	416.7	416.7
TDS (mg/L)	33,932	67,578	286
Boron (mg/L)	5.0	8.8	1.2

Figure 5.2 Schematic diagram and design parameters of configuration 1.

Table 5.7 Calculation of Energy Consumption of Configuration 1

Feed pressure (bar)	57.3
Concentrate pressure (bar)	55.9
Pump flow (m^3/hr)	833.3
Turbine flow (m^3/hr)	416.7
Pumping power (kw)	1,594.8
Recovered power (kw)	540.9
Total power requirement (kw)	1,053.9
Pumping energy (kw-hr/m^3)	2.53

Configuration 2

Table 5.8 Operating Conditions of Configuration 2

Permeate recovery (%)	50	Feed flow (m^3/hr)	833.3 (20,000 m^3/day)
Feed pressure (bar)	57.3	Concentrate pressure (bar)	55.9
Number of vessels	100	Feed pH	8.0 (raw water) 8.45 (feed water)

Table 5.9 Concentrations of Ionic Species in Configuration 2

Constituent	Feed (mg/L)	Permeate (mg/L)	Concentrate (mg/L
pH	8.5	6.4	8.3
Ca	356	0.7	879
Mg	1,200	2.4	2,398
Na	10,669	103	21,235
K	362	4.3	720
CO_3	0.3	0.0	0.6
HCO_3	133	2.1	264
SO_4	2,500	5.6	4,994
Cl	18,700	167	37,233
B	5.0	0.8	9.2
TDS	33,932	286	67,578

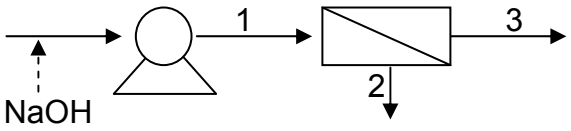

Location	1	2	3
Flow (m^3/hr)	833.3	416.7	416.7
TDS (mg/L)	33,932	67,578	286
Boron (mg/L)	5.0	9.2	0.8

Figure 5.3 Schematic diagram and design parameters of configuration 2.

Table 5.10 Calculation of Energy Consumption of Configuration 2

Feed pressure (bar)	57.3
Concentrate pressure (bar)	55.9
Pump flow (m^3/hr)	833.3
Turbine flow (m^3/hr)	416.7
Pumping power (kw)	1,594.8
Recovered power (kw)	540.9
Total power requirement (kw)	1,053.9
Pumping energy (kw-hr/m^3)	2.53

Configuration 3

Table 5.11 Operating Conditions of Configuration 3

Total system recovery: 49.5% **Total feed flow: 842.3 m^3/hr (20,215 m^3/day)**		
	1st pass (SWRO)	**2nd Pass (BWRO)**
Recovery (%)	50	90
Feed flow (m^3/hr)	842.3	83.3
Feed pressure (bar)	56.9	10.6
Concentrate pressure (bar)	55.5	8.3
Number of vessels	100	10 (7:3 array)
Feed pH	8.0	10.0

Table 5.12 Concentration of Ionic Species in Configuration 3

Constituent	**Feed (mg/L)**	**Permeate (mg/L)**	**Concentrate (mg/L**
pH	8.0	8.8	8.3
Ca	356	0.4	705
Mg	1,200	1.3	2,375
Na	10,669	57.2	21,075
K	362	2.4	715
CO_3	0.3	0	1.2
HCO_3	133	1.1	262
SO_4	2,500	2.7	4,948
Cl	18,700	84	36,951
B	5.0	0.8	9.1
TDS	33,932	150	67,055

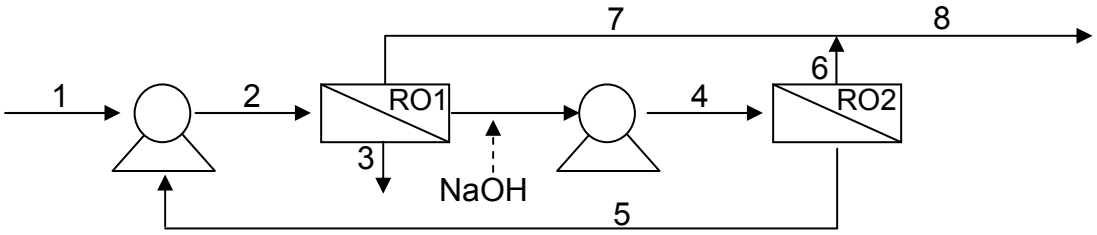

Location	**1**	**2**	**3**	**4**
Flow (m^3/hr)	842.3	850.1	425	83.3
TDS (mg/L)	33,932	33,670	67,055	719
Boron (mg/L)	5.0	5.2	9.1	2.9
Location	**5**	**6**	**7**	**8**
Flow (m^3/hr)	8.3	75	341.7	416.7
TDS (mg/L)	7,960	22	178	150
Boron (mg/L)	23.4	0.6	0.8	0.8

Figure 5.4 Schematic diagram and design parameters of configuration 3.

Table 5.13 Calculation of Energy Consumption of Configuration 3

	RO1	RO2	Total
Feed pressure (bar)	56.9	10.6	-
Concentrate pressure (bar)	55.5	8.3	-
Pump flow (m^3/hr)	850.1	83.3	-
Turbine flow (m^3/hr)	425	-	-
Pumping power (kw)	1,615.5	30.2	1,645.7
Recovered power (kw)	547.7	-	547.7
Total power requirement (kw)	1,067.8	30.2	1,098.0
Pumping energy (kw-hr/m^3)	2.56	0.07	2.64

Configuration 4

Table 5.14 Operating Conditions of Configuration 4

Permeate recovery (%)	50	Feed flow (m^3/hr)	833.3 (20,000 m^3/day)
Feed pressure (bar)	57.3	Concentrate pressure (bar)	56.2
Number of vessels	100	IX Feed flow (m^3/hr)	70

Table 5.15 Concentration of Ionic Species in Configuration 4

Constituent	Feed (mg/L)	Permeate (mg/L)	Concentrate (mg/L
pH	8.0	8.8	8.3
Ca	356	0.7	879
Mg	1,200	2.4	2,398
Na	10,669	103	21,235
K	362	4.3	720
CO_3	0.3	0.0	0.6
HCO_3	133	2.1	264
SO_4	2,500	5.6	4,994
Cl	18,700	167	37,233
B	5.0	0.7	8.8
TDS	33,932	269	67,578

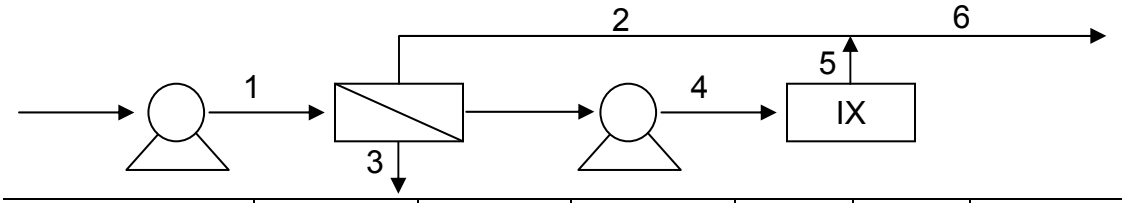

Location	1	2	3	4	5	6
Flow (m^3/hr)	833.3	346.7	416.7	70	70	416.7
TDS (mg/L)	33932	178	67578	719	719	269
Boron (mg/L)	5.0	0.8	8.8	2.9	0.1	0.7
Flow (m^3/hr)	833.3	346.7	416.7	70	70	416.7

Figure 5.5 Schematic diagram and design parameters of configuration 4.

Table 5.16 Calculation of Energy Consumption of Configuration 4

	RO	IX	Total
Feed pressure (bar)	57.3	1	-
Concentrate pressure (bar)	55.9	-	-
Pump flow (m^3/hr)	833.3	70	-
Turbine flow (m^3/hr)	416.7	-	-
Pumping power (kw)	1,594.8	2.8	1,597.6
Recovered power (kw)	540.9	-	540.9
Power requirement (kw)	1,053.9	2.8	1,056.7
Pumping energy (kw-hr/m^3)	2.53	0.01	2.54

Configuration 5

Table 5.17 Operating Conditions of Configuration 5

Total system recovery: 48% **Total feed flow: 466.8 m^3/hr (20,803 m^3/day)**			
	RO1 (SWRO)	**RO2 (BWRO)**	**RO3 (BWRO)**
Recovery (%)	50	80	90
Feed flow (m^3/hr)	866.8	433.3	86.7
Feed pressure	57.3	11.9	15.3
Concentrate pressure	55.9	4.2	11.3
Number of vessels	104	34 (24:10 array)	8 (6:2 array)

Table 5.18 Concentrations of Ionic Species in Configuration 5

Constituent	Feed (mg/L)	Permeate (mg/L)	Concentrate (mg/L
pH	8.0	8.3	8.3
Ca	356	0.0	705
Mg	1,200	0.0	2,375
Na	10,669	7.3	21,075
K	362	0.3	715
CO_3	0.3	0.0	1.2
HCO_3	133	0.3	262
SO_4	2,500	0.0	4,948
Cl	18,700	11.9	36,951
B	5.0	0.3	9.1
TDS	33,932	20.2	67,055

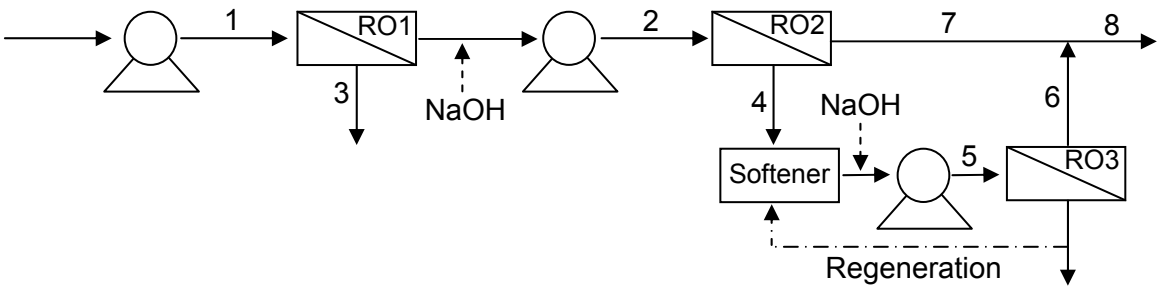

Location	1	2	3	4
Flow (m^3/hr)	866.8	433.4	433.4	433.4
TDS (mg/L)	33932	286	67578	286
Boron (mg/L)	5.0	1.2	9.1	1.2
Location	**5**	**6**	**7**	**8**
Flow (m^3/hr)	86.7	78	346.7	424.7
TDS (mg/L)	1354	95	3.9	21
Boron (mg/L)	4.4	0.4	0.3	0.3

Figure 5.6 Schematic diagram and design parameters of configuration 5.

Table 5.19 Calculation of Energy Consumption of Configuration 5

	RO1	RO2	IX	RO3	Total
Feed pressure (bar)	57.3	11.9	1	15.3	-
Concentrate pressure (bar)	55.9	-	-	-	-
Pump flow (m^3/hr)	866.8	433.4	86.7	86.7	-
Turbine flow (m^3/hr)	433.4	-	-	-	-
Pumping power (kw)	1,658.9	172.3	3.5	44.3	1,878.9
Recovered power (kw)	562.6	-	-	-	562.6
Power requirement (kw)	1,096.3	172.3	3.5	44.3	1,316.3
Pumping energy (kw-hr/m^3)	2.63	0.41	0.01	0.11	3.16

Configuration 6

Table 5.20 Operating Conditions of Configuration 6

Total system recovery: 48%
Total feed flow: 466.8 m^3/hr (20,803 m^3/day)

	RO1 (SWRO)	RO2 (BWRO)	RO3 (BWRO)	RO 4 (BWRO)
Recovery (%)	50	80	90	90
Feed flow (m^3/hr)	866.8	433.3	86.7	78
Feed pressure	57.3	11.9	15.3	8.9
Concentrate pressure	55.9	4.2	11.3	4.7
Number of vessels	104	34 (24:10 array)	8 (6:2 array)	8 (6:2 array)
Feed pH	8.0	9.8	6.5	10.6

Table 5.21 Concentrations of Ionic Species in Configuration 6

Constituent	Feed (mg/L)	Permeate (mg/L)	Concentrate (mg/L
pH	8.0	8.8	8.3
Ca	356	0.0	705
Mg	1,200	0.0	2,375
Na	10,669	1.2	21,075
K	362	0.0	715
CO_3	0.3	0	1.2
HCO_3	133	0.2	262
SO_4	2,500	0.0	4,948
Cl	18,700	1.8	36,951
B	5.0	0.3	9.1
TDS	33,932	3.6	67,055

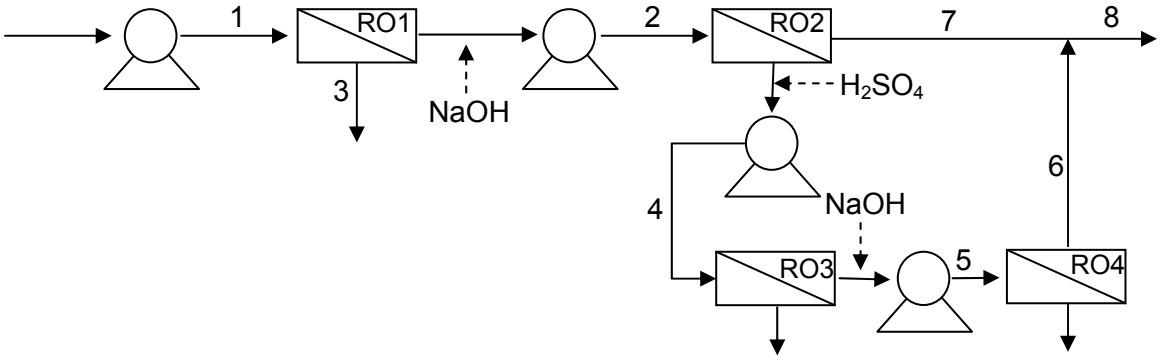

Location	1	2	3	4
Flow (m^3/hr)	866.8	433.4	433.4	86.7
TDS (mg/L)	33,932	6,7578	286	1455
Boron (mg/L)	5.0	8.8	1.2	4.4
Location	**5**	**6**	**7**	**8**
Flow (m^3/hr)	78	346.7	71	417.7
TDS (mg/L)	56	3.9	3.5	3.8
Boron (mg/L)	3.7	0.3	0.4	0.3

Figure 5.7 Schematic diagram and design parameters of configuration 6.

Table 5.22 Calculation of Energy Consumption of Configuration 6

	RO1	RO2	IX	RO3	Total
Feed pressure (bar)	57.3	11.9	15.7	8.9	-
Concentrate pressure (bar)	55.9	-	-	-	-
Pump flow (m^3/hr)	866.8	433.4	86.7	78	-
Turbine flow (m^3/hr)	433.4	-	-	-	-
Pumping power (kw)	1,658.9	172.3	46.5	23.2	1,900.9
Recovered power (kw)	562.6	-	-	-	562.6
Power requirement (kw)	1,096.3	172.3	46.5	23.2	1,338.3
Pumping energy (kw-hr/m^3)	2.63	0.41	0.11	0.06	3.21

Table 5.23 Summary of Water Production Cost

	Configuration	1	2	3	4	5	6
Capital cost ($/m^3)	SWRO Pressure vessel (ea)	100	100	102	100	104	104
	SWRO Membrane element (ea)	800	800	816	800	832	832
	BWRO Pressure vessel (ea)			10		42	50
	BWRO Membrane element (ea)			80		336	400
	Pressure vessels cost($)	240,000	240,000	261,800	240,000	321,000	334,600
	Membrane elements cost($)	440,000	440,000	492,800	440,000	642,400	677,600
	RO trains cost ($)	444,000	444,000	481,880	444,000	583,980	607,260
	Other RO equipment ($)	1,124,000	1,124,000	1,236,480	1,124,000	1,547,380	1,619,460
	RO pretreatment equipment ($)	1,000,000	1,000,000	1,010,101	1,000,000	1,250,000	1,250,000
	Site and construction ($)	1,500,000	1,500,000	1,600,000	1,600,000	1,700,000	1,700,000
	Engineering cost ($)	949,600	949,600	1,016,612	969,600	1,208,952	1,237,784
	Indirect cost ($)	2,374,000	2,374,000	2,541,531	2,424,000	3,022,380	3,094,460
	Contingency ($)	474,800	474,800	508,306	484,800	604,476	618,892
	Ion exchange equipment ($)				150,000		
	Total system cost ($)	8,546,400	8,546,400	9,149,510	8,876,400	10,880,568	11,140,056
		0.227	0.227	0.243	0.236	0.289	0.296
		(0.86 $/1,000gal)	(0.86 $/1,000gal)	(0.92 $/1,000gal)	(0.89 $/1,000gal)	(1.09 $/1,000gal)	(1.12 $/1,000gal)
Operation cost ($/m^3)	Pumping energy (kw-hr/m^3)	2.53	2.53	2.64	2.54	3.16	3.21
	Pumping energy + auxiliary power (kw-hr/m^3)	3.03	3.03	3.14	3.04	3.66	3.71
	Power cost ($/m$^{3)}$	0.1515	0.1515	0.157	0.152	0.183	0.1855
	1st pass chemical cost ($/m^3)	0.0450	0.0470	0.0455	0.0450	0.0468	0.0468
	2nd pass chemical cost ($/m^3)			0.003	0.007	0.018	0.018
	Membrane replacement ($/m^3)	0.0201	0.0201	0.0225	0.0201	0.0293	0.0309
	Maintenance ($/m^3)	0.0015	0.0015	0.0016	0.0015	0.0020	0.0020
	Labor ($/m^3)	0.0731	0.0731	0.0731	0.0731	0.0731	0.0731
		0.291	0.293	0.303	0.299	0.352	0.356
		(1.10 $/1,000gal)	(1.11 $/1,000gal)	(1.15 $/1,000gal)	(1.13 $/1,000gal)	(1.33 $/1,000gal)	(1.35 $/1,000gal)
Water production cost= Capital + Operation cost ($/m^3)		0.518	0.520	0.545	0.534	0.641	0.652
		(1.96 $/1,000gal)	(1.96 $/1,000gal)	(2.06 $/1,000gal)	(2.02 $/1,000gal)	(2.43 $/1,000gal)	(2.47 $/1,000gal)

5.5 Discussion

Estimated water production costs ranged from \$0.518/m^3 to \$0.652/m^3 (from \$1.96/1,000 gal to \$2.47/1,000 gal). Estimated cost for each configuration was: \$0.518/m^3 (\$1.96/1,000 gal) for configuration 1 (lowest), \$0.520/m^3 (\$1.96/1,000 gal) for configuration 2, \$0.534 /m^3 (\$2.02/1,000 gal) for configuration 4, \$0.545/m^3 (\$2.06/1,000 gal) for configuration 3, \$0.641/m^3 (\$2.43/1,000 gal) for configuration 5, and \$0.652/m^3 (\$2.47/1,000 gal) for configuration 6 (highest) and generally increased as additional equipments were used (figure 5.8). Water cost for the system designed to produce water with

<1 mg/L boron (configurations 2, 3 and 4) was in the range of \$0.52~0.55/m^3. Systems with permeate boron concentrations < 0.5 mg/L (configurations 5 and 6) would require approximately 20 to 25% increase of water production cost.

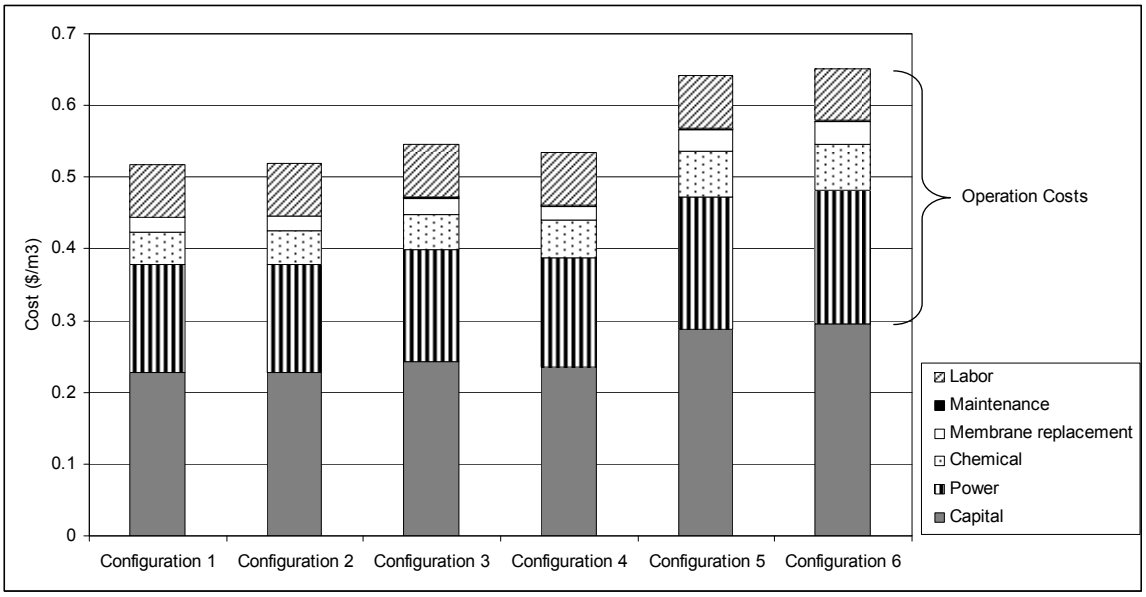

Figure 5.8 Estimated water production cost for each configuration.

Capital costs accounted for approximately 43 to 45% of overall water production cost and ranged from \$0.227 (configurations 1 and 2) to \$0.296/m^3 of permeate (configuration 6) (from 0.86 \$/1,000 gal to 1.12 \$/1,000 gal). Capital cost was mostly affected by the cost of membrane equipment. Equipment cost comprised 38 to 40% of capital costs depending on the configuration. Operation costs accounted for 55 to 57% of overall water production cost and ranged from \$0.291/m^3 (\$1.10/1,000 gal) (configurations 1 and 2) to \$0.356/m^3 (\$1.35/1,000 gal) (configuration 6). Power costs accounted for the largest portion of the operation costs for all system configurations, comprising approximately 50% of the total operation cost. The second largest portion of operation cost was due to labor, which accounted for approximately 25% of operation cost.

The simulation of process performance suggested that although a simple single-pass SWRO system (configuration 1) should be able to produce permeate with an acceptable salinity (< 500 mg/L TDS), it would be difficult to maintain permeate boron concentrations below 1 mg/L. However, by increasing the pH of the feed water to 8.5, permeate boron concentration of 0.8 mg/L in the single-pass RO configuration could be achieved (configuration 2). It might be possible to achieve higher rejection of boron by raising pH over 8.5, but operation at higher pH would require antiscalant treatment. Capital cost calculations showed that configurations 1 and 2 had the same capital costs of \$0.227/m^3 (\$0.86/1,000 gal) since the two systems were virtually identical except NaOH dosing, which was a

negligible marginal cost ($0.002/$m^3$). Compared to configuration 1, there was a $0.002/$m^3$ increase of the operation cost in configuration 2 due to the increased chemical (NaOH) consumption.

By processing part of the SWRO permeate with either a BWRO unit or a boron-specific ion exchange unit (configurations 3 and 4), a permeate boron concentration of ≤1.0 mg/L might be obtained. For the representative systems in this study in which 16% of the first RO permeate was treated, permeate boron concentrations of 0.8 mg/L (configuration 3) and 0.7 mg/L (configuration 4) were achieved. Increasing the partial treatment ratio greater than 16% will decrease the permeate boron concentration, but increase the capital costs. Comparing configurations 2, 3, and 4, which showed similar boron removal performance, vonfiguration 2 had much lower estimated costs than configurations 3 and 4. Total water production costs for configuration 2 were $0.026/$m^3$ ($0.096/1,000 gal) and $0.014/$m^3$ ($0.052/1,000 gal) lower than those for configuration 3 and configuration 4, respectively. This was mainly due to the lower capital costs. In case scale formation is controllable and system material is resistant to the high pH condition, configuration 2 might be a promising option to obtain permeates boron concentration less than 1.0 mg/L.

To meet the 0.5 mg/L permeate boron concentration, a full double-pass RO system would be necessary. The double-pass RO process combined with a softener and RO treatment of second pass concentrate (configuration 5) and the double-pass RO process with two-stage RO treatment of second pass concentrate (configuration 6) both showed the same permeate boron concentration of 0.3 mg/L. The associated water production costs were much higher than that for other configurations due to the additional membrane units. Configuration 5 appeared to have a better cost efficiency for boron removal than configuration 6 ($0.011/$m^3$ ($0.042/1,000 gal) lower total water production cost).

Water production costs of RO processes will be largely affected by the boron removal performance of the membranes. Based on the projection from the IMS software, if SWRO membranes with boron rejection over 96% were installed, even a single-pass RO system might be able to produce permeate with the boron concentration under 1 mg/L, thereby drastically improving the cost efficiency of boron removal by RO. Improving boron rejection by BWRO membranes will also have a positive effect on process economics. In the seawater desalination system where BWRO is employed as a second-pass unit, this effect will be limited to the reduction of NaOH dose and cost savings will be marginal. In contrast, BWRO membranes with improved boron rejection capabilities can result in significant cost savings when they are used for brackish water treatment. However, boron levels in brackish water are typically much lower and might not raise concern.

References

Agency for Toxic Substances and Disease Registry (ATSDR), 1992. *Toxicological Profile for Boron*, U.S. Department of Health and Human Services, Public Health Service, Atlanta, Georgia

Bader, H., J. Hoigné, 1981. "Determination of Ozone in Water by the Indigo Method." *Water Research*, 15, 449-456

Badruk, M., N. Kabay, M. Demircioglu, H. Mordogan, U. Ipekoglu, 1999. "Removal of Boron from Wastewater of Geothermal Power Plant by Selective Ion-Exchange Resins. I. Batch Sorption-Elution Studies." *Separation Science and Technology*, 34(13), 2553-2569.

Badruk, M, N. Kabay, M. Demircioglu, H. Mordogan, U. Ipekoglu, 1999. "Removal of Boron from Wastewater of Geothermal Power Plant by Selective Ion-Exchange Resins. II. Column Sorption-Elution Studies." *Separation Science and Technology*, 34(15), 2981-2995.

Busch, M., W.E. Mickols, S. Jons, J. Redondo, J. De Witte, 2003. "Boron Removal in Sea Water Desalination." *Proceedings of International Desalination Association Annual Conference*, Bahama.

Childress, A. E. and M. Elimelech, 2000. "Relating nanofiltration membrane performance to membrane charge (electrokinetic) characteristics." *Environmental Science & Technology*, 34(17), 3710-3716.

Choi, W.-W. and K.Y. Chen, 1979. "Evaluation of Boron Removal by Adsorption on Solids." *Environmental Science & Technology*, 13(2), 189-196.

Diaz-caneja, J. et al., 1991. "Spanish cost data illustrate RO's competitiveness," *Desalination & Water Reuse*, 15(1), 10 – 28.

EPA, 1975. *Preliminary Investigation of Effects on the Environment of Boron, Indium, Nickel, Selenium, Tin, Vanadium, and Their Compounds*, Vol. 1. Boron, Rep. 56/2-75-005A.

EPA, 2001. *Toxicological Review of Boron and Compounds*, CAS No. 7440-42-8.

EPA, 2003. *Technical Support Document for the Assessment of Detection and Quantitation Approaches*, EPA-821-R-03-005.

Gieskes, J. M, 1974. *The Sea*, Wiley-Interscience.

Glueckstern, P. and M. Priel, 2003. "Optimization of Boron Removal in Old and New SWRO Systems." *Desalination*, 156, 219-228.

Kiernan, J., 2005. "Start –up of the Trinidad Sea water Desalination project," *Proceedings AMTA Workshop*, Norfolk, VA.

Lee, S., G. Amy, and J. Cho, 2004. "Applicability of Sherwood correlations for natural organic matter (NOM) transport in nanofiltration (NF) membranes." Journal of Membrane Science, 240(1-2), 49-65.

Leitner, G., 1989. "Cost of sea water desalination in real terms, 1979 trough 1989, and projections for 1999," *Desalination*, 76, 201-213.

Magara, Y., T. Aizawa, S. Kunikane, M. Itoh, M. Kohki, M. Kawasaki, H. Takeuti, 1996. "The Behavior of Inorganic Constituents and Disinfection By-Products in Reverse Osmosis Water Desalination Processes." *Water Science and Technology*, 34, 141-148.

Magara, Y., A. Tabata, M. Kohki, M. Kawasaki, M. Hirose, 1998. "Development of Boron Reduction System for Sea Water Desalination." *Desalination*, 118, 25-34.

Mariñas, B. J., 1991. "Reverse Osmosis Technology for Wastewater Reuse." *Water Science and Technology*, 24(9), 215-227.

Marinas, B. J. and R.E. Selleck, 1992. "Reverse-Osmosis Treatment of Multicomponent Electrolyte-Solutions." *Journal of Membrane Science*, 72(3), 211-229.

Melnik, L., O. Vysotskaja, B. Kornilovich, 1999. "Boron Behavior During Desalination of Sea and Underground Water by Electrodialysis." *Desalination*, 124, 125-130.

Mi, B., C.L. Eaton, J.H. Kim, C.K. Colvin, J.C. Lozier, B.J. Mariñas, 2004. "Removal of Biological and Non-Biological Viral Surrogates by Spiral-Wound Reverse Osmosis Membrane Elements with Intact and Compromised Integrity." *Water Research*, 38, 3821-3832.

Moss, S.A. and N.K. Nagpal, 2003. *Ambient Water Quality Guidelines for Boron*, Ministry of Water Land and Air Protection in Canada.

Murthy, Z.V.P. and S.K. Gupta, 1997. "Estimation of mass transfer coefficient using a combined nonlinear membrane transport and film theory model." *Desalination*, 109(1), 39-49.

Murthy, Z.V.P. and S.K. Gupta, 1999. "Sodium cyanide separation and parameter estimation for reverse osmosis thin film composite polyamide membrane." *Journal of Membrane Science*, 154(1), 89-103.

Nadav, N., 1999. "Boron Removal from Sea water Reverse Osmosis Permeate Utilizing Selective Ion Exchange Resin." *Desalination*, 124, 131-135.

Nakao, S. and S. Kimura, 1981. "Analysis of Solutes Rejection in Ultrafiltration." *Journal of Chemical Engineering of Japan*, 14(1), 32-37.

Okay, H., H. Guclu, E. Soner, T. Balkas, 1985. "Boron Pollution in the Simav River, Turkey and Various methods of Boron Removal." *Water Research*, 19(7), 857-862.

Parekh, B.S., 1988. *Reverse osmosis technology*, Marcel Dekker Inc.

Petersen, R.J., 1993. "Composite Reverse-Osmosis and Nanofiltration Membranes." *Journal of Membrane Science*, 83(1), 81-150.

Popat, K.M., P.S. Anand, B.D. Dasare, 1988. "Synthesis and Characterization of Boron-Selective Porous Condensate Cation Exchanger." *Reactive Polymers*, 8, 143-151.

Prats, D., M.F. Chillon-Arias, M. Rodrígez-Pastor, 2000. "Analyses of the Influence of pH and Pressure on the Elimination of Boron in Reverse Osmosis." *Desalination*, 128, 269-273.

Recepoglu O., Beker, U., 1991. "A Preliminary Study of Boron Removal from Kizildere/Turkey Geothermal Waste Water." *Geothermics*, 20(1/2), 83-89.

Redondo, J., M. Busch, A. Ferrandiz-Ruiz, M.F. Chillon, D. Prats Rico, 2001. "Boron Removal from Sea water Using FILMTEC^{TM} High Rejection SWRO Membranes." *Desalination*, Vol. 156, pp. 229-238.

Ristic, M.D., L.V. Rajakovik, 1996. "Boron Removal by Anion Exchangers Impregnated with Citric and Tartaric Acids." *Separation Science and Technology*, 31(20), 2805-2814.

Rodrígez-Pastor, M., A. Ferrándiz-Ruiz, M.F. Chillón, D. Prats Rico, 2001. "Influence of pH in the Elimination of Boron by means of Reverse Osmosis." *Desalination*, 140, 145-152.

Redondo, J., M. Busch, J.-P. De Witte, 2003. "Boron Removal from Sea water Using FILMTEC^{TM} High Rejection SWRO Membranes." *Desalination*, 156, 229-238.

Riley, J. P. and G. Skirrow, 1975. *Chemical Oceanography*, Academic, New York.

Sagiv, A. and R. Semiat, R., 2004. "Analysis of parameters affecting boron permeation through reverse osmosis membranes." *Journal of Membrane Science*, 243, 79-87.

Simonnot, M.-O., C. Castel, M. Nicolai, C. Rosin, M. Sardin, H. Jauffret, 2000. "Boron Removal from Drinking Water with a Boron Selective Resin: Is the Treatment really Selective?" *Water Research*, 34(1), 109-116.

Smith, B.M., P. Todd, C.N. Bowman, 1995. "Boron Removal by Polymer-Assisted Ultrafiltration." *Separation Science and Technology*, 30(20), 3849-3859.

Sourirajan, S., 1970. *Reverse osmosis*, Logos Press Ltd.

Sutzkover, I., D. Hasson, R. Semiat, 2000. "Simple technique for measuring the concentration polarization level in a reverse osmosis system." *Desalination*, 131(1-3), 117-127.

Taniguchi, M. and S. Kimura, 2000. "Estimation of transport parameters of RO membranes for sea water desalination." *Aiche Journal*, 46(10), 1967-1973.

Taniguchi, M., M. Kurihara, S. Kimura, 2001. "Boron reduction performance of reverse osmosis sea water desalination process." *Journal of Membrane Science*, 183(2), 259-267.

Urama, R.I., B.J. Marinas, 1997. "Mechanistic interpretation of solute permeation through a fully aromatic polyamide reverse osmosis membrane." *Journal of Membrane Science*, 123(2), 267-280.

Vaarapeneni, S, et al., 2003. "The validity of expectation for improved SWRO cost", *Proceedings of IDA Conference*, Bahamas.

Voutchkov, N., 2005. *Personal communication*.

Waggott, A., 1969. "An Investigation of the Potential Problem of Increasing Boron Concentrations in Rivers and Water Courses." *Water Research*, 3, 749-765.

Weinthal, E. P., Y. Vengosh, A. Muti, W. Kloppmann, 2005. "The EU Drinking Water Directive: The Boron Standard and Scientific Uncertainty" *European Environment,* 15, 1-12.

Winograd, Y., A. Solan, M. Toren, 1973. "Mass-Transfer in Narrow Channels in Presence of Turbulence Promoters." *Desalination*, 13(2), 171-186.

Woods, W.G. (1994). "An Introduction to Boron: History, Sources, Uses, and Chemistry." *Environmental Health Perspectives,* 102, Supplement 7, 1-11.

World Health Organization, 1998. Addendum to Guidelines for Drinking Water Quality Volume 1. Recommendations, 2nd edition, Geneva.

Project Abstract

Seawater desalination has become an important process in many areas of the United States and worldwide due to increased water demand and decreased suitable water sources. As our knowledge of trace contaminant occurrence and related environmental and human health impacts expands and water quality standards become increasingly stringent, seawater desalination processes will continue to be challenged by new types of contaminants, such as boron. Boron is naturally occurring and is present in seawater at an average concentration of 4.6 mg/L. While boron is a vital element for organism growth, excessive exposure can cause detrimental effects to plants, animals, and possibly humans. Consequently, World Health Organization Guidelines for Drinking Water Quality proposes a maximum recommended boron concentration of 0.5 mg/L. This value is considered provisional due to the lack of a comprehensive toxicological assessment and the limited availability of technologies to remove boron. Boron is also on the EPA's Drinking Water Contaminant Candidate List, but there is little information on the occurrence of boron in drinking water supplies in the United States.

The three major objectives of this project were (1) to understand the mechanism of boron rejection by and transport through RO membranes while elucidating the effect of operating conditions such as pH and temperature on boron transport; (2) to perform a national reconnaissance study on ambient boron concentrations and evaluate boron removal at selected full- or pilot-scale seawater and brackish RO plants; and (3) to develop cost estimates for RO processes designed for boron removal.

Rejection of boron and ionic species by six commercial SWRO membranes was evaluated using a laboratory-scale cross-flow filtration apparatus. Experiments were performed using synthetic seawater (5 mg/L boron) and an orthogonal matrix of operating pressures (600 to 1,000 psi), pHs (6.2 to 9.5), and temperatures (15 to 30 °C). Experimental results were analyzed using the nonequilibrium thermodynamic model coupled with film theory. The key model parameters such as overall permeability constant (P_s) and reflection coefficient (σ) for boron transport were estimated based on nonlinear optimization of the experimental data. From the parameters, the model successfully predicted boron transport through different SWRO membranes under various pressure, temperature, and pH conditions. The model prediction suggested that, due to charge repulsion, borate ions were more easily removed than boric acid by negatively charged membranes. That is, boron transport is largely governed by pH. The overall permeability constant and reflection coefficient of boron were dependent on the change of pH and temperature. Equations were developed to predict the model parameters at various pH and temperature conditions. When

the permeability constants of boric acid and borate are known at one temperature, overall permeability constants of boron at other temperatures and pHs can be predicted from the following equation developed in this study:

$$P_{s,B} = \alpha_0 \times P_{s(H_3BO_3)25} \exp(a(T-298)) + \alpha_1 \times P_{s(H_2BO_3^-)25} \exp(b(T-298)) \quad (31)$$

where T = absolute temperature [K]; α_0 = fraction of boric acid [dimensionless]; and α_1 = fraction of borate [dimensionless]; a = pre-exponent number of boric acid [T^{-1}]; and b = pre-exponent number of borate [T^{-1}]. The following equation was also developed to predict the reflection coefficient of boron at any pH:

$$\sigma_B = \alpha_0 \times \sigma_{(H_3BO_3)} + \alpha_1 \times \sigma_{(H_2BO_3^-)} \quad (25)$$

where $\sigma_{(H3BO3)}$ = reflection coefficient of boric acid [dimensionless] and $\sigma_{(H2BO3-)}$ = reflection coefficient of boric acid [dimensionless]. The impact of temperature on the reflection coefficient was negligible under the experimental conditions of this study. In the above equations, $P_{s(H3BO3)25}$, $P_{s(H2BO3-)25}$, a, b, $\sigma_{(H3BO3)}$, and $\sigma_{(H2BO3-)}$ are membrane-specific and should be evaluated by bench-scale experiments before the model is applied to simulate larger scale systems.

The above parameters that characterized boron transport across SWRO membranes did not correlate well with essential membrane properties such as surface charge, roughness, and hydrophilicity of membrane surfaces, which were determined by electrokinetic analyses, atomic force microscopy, and contact angle measurements, respectively. Membrane test indicated that boron transport was governed by its speciation, thereby validating equations (31) and (25). Boron transport was also compared with the transport of other ionic species, including sodium, chloride, magnesium, calcium, and sulfate. While the observed transport behaviors of these ionic species were consistent with the current understanding of the RO process, they did not show any meaningful relationship with the transport of boric acid or borate. For example, a membrane with higher salt rejection did not necessarily achieve a higher level of boron rejection. This suggests that it is not possible to predict the rejection of boron based on other readily measurable parameters for SWRO membranes.

Samples of feed, permeate, and concentrate from the six seawater and three brackish RO plants (six national and three international) were analyzed and compared with the bench-scale experiment results. Concentrations of representative ionic species such as sodium, chloride, calcium, magnesium, and sulfate as well as that of boron were measured. General ionic species were rejected at over over 99%; boron rejection in the SWRO desalination plants reached only 65~85% and depended largely on membrane type, operating conditions, and sampling locations (brine side or feed side). Full- and pilot-scale

permeate boron concentrations ranged from 0.53 to 1.52 mg/L. Boron concentrations in the permeates from the seawater treatment plants were higher than the current WHO guideline of 0.5 mg/L, but in compliance with a currently applicable regulation in the United States (the California Department of Health Services action level of 1 mg/L). Since raw water in brackish water treatment plants contained low concentrations of boron, boron concentrations in the permeate were low in spite of mediocre boron rejection by the BWRO membranes. Due to their higher recovery, boron rejection was much lower in the full- or pilot-scale systems than that observed during the bench-scale experiments. Accurate extrapolation of bench-scale boron rejection data to full- or pilot-scale performance would require mathematical models (Mi et al., 2005) that account for nonhomogenous conditions along the membrane elements. The equations developed in this study, such as equations (25) and (31), can serve as a basis for such models.

In this study, the economics of six hypothetical RO process options for boron removal was evaluated. Configurations included single-pass RO (configuration 1), single-pass RO with increased feed pH (configuration 2), partial double-pass RO (configuration 3), single-pass RO with ion exchange polishing (configuration 4), double-pass RO with softening and RO treatment of second-pass concentrate (configuration 5), and double-pass RO with two-stage RO treatment of second-pass concentrate (configuration 6). Costs for configuration 1 were estimated to be approximately $\$0.518/m^3$ ($1.96/1,000 gal) and permeate from this system would contain 1.2 mg/L boron. Among configurations 2, 3, and 4, each of which could produce permeate containing < 1 mg/L boron, configuration 2 would be the most cost-effective option. The estimate of water production cost for configuration 2 was comparable to that of configuration 1. To achieve a permeate boron concentration < 0.5 mg/L (configurations 5 and 6), a 20 to 25% increase in water production costs would be required. From the result of cost analysis, it is concluded that the economics of boron removal processes is expected to be governed by the target permeate water quality driven by the regulations. In addition, when the boron removal is of concern in the SWRO process, the development of RO membranes with improved boron rejection capabilities is critical to achieve target boron removal in full-scale membrane plants.

This project was a collaborative effort between the Georgia Institute of Technology, two leading membrane manufacturers (Hydranautics and Saehan Industry, Inc.), an engineering consulting firm (Carollo Engineers), and several desalination utilities. Phase II of this project will focus on developing a mathematical model for larger-scale RO processes targeting boron removal. The model, which will be adjusted and validated using pilot-scale experiments, will be based on the six RO configurations studied during Phase I of this project.

Appendix A: Sampling Instructions

Preparation

(1) Sampling Bottles

Use 150~200 mL sampling bottle made with HDPE, PE, or PP.

Glass containers cannot be used since it could contaminate samples with boron.

Prepare three sampling bottles for each sampling point; three bottles for feed water, three bottles for concentrate water, and three bottles for product (permeate).

(2) Gloves (latex)

(3) Thermometer (Not necessary, in case your facility checks temperature of feed and permeate water with other methods)

Sampling steps

(1) Label the bottles with date, the name of person, sampling location, and sample number (for example, Feed 1, Feed 2, Feed 3, Concentrate 1, Concentrate 2, Concentrate 3, Permeate 1, Permeate 2, and Permeate 3)

(2) Put on gloves during bottle handling and sampling.

(3) Rinse the bottle 3 times with sample water.

(4) Fill the each bottle with at least 100 mL of sample water. After sampling, make sure the cap of the bottle is tightly closed.

(5) Triplicate for each sampling point.

(6) Measure the water temperature during sampling.

(7) After finishing sampling, fill out the SAMPLE INFORMATION for each set of sampling. This form should be filled at the site of sampling immediately after the sampling.

(8) Place the form and the sampling bottles into the shipping package and seal carefully. Send the package within two days after sampling through the U.S. Postal Service Priority Mail or commercial ground carriers such as UPS, Fedex, etc. It is not necessary to freeze the samples nor use coolers for shipping.

NOTE: You may want to fill the information in the SAMPLING INFORMATION FORM that is same for all the samplings before you print out the form. For example, type in the Facility name, Address, and Personnel (if one person is sampling) before you print out to avoid hand writing these again and again.

SAMPLING INFORMATION FORM

Facility	***Personnel (please print)***
Facility name _____	Name _____
_____	Date _____
Address _____	Signature _____
_____	E-mail _____
_____	Phone _____ Fax _____

Sample Information

Details of Conductivity _____ _____

Comment _____

_____

2. Concentrate

Sampling date and time _____ Concentrate flow rate _____

Concentrate pressure _____ Conductivity _____

Comment _____

_____

3. Permeate

Sampling date and time _____ Temperature _____

Permeate flow rate _____ pH _____

Conductivity _____

Comment _____ _____

Appendix B: Data Record

B.1. pH Effect Experiment

Conductivity Passage (%) Figure 3.15		SR				SWC4+				XLE			
	psi	pH 6.2	pH 7.5	pH 8.5	pH 9.5	pH 6.2	pH 7.5	pH 8.5	pH 9.5	pH 6.2	pH 7.5	pH 8.5	pH 9.5
	1,000	0.488	0.471	0.477	0.501	0.236	0.226	0.230	0.243	0.582	0.536	0.531	0.545
	900	0.515	0.514	0.512	0.532	0.259	0.240	0.246	0.269	0.613	0.564	0.557	0.564
	800	0.575	0.564	0.566	0.582	0.296	0.269	0.274	0.290	0.650	0.619	0.600	0.590
	700	0.666	0.631	0.668	0.663	0.334	0.323	0.316	0.331	0.706	0.652	0.630	0.648
	600	0.809	0.861	0.778	0.804	0.415	0.405	0.388	0.427	0.822	0.778	0.731	0.743
		LE				TM820				TM820A			
	psi	pH 6.2	pH 7.5	pH 8.5	pH 9.5	pH 6.2	pH 7.5	pH 8.5	pH 9.5	pH 6.2	pH 7.5	pH 8.5	pH 9.5
	1,000	0.221	0.208	0.213	0.224	0.217	0.207	0.209	0.217	0.341	0.335	0.352	0.359
	900	0.240	0.219	0.226	0.241	0.235	0.219	0.222	0.234	0.383	0.362	0.364	0.388
	800	0.275	0.250	0.250	0.261	0.264	0.247	0.245	0.254	0.436	0.410	0.410	0.430
	700	0.308	0.296	0.286	0.297	0.298	0.283	0.275	0.279	0.491	0.494	0.480	0.495
	600	0.376	0.367	0.348	0.374	0.357	0.350	0.334	0.347	0.609	0.622	0.587	0.641

Flux (gfd) Figure 3.8		SR				SWC4+				XLE			
	psi	pH 6.2	pH 7.5	pH 8.5	pH 9.5	pH 6.2	pH 7.5	pH 8.5	pH 9.5	pH 6.2	pH 7.5	pH 8.5	pH 9.5
	1,000	12.32	12.24	12.48	12.58	16.29	16.20	16.53	16.43	16.18	16.22	16.53	16.46
	900	10.84	10.74	10.41	10.60	14.24	14.42	14.25	14.31	14.50	14.15	13.90	14.04
	800	9.05	8.74	9.04	8.66	12.02	11.79	11.92	12.20	11.91	11.62	12.09	11.56
	700	7.53	7.25	7.45	7.26	10.32	10.20	9.97	9.95	9.96	9.68	10.08	10.06
	600	5.58	5.67	5.67	6.48	7.86	7.61	7.80	7.36	7.47	7.23	7.64	7.63
		LE				TM820				TM820A			
	psi	pH 6.2	pH 7.5	pH 8.5	pH 9.5	pH 6.2	pH 7.5	pH 8.5	pH 9.5	pH 6.2	pH 7.5	pH 8.5	pH 9.5
	1,000	14.87	14.82	15.03	15.05	16.18	15.85	16.03	15.96	15.49	15.27	15.50	15.60
	900	12.95	13.22	12.99	13.17	14.07	14.11	13.93	14.03	13.46	13.59	13.51	13.69
	800	10.90	10.83	10.89	11.19	11.95	11.59	11.69	11.94	11.43	11.16	11.33	11.60
	700	9.41	9.34	9.13	9.14	10.25	10.05	9.80	9.77	9.83	9.67	9.51	9.51
	600	7.16	6.97	7.15	6.80	7.84	7.52	7.70	7.29	7.53	7.24	7.47	7.06

Boron Passage (%) Figure 3.9		SR				SWC4+				XLE			
	psi	pH 6.2	pH 7.5	pH 8.5	pH 9.5	pH 6.2	pH 7.5	pH 8.5	pH 9.5	pH 6.2	pH 7.5	pH 8.5	pH 9.5
	1,000	13.83	13.37	10.39	3.82	7.51	7.26	5.64	1.58	9.19	9.03	7.12	2.63
	900	14.27	14.40	11.40	4.00	8.00	7.70	6.10	1.63	9.42	9.46	7.60	2.74
	800	15.85	16.03	12.88	4.34	8.67	8.64	6.64	1.72	10.63	10.66	8.41	2.83
	700	18.10	17.71	14.24	5.13	9.75	9.53	7.52	2.10	11.76	11.51	9.12	3.21
	600	20.82	22.32	17.12	6.07	11.82	12.00	9.13	2.67	13.59	14.25	10.68	3.72
		LE				TM820				TM820A			
	psi	pH 6.2	pH 7.5	pH 8.5	pH 9.5	pH 6.2	pH 7.5	pH 8.5	pH 9.5	pH 6.2	pH 7.5	pH 8.5	pH 9.5
	1,000	7.34	7.06	5.67	1.55	9.13	8.60	6.87	1.85	5.93	5.54	4.22	1.15
	900	7.62	7.53	6.02	1.57	9.34	9.23	7.35	2.01	6.18	5.86	4.59	1.23
	800	8.64	8.38	6.48	1.74	10.39	10.24	7.98	2.14	6.83	6.56	4.90	1.37
	700	9.46	9.37	7.41	2.05	11.42	11.29	9.00	2.50	7.63	7.34	5.75	1.62
	600	11.23	11.95	9.02	2.67	13.58	14.13	10.82	3.17	9.25	9.45	7.07	2.16

Na Passage (%) Figure 3.10

	SR				SWC4+				XLE			
psi	pH 6.2	pH 7.5	pH 8.5	pH 9.5	pH 6.2	pH 7.5	pH 8.5	pH 9.5	pH 6.2	pH 7.5	pH 8.5	pH 9.5
1,000	0.500	0.536	0.502	0.552	0.163	0.101	0.086	0.075	0.574	0.538	0.543	0.595
900	0.561	0.556	0.563	0.568	0.192	0.135	0.143	0.135	0.628	0.561	0.550	0.619
800	0.631	0.631	0.635	0.664	0.246	0.161	0.121	0.141	0.746	0.673	0.624	0.660
700	0.815	0.752	0.761	0.831	0.249	0.235	0.198	0.195	0.788	0.728	0.667	0.682
600	1.023	1.104	0.948	0.996	0.337	0.280	0.277	0.300	0.948	0.910	0.818	0.854
	LE				TM820				TM820A			
psi	pH 6.2	pH 7.5	pH 8.5	pH 9.5	pH 6.2	pH 7.5	pH 8.5	pH 9.5	pH 6.2	pH 7.5	pH 8.5	pH 9.5
1,000	0.115	0.064	0.084	0.081	0.163	0.049	0.101	0.072	0.243	0.172	0.215	0.215
900	0.121	0.089	0.101	0.121	0.135	0.072	0.086	0.078	0.240	0.206	0.198	0.257
800	0.192	0.115	0.152	0.118	0.163	0.155	0.158	0.149	0.289	0.317	0.263	0.306
700	0.178	0.200	0.146	0.161	0.212	0.195	0.138	0.186	0.391	0.377	0.363	0.340
600	0.266	0.243	0.226	0.223	0.314	0.246	0.180	0.166	0.508	0.568	0.471	0.545

Cl Passage (%) Figure 3.11

	SR				SWC4+				XLE			
psi	pH 6.2	pH 7.5	pH 8.5	pH 9.5	pH 6.2	pH 7.5	pH 8.5	pH 9.5	pH 6.2	pH 7.5	pH 8.5	pH 9.5
1,000	0.476	0.485	0.468	0.468	0.250	0.238	0.228	0.243	0.559	0.532	0.512	0.528
900	0.516	0.525	0.499	0.523	0.274	0.252	0.242	0.269	0.606	0.566	0.537	0.574
800	0.579	0.578	0.563	0.564	0.315	0.289	0.305	0.293	0.645	0.616	0.590	0.575
700	0.674	0.645	0.676	0.645	0.351	0.347	0.327	0.337	0.704	0.654	0.632	0.633
600	0.842	0.902	0.792	0.802	0.444	0.432	0.409	0.440	0.828	0.790	0.733	0.740
	LE				TM820				TM820A			
psi	pH 6.2	pH 7.5	pH 8.5	pH 9.5	pH 6.2	pH 7.5	pH 8.5	pH 9.5	pH 6.2	pH 7.5	pH 8.5	pH 9.5
1,000	0.233	0.219	0.206	0.223	0.222	0.211	0.199	0.204	0.351	0.368	0.358	0.360
900	0.257	0.226	0.218	0.240	0.244	0.227	0.212	0.220	0.404	0.374	0.377	0.393
800	0.291	0.261	0.312	0.260	0.280	0.254	0.256	0.237	0.469	0.435	0.477	0.438
700	0.319	0.311	0.317	0.302	0.310	0.293	0.276	0.266	0.528	0.529	0.528	0.515
600	0.410	0.390	0.390	0.386	0.381	0.367	0.336	0.341	0.657	0.678	0.643	0.685

Ca Passage (%) Figure 3.12

	SR				SWC4+				XLE			
psi	pH 6.2	pH 7.5	pH 8.5	pH 9.5	pH 6.2	pH 7.5	pH 8.5	pH 9.5	pH 6.2	pH 7.5	pH 8.5	pH 9.5
1,000	0.117	0.118	0.128	0.131	0.067	0.045	0.053	0.062	0.389	0.334	0.316	0.329
900	0.126	0.132	0.135	0.136	0.065	0.046	0.048	0.057	0.393	0.347	0.323	0.364
800	0.136	0.125	0.136	0.137	0.066	0.054	0.053	0.058	0.419	0.357	0.337	0.319
700	0.153	0.145	0.181	0.146	0.074	0.063	0.058	0.065	0.406	0.354	0.332	0.315
600	0.176	0.239	0.179	0.179	0.087	0.074	0.075	0.082	0.438	0.380	0.339	0.346
	LE				TM820				TM820A			
psi	pH 6.2	pH 7.5	pH 8.5	pH 9.5	pH 6.2	pH 7.5	pH 8.5	pH 9.5	pH 6.2	pH 7.5	pH 8.5	pH 9.5
1,000	0.072	0.050	0.053	0.065	0.069	0.036	0.039	0.041	0.150	0.118	0.121	0.126
900	0.065	0.046	0.050	0.050	0.056	0.037	0.032	0.029	0.151	0.113	0.116	0.114
800	0.080	0.058	0.051	0.051	0.057	0.040	0.039	0.030	0.162	0.119	0.120	0.115
700	0.084	0.065	0.067	0.061	0.065	0.040	0.039	0.033	0.164	0.140	0.133	0.144
600	0.090	0.088	0.068	0.071	0.066	0.049	0.041	0.032	0.193	0.172	0.155	0.155

Mg Passage (%) Figure 3.13		SR				SWC4+				XLE			
	psi	pH 6.2	pH 7.5	pH 8.5	pH 9.5	pH 6.2	pH 7.5	pH 8.5	pH 9.5	pH 6.2	pH 7.5	pH 8.5	pH 9.5
	1,000	0.114	0.112	0.122	0.137	0.049	0.043	0.044	0.050	0.390	0.327	0.321	0.335
	900	0.123	0.124	0.125	0.134	0.053	0.042	0.043	0.054	0.407	0.341	0.328	0.354
	800	0.130	0.124	0.132	0.128	0.059	0.047	0.045	0.051	0.408	0.361	0.338	0.317
	700	0.145	0.133	0.178	0.140	0.063	0.056	0.049	0.058	0.406	0.350	0.326	0.319
	600	0.167	0.231	0.172	0.171	0.075	0.066	0.060	0.074	0.432	0.381	0.343	0.340
		LE				TM820				TM820A			
	psi	pH 6.2	pH 7.5	pH 8.5	pH 9.5	pH 6.2	pH 7.5	pH 8.5	pH 9.5	pH 6.2	pH 7.5	pH 8.5	pH 9.5
	1,000	0.053	0.046	0.045	0.052	0.047	0.031	0.029	0.030	0.118	0.101	0.107	0.110
	900	0.054	0.042	0.044	0.048	0.041	0.030	0.028	0.031	0.122	0.101	0.098	0.101
	800	0.062	0.046	0.046	0.049	0.046	0.032	0.028	0.028	0.137	0.105	0.103	0.107
	700	0.066	0.059	0.051	0.054	0.048	0.038	0.030	0.029	0.143	0.130	0.122	0.119
	600	0.075	0.069	0.059	0.066	0.051	0.044	0.037	0.033	0.168	0.155	0.137	0.147

SO_4 Passage (%) Figure 3.14		SR				SWC4+				XLE			
	psi	pH 6.2	pH 7.5	pH 8.5	pH 9.5	pH 6.2	pH 7.5	pH 8.5	pH 9.5	pH 6.2	pH 7.5	pH 8.5	pH 9.5
	1,000	0.131	0.141	0.148	0.155	0.115	0.088	0.089	0.092	0.374	0.329	0.335	0.341
	900	0.132	0.142	0.143	0.139	0.111	0.088	0.083	0.091	0.371	0.301	0.316	0.345
	800	0.134	0.149	0.155	0.152	0.133	0.089	0.102	0.094	0.363	0.355	0.333	0.318
	700	0.153	0.154	0.200	0.165	0.275	0.121	0.097	0.101	0.373	0.330	0.338	0.311
	600	0.183	0.231	0.188	0.194	0.124	0.104	0.112	0.115	0.402	0.357	0.325	0.323
		LE				TM820				TM820A			
	psi	pH 6.2	pH 7.5	pH 8.5	pH 9.5	pH 6.2	pH 7.5	pH 8.5	pH 9.5	pH 6.2	pH 7.5	pH 8.5	pH 9.5
	1,000	0.095	0.087	0.075	0.083	0.095	0.083	0.084	0.085	0.135	0.151	0.171	0.130
	900	0.251	0.081	0.073	0.086	0.112	0.112	0.084	0.090	0.156	0.119	0.131	0.127
	800	0.107	0.082	0.129	0.081	0.099	0.101	0.098	0.084	0.178	0.133	0.162	0.132
	700	0.106	0.121	0.116	0.087	0.105	0.102	0.097	0.094	0.146	0.152	0.156	0.145
	600	0.315	0.129	0.129	0.102	0.140	0.139	0.110	0.103	0.191	0.189	0.181	0.162

B.2. Temperature Effect Experiment at pH 6.2

Flux (gfd) Figure 3.16		SR			SWC4+			XLE		
	psi	15 °C	25 °C	35 °C	15 °C	25 °C	35 °C	15 °C	25 °C	35 °C
	1,000	10.99	15.76	19.83	12.10	16.61	23.68	14.27	22.65	29.76
	900	9.64	13.32	17.46	10.73	14.61	20.51	12.79	19.02	26.76
	800	8.12	11.05	14.32	9.30	12.49	16.70	10.15	15.11	22.47
	700	6.87	9.53	12.43	7.66	10.30	14.08	8.91	13.63	17.94
	600	4.74	6.88	8.29	5.60	8.08	10.48	6.53	10.09	12.34
		LE			TM820			TM820A		
	psi	15 °C	25 °C	35 °C	15 °C	25 °C	35 °C	15 °C	25 °C	35 °C
	1,000	11.15	15.48	22.33	13.24	17.20	23.58	11.25	15.49	21.78
	900	9.79	13.97	19.35	11.42	15.23	20.42	9.81	13.74	18.89
	800	8.49	11.80	15.75	9.95	12.86	16.49	8.55	11.58	15.36
	700	6.95	9.77	13.46	8.20	10.58	14.08	7.01	9.55	13.12
	600	5.26	7.63	10.02	6.16	8.30	10.67	5.25	7.53	9.86

Boron Passage (%) Figure 3.17		SR			SWC4+			XLE		
	psi	15 °C	25 °C	35 °C	15°C	25 °C	35 °C	15 °C	25 °C	35 °C
	1,000	8.10	11.72	14.93	4.20	6.44	8.86	6.84	9.68	12.04
	900	8.96	12.14	15.83	4.46	6.80	9.55	6.63	9.57	12.52
	800	9.66	14.33	18.70	5.17	7.73	11.06	7.36	10.76	13.69
	700	10.85	16.21	22.33	5.63	8.57	12.19	8.08	11.93	15.59
	600	14.18	20.25	27.69	7.32	10.64	14.49	10.03	14.54	18.23
		LE			TM820			TM820A		
	psi	15 °C	25 °C	35 °C	15°C	25 °C	35 °C	15 °C	25 °C	35 °C
	1,000	4.70	7.04	9.27	5.25	8.23	10.63	3.34	4.92	6.35
	900	4.99	7.15	9.69	5.80	8.70	11.50	3.55	5.19	6.94
	800	5.53	8.18	11.68	6.58	9.72	13.40	4.06	5.92	8.35
	700	6.23	9.18	12.59	7.15	10.83	14.69	4.45	6.79	9.30
	600	7.95	11.17	14.95	9.18	13.17	17.17	5.83	8.43	10.81

Na Passage (%) Figure 3.18		SR			SWC4+			XLE		
	psi	15 °C	25 °C	35 °C	15 °C	25 °C	35 °C	15 °C	25 °C	35 °C
	1,000	0.735	0.487	0.557	0.474	0.446	0.392	0.296	0.314	0.338
	900	1.116	0.540	0.575	0.440	0.555	0.510	0.268	0.335	0.370
	800	0.745	0.639	1.328	0.494	0.474	0.623	0.324	0.374	0.448
	700	0.829	0.699	2.515	0.530	0.552	0.592	0.271	0.352	0.508
	600	1.253	1.045	4.652	0.569	0.592	0.670	0.388	0.494	0.586
		LE			TM820			TM820A		
	psi	15 °C	25 °C	35 °C	15 °C	25 °C	35 °C	15 °C	25 °C	35 °C
	1,000	0.465	0.583	0.426	0.322	0.651	0.412	0.527	0.738	0.454
	900	0.443	0.510	0.566	0.317	0.437	0.449	0.494	0.631	0.620
	800	0.508	0.502	0.603	0.508	0.519	0.505	0.623	0.704	0.687
	700	0.510	0.597	0.617	0.524	0.522	0.530	0.710	0.648	0.729
	600	0.648	0.606	0.783	0.564	0.609	0.802	0.859	0.844	0.912

Cl Passage (%) Figure 3.19		SR			SWC4+			XLE		
	psi	15 °C	25 °C	35 °C	15 °C	25 °C	35 °C	15 °C	25 °C	35 °C
	1,000	0.851	0.528	0.575	0.164	0.205	0.245	0.306	0.322	0.473
	900	1.262	0.558	0.630	0.175	0.217	0.260	0.307	0.324	0.411
	800	0.883	0.620	1.441	0.206	0.243	0.312	0.343	0.337	0.468
	700	0.932	0.783	2.504	0.226	0.286	0.340	0.342	0.394	0.536
	600	1.403	1.090	3.839	0.288	0.361	0.418	0.438	0.516	0.678
		LE			TM820			TM820A		
	psi	15 °C	25 °C	35 °C	15 °C	25 °C	35 °C	15 °C	25 °C	35 °C
	1,000	0.148	0.190	0.232	0.143	0.187	0.218	0.287	0.310	0.330
	900	0.158	0.198	0.249	0.156	0.197	0.233	0.307	0.330	0.353
	800	0.179	0.229	0.304	0.177	0.223	0.277	0.369	0.383	0.429
	700	0.199	0.263	0.330	0.199	0.258	0.301	0.419	0.460	0.464
	600	0.253	0.328	0.410	0.255	0.319	0.364	0.558	0.592	0.590

Ca Passage (%) Figure 3.20		SR			SWC4+			XLE		
	psi	15 °C	25 °C	35 °C	15 °C	25 °C	35 °C	15 °C	25 °C	35 °C
	1,000	0.501	0.287	0.217	0.056	0.050	0.040	0.186	0.140	0.114
	900	0.796	0.330	0.236	0.053	0.040	0.041	0.173	0.143	0.116
	800	0.466	0.295	0.889	0.065	0.050	0.041	0.168	0.123	0.110
	700	0.505	0.356	1.815	0.063	0.059	0.049	0.174	0.118	0.111
	600	0.695	0.469	3.422	0.080	0.065	0.062	0.189	0.131	0.125
		LE			TM820			TM820A		
	psi	15 °C	25 °C	35 °C	15 °C	25 °C	35 °C	15 °C	25 °C	35 °C
	1,000	0.040	0.036	0.033	0.026	0.031	0.022	0.119	0.101	0.086
	900	0.037	0.038	0.025	0.028	0.026	0.019	0.124	0.107	0.076
	800	0.040	0.038	0.041	0.035	0.029	0.028	0.143	0.120	0.092
	700	0.049	0.040	0.040	0.036	0.035	0.033	0.151	0.130	0.102
	600	0.062	0.051	0.043	0.048	0.041	0.036	0.207	0.162	0.128

Mg Passage (%) Figure 3.21		SR			SWC4+			XLE		
	psi	15 °C	25 °C	35 °C	15 °C	25 °C	35 oC	15 °C	25 °C	35 °C
	1,000	0.611	0.288	0.220	0.046	0.047	0.035	0.191	0.148	0.131
	900	1.060	0.329	0.242	0.046	0.042	0.035	0.180	0.155	0.129
	800	0.555	0.297	0.919	0.055	0.046	0.038	0.177	0.135	0.123
	700	0.604	0.359	1.894	0.056	0.052	0.043	0.180	0.125	0.124
	600	0.855	0.486	3.683	0.069	0.063	0.051	0.190	0.139	0.139
		LE			TM820			TM820A		
	psi	15 oC	25 oC	35 oC	15 oC	25 oC	35 oC	15 oC	25 oC	35 oC
	1,000	0.035	0.032	0.027	0.027	0.031	0.022	0.114	0.096	0.078
	900	0.039	0.031	0.025	0.028	0.028	0.021	0.110	0.096	0.077
	800	0.041	0.034	0.030	0.034	0.031	0.025	0.134	0.105	0.089
	700	0.044	0.038	0.031	0.035	0.037	0.027	0.136	0.125	0.094
	600	0.054	0.049	0.040	0.048	0.044	0.032	0.174	0.153	0.114

SO_4 Passage (%) Figure 3.22		SR			SWC4+			XLE		
	psi	15 °C	25 °C	35 °C	15 °C	25 °C	35 °C	15 °C	25 °C	35 °C
	1,000	0.570	0.266	0.217	0.075	0.080	0.074	0.209	0.182	0.206
	900	0.897	0.264	0.249	0.075	0.076	0.075	0.196	0.175	0.154
	800	0.499	0.270	0.902	0.081	0.081	0.066	0.215	0.151	0.161
	700	0.482	0.333	1.787	0.079	0.082	0.078	0.185	0.156	0.160
	600	0.737	0.417	3.082	0.087	0.088	0.078	0.197	0.180	0.163
		LE			TM820			TM820A		
	psi	15 °C	25 °C	35 °C	15 °C	25 °C	35 °C	15 °C	25 °C	35 °C
	1,000	0.067	0.068	0.058	0.074	0.080	0.071	0.109	0.111	0.104
	900	0.069	0.069	0.065	0.072	0.079	0.075	0.104	0.113	0.104
	800	0.072	0.071	0.062	0.080	0.082	0.075	0.119	0.119	0.112
	700	0.069	0.072	0.061	0.079	0.087	0.080	0.122	0.129	0.121
	600	0.072	0.075	0.067	0.092	0.094	0.083	0.147	0.144	0.129

B.3. Temperature Effect Experiment at pH 9.5

		SR			SWC4+			XLE		
	psi	15 °C	25 °C	35 °C	15 °C	25 °C	35 °C	15 °C	25 °C	35 °C
	1,000	9.31	12.58	15.74	12.30	17.61	21.66	12.31	16.46	21.38
	900	8.05	10.60	13.61	11.07	15.16	19.44	10.56	14.04	18.90
	800	6.56	8.66	11.59	9.10	12.89	15.48	8.73	11.56	15.36
	700	5.49	7.26	9.30	7.65	10.69	13.11	7.50	10.06	12.88
Flux (gfd) Figure 3.23	600	4.13	6.48	7.10	5.86	7.93	9.66	5.51	7.63	9.47
		LE			TM820			TM820A		
	psi	15 °C	25 °C	35 °C	15 °C	25 °C	35 °C	15 °C	25 °C	35 °C
	1,000	11.09	16.18	20.47	12.86	17.30	20.33	11.08	15.77	19.71
	900	9.97	14.10	18.30	11.50	14.87	18.22	9.86	13.66	17.83
	800	8.27	11.94	14.63	9.38	12.57	14.61	8.19	11.66	14.27
	700	6.94	9.92	12.47	7.87	10.37	12.43	6.86	9.63	12.17
	600	5.32	7.34	9.21	6.02	7.72	9.13	5.29	7.18	9.00

		SR			SWC4+			XLE		
	psi	15°C	25°C	35°C	15°C	25°C	35°C	15°C	25°C	35°C
	1,000	2.76	3.82	4.79	1.03	1.32	1.70	1.91	2.63	3.45
	900	2.83	4.00	5.25	1.14	1.54	1.88	2.00	2.74	3.65
	800	3.15	4.34	5.37	1.24	1.86	2.11	2.14	2.83	3.62
	700	3.75	5.13	6.32	1.53	2.07	2.44	2.43	3.21	4.18
Boron Passage (%) Figure 3.24	600	4.65	6.07	7.98	2.05	2.63	3.13	2.97	3.72	4.96
		LE			TM820			TM820A		
	psi	15°C	25°C	35°C	15°C	25°C	35°C	15°C	25°C	35°C
	1,000	1.12	1.34	1.87	1.26	1.66	2.17	0.84	1.09	1.31
	900	1.19	1.57	2.06	1.41	1.95	2.35	0.91	1.21	1.45
	800	1.42	1.94	2.25	1.70	2.21	2.59	1.06	1.48	1.62
	700	1.73	2.17	2.56	1.91	2.54	3.00	1.27	1.64	1.83
	600	2.15	2.79	3.25	2.50	3.16	3.72	1.67	2.09	2.44

		SR			SWC4+			XLE		
	psi	15 °C	25 °C	35 °C	15 °C	25 °C	35 °C	15 °C	25 °C	35 °C
	1,000	0.453	0.552	0.649	0.488	0.387	0.314	0.507	0.595	0.773
	900	0.432	0.568	0.732	0.479	0.463	0.212	0.480	0.619	0.872
	800	0.502	0.664	0.788	0.339	0.435	0.229	0.532	0.660	0.847
	700	0.604	0.831	0.953	0.508	0.510	0.260	0.581	0.682	1.052
	600	0.775	0.996	1.311	0.437	0.698	0.377	0.718	0.854	1.264
Na Passage (%) Figure 3.25		LE			TM820			TM820A		
	psi	15 °C	25 °C	35 °C	15 °C	25 °C	35 °C	15 °C	25 °C	35 °C
	1,000	0.409	0.440	0.297	0.491	0.370	0.294	0.654	0.575	0.343
	900	0.409	0.446	0.186	0.412	0.499	0.183	0.628	0.673	0.289
	800	0.378	0.465	0.223	0.440	0.463	0.175	0.547	0.640	0.360
	700	0.463	0.527	0.158	0.336	0.569	0.178	0.682	0.839	0.406
	600	0.499	0.715	0.369	0.502	0.620	0.300	0.932	1.032	0.562

		SR			SWC4+			XLE		
	psi	15 °C	25 °C	35 °C	15 °C	25 °C	35 °C	15 °C	25 °C	35 °C
	1,000	0.429	0.468	0.536	0.178	0.198	0.277	0.475	0.528	0.682
	900	0.436	0.497	0.604	0.190	0.226	0.293	0.502	0.545	0.724
	800	0.469	0.564	0.632	0.217	0.261	0.334	0.521	0.575	0.741
Cl Passage (%) Figure 3.26	700	0.553	0.645	0.773	0.234	0.305	0.382	0.554	0.633	0.843
	600	0.679	0.802	0.975	0.298	0.390	0.502	0.654	0.740	1.005
		LE			TM820			TM820A		
	psi	15 °C	25 °C	35 °C	15 °C	25 °C	35 °C	15 °C	25 °C	35 °C
	1,000	0.154	0.180	0.275	0.155	0.179	0.241	0.342	0.318	0.367
	900	0.162	0.202	0.292	0.166	0.199	0.259	0.371	0.366	0.399
	800	0.192	0.237	0.326	0.192	0.225	0.288	0.415	0.442	0.455
	700	0.197	0.277	0.384	0.209	0.258	0.326	0.458	0.564	0.535
	600	0.252	0.346	0.485	0.271	0.324	0.416	0.591	0.708	0.716

		SR			SWC4+			XLE		
	psi	15 °C	25 °C	35 °C	15 °C	25 °C	35 °C	15 °C	25 °C	35 °C
	1,000	0.195	0.131	0.081	0.050	0.034	0.035	0.366	0.329	0.372
	900	0.178	0.136	0.095	0.048	0.041	0.039	0.377	0.364	0.386
	800	0.170	0.137	0.101	0.052	0.047	0.040	0.370	0.319	0.344
Ca Passage (%) Figure 3.27	700	0.190	0.146	0.105	0.049	0.054	0.042	0.373	0.315	0.351
	600	0.214	0.179	0.136	0.060	0.069	0.050	0.383	0.346	0.380
		LE			TM820			TM820A		
	psi	15 °C	25 °C	35 °C	15 °C	25 °C	35 °C	15 °C	25 °C	35 °C
	1,000	0.040	0.027	0.040	0.028	0.022	0.020	0.138	0.094	0.091
	900	0.038	0.031	0.032	0.024	0.026	0.020	0.141	0.105	0.090
	800	0.040	0.040	0.032	0.028	0.032	0.023	0.141	0.127	0.091
	700	0.039	0.044	0.037	0.030	0.035	0.027	0.140	0.185	0.093
	600	0.043	0.049	0.041	0.040	0.040	0.029	0.170	0.207	0.113

		SR			SWC4+			XLE		
	psi	15 oC	25 oC	35 oC	15 oC	25 oC	35 oC	15 oC	25 oC	35 oC
	1,000	0.179	0.137	0.084	0.045	0.034	0.036	0.363	0.335	0.376
	900	0.162	0.134	0.089	0.045	0.037	0.034	0.372	0.354	0.377
	800	0.164	0.128	0.090	0.047	0.049	0.041	0.376	0.317	0.341
Mg Passage (%) Figure 3.28	700	0.173	0.140	0.100	0.049	0.053	0.041	0.364	0.319	0.345
	600	0.199	0.171	0.120	0.058	0.063	0.051	0.380	0.340	0.373
		LE			TM820			TM820A		
	psi	15 °C	25 °C	35 °C	15 °C	25 °C	35 °C	15 °C	25 °C	35 °C
	1,000	0.035	0.029	0.032	0.028	0.025	0.025	0.135	0.093	0.087
	900	0.036	0.031	0.032	0.030	0.027	0.024	0.142	0.101	0.086
	800	0.038	0.041	0.033	0.033	0.032	0.026	0.135	0.127	0.092
	700	0.040	0.044	0.036	0.032	0.034	0.026	0.142	0.177	0.096
	600	0.046	0.051	0.044	0.050	0.042	0.028	0.158	0.199	0.116

		SR			SWC4+			XLE		
	psi	15 °C	25 °C	35 °C	15 °C	25 °C	35 °C	15 °C	25 °C	35 °C
	1,000	0.203	0.155	0.107	0.084	0.074	0.080	0.360	0.341	0.374
	900	0.184	0.139	0.128	0.078	0.076	0.083	0.376	0.345	0.377
	800	0.179	0.152	0.131	0.084	0.088	0.083	0.352	0.318	0.362
SO_4 Passage (%) Figure 3.29	700	0.170	0.165	0.121	0.079	0.089	0.090	0.344	0.311	0.360
	600	0.200	0.194	0.163	0.088	0.101	0.100	0.354	0.323	0.354
		LE			TM820			TM820A		
	psi	15 °C	25 °C	35 °C	15 °C	25 °C	35 °C	15 °C	25 °C	35 °C
	1,000	0.074	0.067	0.072	0.078	0.073	0.083	0.138	0.116	0.128
	900	0.071	0.069	0.072	0.081	0.079	0.086	0.142	0.127	0.134
	800	0.074	0.077	0.072	0.086	0.090	0.087	0.141	0.152	0.139
	700	0.073	0.064	0.076	0.085	0.085	0.085	0.141	0.191	0.149
	600	0.078	0.086	0.084	0.103	0.105	0.104	0.151	0.222	0.178